The Impact of the Mesoprefrontal System on the Development of Murine Prefrontal Cortex

Dissertation

zur

Erlangung des Doktorgrades (Dr. rer. nat.)

der

Mathematisch-Naturwissenschaftlichen Fakultät

der

Rheinischen Friedrich-Wilhelms-Universität Bonn

vorgelegt von

Khondker Ushna Sameen Islam

aus

Dhaka, Bangladesch

Bonn, 2024

Angefertigt mit Genehmigung der Mathematisch-Naturwissenschaftlichen Fakultät der
Rheinischen Friedrich-Wilhelms-Universität Bonn

Gutachterin/Betreuerin: Prof. Dr. Sandra Blaess

Gutachter: Prof. Dr. Walter Witke

Tag der Promotion: 19/07/2024
Erscheinungsjahr: 2025

TABLE OF CONTENTS

Abbreviations

5-HT	5-hydroxy tryptamine / serotoninn
5-HTT/SERT	serotonin transporter
ADHD	attention deficit/hyperactivity disorder
AIS	axon initial segment
APOER2	apolipoprotein E receptor 2
ASD	autism spectrum disorder
BAC	bacterial artificial chromosome
CALB 1	calbindin 1
CB	calbindin
CGE	caudal ganglionic eminence
CgII	caudal cingulate cortex
CgI	cingulate cortex
CP	cortical plate
CR	calretinin
CXCL12	chemokine (C-X-C motif) ligand 12
DA	dopamine
DAT	dopamine transporter
DBH	dopamine beta hydroxylase
DCC	deleted in colorectal cancer receptor
DOPAC	dihydroxyphenylacetic acid
DR	dorsal raphe
DRD	dopamine receptor
E/I	excitatory / inhibitory
EGFP	enhanced green fluorescent protein
EN1/2	engrailed 1/2
FGF8	fibroblast growth factor 8
FOXA1/2	forkhead box A1/2
GABA	gamma amino butyric acid
GAD	glutamate decarboxylase
GBX2	gastrulation brain homeobox 2
GIFM	genetic inducible fate mapping
GIRK2	G-protein-regulated inward-rectifier potassium channel 2
glyco-DAT	glycosylated active form of the dopamine transporter
GPCR	G-protein coupled receptor
HVA	homovanillic acid
IL	Infralimbic cortex
L1CAM	L1 cell adhesion molecule
LC	locus coeruleus
LiN	linear nucleus
LMX1A/B	LIM homeobox transcription factor 1 alpha and beta
mDA	midbrain dopaminergic
MFB	medial forebrain bundle
MGE	medial ganglionic eminence
mPFC	medial prefrontal cortex
MZ	marginal zone
NA	noradrenaline/norephinephrine
NAc	nucleus accumbens
NET	noradrenaline/norepinephrine transporter
NEUROG2	neurogenin 2
NURR1	nuclear receptor related 1 protein
OB	olfactory bulb

OTX2	orthodenticle homolog 2
PAX	paired box transcription factors
PFC	prefrontal cortex
PITX3	pituitary homeobox 3
PP	preplate
PrL	Prelimbic cortex
PTCH	cell surface receptor patched
PTPRZ1	protein tyrosine phosphatase, receptor type Z, polypeptide 1
PV	parvalbumin
qPCR	quantitative polymerase chain reaction
SHH	sonic hedgehog
SMO	cell surface receptor smoothened
SNpc	substantia nigra pars compacta
SNpr	substantia nigra pars reticulata
SOX6	SRY-Box Transcription Factor 6
SP	subplate
TH	tyrosine hydroxylase
UNC5	uncoordinated 5 receptor
vGLUT2	vesicular glutamate transporter 2
VLDLR	very low density lipoprotein receptor
VMAT-2	vesicular monoamine transporter-2
VTA	ventral tegmental area
VZ	ventricular zone
WNT 1	wingless-related MMTV integration site 1

Summary

The prefrontal cortex (PFC) is involved in important cognitive processes and undergoes a lengthy functional and anatomical maturation process during postnatal development, which in mammals lasts until early adulthood. Afferent inputs, local microcircuits and the GABAergic interneurons mature during this time, and changes in their development likely contribute to susceptibility to mental illnesses such as schizophrenia. A subset of midbrain dopaminergic neurons (mDA) in the ventral tegmental area (VTA) projects to the PFC, and this so-called mesoprefrontal system modulates the function of the PFC. The development of the mesoprefrontal system is also relatively protracted and correlates temporally with the maturation of the PFC: dopaminergic innervation and dopamine content in the PFC increase strongly during the transition from adolescence to adulthood. This suggests that the appropriate development of mesoprefrontal input may play a key role in the maturation of the PFC microcircuits. To investigate how changes in mesoprefrontal signaling might affect the circuit elements of the PFC, we used a conditional *Gli2* knockout (cKO) mouse model in which the mDA projections to the PFC are not established. In this model, we followed the development of parvalbumin (PV), calretinin (CR) and calbindin (CB) expressing GABAergic interneurons of the medial (m)PFC and could show that the maturation process of PV and CB interneuron populations was impaired in the mPFC of *Gli2* cKO animals. In particular, PV interneurons are sensitive to the lack of dopaminergic input in *Gli2* cKO mice, as they are unable to maintain adequate PV expression during late adolescence and adulthood, which is associated with a concomitant decrease in their Gad1 expression. In *Gli2* cKO mice, the expression of DA receptor transcripts was also altered during development. However, other monoaminergic innervations were not affected by the absence of mDA projections, as the innervation pattern and density of serotonergic and noradrenergic projections in the mPFC of *Gli2* cKO mice remained unchanged. To determine the functional impact of impaired mesoprefrontal DA signaling, a spatial working memory task was performed with the *Gli2*-cKO mice, which revealed that a proportion of *Gli2* cKO mice have severe deficits in working memory. Our study shows that adolescence is a sensitive period in which the dopaminergic mesoprefrontal input plays a crucial role in the postnatal maturation of specific subsets of interneurons. The results of this study may contribute to a better understanding of the role of a developmentally dysregulated mesoprefrontal system in the pathophysiology of neurodevelopmental disorders.

Zusammenfassung

Der präfrontale Kortex (PFC) ist an wichtigen kognitiven Prozessen beteiligt und durchläuft während der postnatalen Entwicklung einen langwierigen funktionellen und anatomischen Reifungsprozess, der bei Säugetieren bis zum frühen Erwachsenenalter andauert. Afferente Eingänge, lokale Mikroschaltkreise und die GABAergen Interneurone reifen in dieser Zeit aus, und Veränderungen in ihrer Entwicklung tragen wahrscheinlich zur Anfälligkeit für psychische Erkrankungen wie Schizophrenie bei. Eine Untergruppe der mesencephalen dopaminergen Neuronen (mDA) im ventralen tegmentalen Areal (VTA) projiziert zum PFC, und dieses sogenannte mesopräfrontale System moduliert die Funktion des PFC. Die Entwicklung des mesopräfrontalen Systems ist ebenfalls relativ langwierig und korreliert zeitlich mit dem Reifungsprozess des PFC: die dopaminerge Innervation und der Dopamingehalts im PFC steigen während des Übergangs vom Jugend- zum Erwachsenenalter stark an. Dies deutet darauf hin, dass die angemessene Entwicklung des mesopräfrontalen Inputs eine Schlüsselrolle bei der Reifung der PFC-Mikroschaltkreise spielen könnte. Um zu untersuchen, wie sich Veränderungen im mesopräfrontalen Signalweg auf die Schaltkreiselemente des PFC auswirken könnten, verwendeten wir ein konditionales *Gli2*-Knockout (cKO)-Mausmodell, bei dem die mDA-Projektionen zum PFC nicht ausgebildet werden. In diesem Modell, verfolgten wir die Entwicklung von Parvalbumin (PV), Calretinin (CR) und Calbindin (CB) exprimierenden GABAergen Interneuronen des medialen (m)PFC und konnten zeigen, dass der Reifungsprozess von PV- und CB-Interneuronenpopulationen im mPFC der *Gli2* cKO Tiere gestört war. Insbesonder die PV-Interneuronen reagieren empfindlich auf den fehlenden dopaminergen Input in den *Gli2* cKO Mäusen, da sie nicht in der Lage sind, eine adäquate PV-Expression während der späten Adoleszenz und im Erwachsenenalter aufrechtzuerhalten, was mit einer gleichzeitigen Abnahme ihrer *Gad1*-Expression einhergeht. In den Gli2-cKO Mäusen war außerdem die Expression der DA-Rezeptor-mRNAs während der Entwicklung verändert. Andere monoaminerge Innervationen wurden durch das Fehlen der mDA Projektionen allerding nicht beeinflusst, da das Innervationsmuster und die Dichte der serotonergen und noradrenergen Projektionen im mPFC der *Gli2* cKO-Mäuse unverändert blieb. Um die funktionelle Auswirkung der gestörten mesopräfrontalen DA-Signalgebung zu bestimmen, wurde außerdem eine räumliche Arbeitsgedächtnisaufgabe mit den Gli2-cKO Mäusen durchgeführt, die zeigte, dass ein Teil der *Gli2*-cKO Mäuse starke Defizite im Arbeitsgedächtnis hat. Zusammenfassend zeigt unsere Studie, dass die Adoleszenz ein sensibler Zeitraum ist, in dem der dopaminerge mesopräfrontale Input eine entscheidende Rolle bei der postnatalen Reifung bestimmter Untergruppen von Interneuronen spielt. Die Ergebnisse dieser Studie können dazu beitragen, die Rolle eines entwicklungsbedingt

dysregulierten mesopräfrontalen Systems in der Pathophysiologie neurologischer Entwicklungsstörungen besser zu verstehen.

1. Introduction

1.1 The prefrontal cortex (PFC)

The prefrontal cortex (PFC) comprises cortical areas located at the rostral pole of the mammalian brain that are implicated in higher order cognitive functions such as planning, inhibitory control, decision making and working memory. The PFC is connected to other cortical regions and subcortical centers such as the thalamus, the limbic system, the basal ganglia and the brainstem. The executive functions of the PFC are dependent on its extensive interactions with other brain regions and are governed by its primary function of integration of information to execute actions in accordance with internally represented goals (Fuster, 2001; Miller et al., 2002).

1.1.1 Neuronal population of PFC

Similar to other parts of the cortex, the cytoarchitecture of PFC is multilayered, with distinct cellular and molecular composition assigned to each layer. The neuronal population of PFC is made up of 75–80% glutamatergic pyramidal neurons, and 20–25% GABAergic local interneurons (Kroon et al., 2019; Santana & Artigas, 2017).

On the basis of morphology and electrophysiological characteristics, various subtypes of pyramidal neurons are found across the cortical layers of PFC. For instance, in layer V, pyramidal neurons that exhibit adaptive firing pattern have only slender tufted apical dendrites but in layer III the adaptive firing subtype present either slender tufted or broad tufted apical dendrites. Layer VI pyramidal neurons show the greatest diversity in their morphology and mainly project to the thalamus. The most distinctive pyramidal neurons in the rodent PFC are the regular spiking subtype of layer V with broad tufted apical dendrites, which are involved in sending out long-range axonal projections (Van Aerde & Feldmeyer). During the early postnatal weeks, dendritic morphology and intrinsic membrane function of layer III and layer V pyramidal neurons develop rapidly in parallel. The development trajectory of ratio of excitatory to inhibitory (E/I) synaptic innervation received by the pyramidal neurons, however, is layer specific. At 2nd postnatal week, the excitatory inputs and inhibitory inputs are proportional in layer V but the E/I is much higher in layer III, demonstrating differential development in E/I balance across the cortical layers (Kroon et al., 2019). PFC pyramidal neurons contribute to maintenance of working memory and changes in their properties are implicated in neuropsychiatric disorders such as schizophrenia (Black et al., 2004; Glantz & Lewis, 2000; Lewis, 1997; Vogel et al., 2022).

GABAergic interneurons within the PFC form inhibitory microcircuits and control the temporal dynamics of pyramidal neuron spiking. They participate in generating cortical rhythmic activity and network synchrony and gate long-range input that contribute to the processing of PFC-dependent cognitive and emotional behavior (Rudy, 2013; S. S. Yang et al., 2021). The interneurons that coordinate these functions can be classified into subpopulations with distinct morphological, molecular and functional characteristics (Lim et al., 2018; Rudy, 2013). Interneurons expressing calcium-binding proteins calretinin (CR), calbindin (CB) and parvalbumin (PV) make up 80% of the GABAergic interneuron population in the rodent frontal cortex (Gabbott et al., 1997). CR expressing interneurons in rat agranular frontal cortex (see section 1.2) frequently colocalize with vasoactive intestinal peptide. In layer II/III, bipolar CR cells of bursting firing type and multipolar CR cells with adaptive firing pattern have been found to preferentially innervate other classes of interneurons, including their own type (Caputi et al., 2009; Kubota et al., 1994). CB expressing interneurons are regularly co-detected with other molecular markers such as somatostatin, neuropeptide Y, parvalbumin and sometimes nitric oxide synthase. They are the most heterogenous group of cortical interneurons, possessing a wide range of morphological and electrophysiological characteristics. Their postsynaptic target location also varies, depending on the specific subclass (Gabbott et al., 1997; Kubota et al., 1994; Lim et al., 2018). PV expressing interneurons are the largest group of GABAergic interneurons in the rodent PFC, functionally recognized by their distinctive fast-spiking characteristic. PV interneurons are categorized into PV basket cells, which form synapses at the soma and proximal dendrite of pyramidal neurons, and PV chandelier cells that form synapses onto the axon initial segment (AIS) of pyramidal neurons (Gabbott et al., 1997; Lim et al., 2018; Rudy, 2013). The participation of PV interneurons is essential for the performance of working memory and social interaction (Murray et al., 2015; S. S. Yang et al., 2021). PV neurons are involved in generating gamma-frequency oscillations (30-100 Hz), which have been shown to augment cortical signal processing, facilitating higher cognitive functions (Sohal et al., 2009; Uhlhaas & Singer, 2011). In schizophrenia, patients often exhibit disrupted gamma oscillatory activity during execution of cognitive tasks. This could be associated with deficits in PV activity since reduced PV expression has been detected in brain samples of schizophrenic patients. Downregulation of PV at both protein and transcript levels is also seen in individuals with autism, suggesting a potentially crucial role of PV in the pathophysiology of neurodevelopmental disorders (Filice et al., 2016; Le Magueresse & Monyer, 2013).

1.2 PFC terminologies across species

Before discussing further on the structure and development of the PFC, the definitions of the terms PFC and medial PFC (mPFC) need to be clarified, especially when evaluating rodent

studies. Due to disagreement regarding the subdivisions of prefrontal cortical areas in different species, there is still no clear definition on which frontal cortex regions comprise the PFC. Functionally, the human PFC is subdivided into dorsolateral, dorsomedial, ventrolateral, ventromedial, and orbital prefrontal cortex. These areas mostly show a six-layered laminar organization with a distinct granular layer IV. However, some parts of the primate PFC consist of dysgranular cortex with an indistinct layer IV or agranular cortex in which layer IV is completely absent, such as the anterior cingulate cortex. In contrast, all frontal cortical areas are agranular in rodents and lack the subdivision into granular and dysgranular cortices (Carlén, 2017; Laubach et al., 2018). Although the equivalent of a primate dorsolateral cortex, which is involved in processes such as attention and working memory, is absent in rodents, functional data suggest that the prelimbic (PrL), infralimbic (IL), and anterior cingulate (CgI) cortices of rodent have functions that can be attributed to the dorsolateral PFC and anterior cingulate cortices in primates (Uylings et al., 2003; Seamans et al., 2008). The prelimbic, infralimbic and cingulate cortices are thus classified as prefrontal regions in rodents. These cortices are located in the medial frontal area in rodents, similar to the anterior cingulate cortex occupying the medial frontal cortex in primates and are therefore labeled mPFC in most rodent studies (Laubach et al., 2018). In this thesis, the term mPFC is used to describe the anatomical region of the rodent PFC consisting of prelimbic, infralimbic, and anterior cingulate cortices. The cingulate cortex that extends from the genu of corpus callosum caudally, the anatomical region immediately posterior to the mPFC, is referred to as caudal cingulate cortex (CgII). As for studies in which prefrontal subdivisions are not specified in terms of the aforementioned definitions, the terminologies from the original publications are used.

1.3 Structural organization of PFC

The series of events that leads to the laminar organization of the cerebral cortex begins during embryonic development and involves similar progressing steps in humans, non-human primates, and rodents (Chini & Hanganu-Opatz, 2021; Kolk & Rakic, 2022). The cerebral cortex arises from the dorsal part of the telencephalon. The neuroepithelial cells give rise to the radial glial cells from which the cortical projection neurons are generated in the ventricular zone (VZ) in a temporally regulated manner. The earliest born cortical neurons arrange above the VZ to form the preplate (PP). The next generation of neurons that migrate into the PP starts to form the cortical plate, splitting the PP into subplate (SP) and marginal zone (MZ). As cortical development proceeds, successive batches of neurons migrate radially from the VZ towards the pial surface via the support of radial glial processes, through preformed layers of earlier-born neurons. Thus, early-born projection neurons form the deeper cortical layers, while later-born neurons form the upper cortical layers, resulting in the inside-out formation of

the cerebral cortex. In mice, deep layer neurons are born between embryonic day (E)12.5 and E13.5 and upper layer neurons are born between E14.5 and E17.5. The MZ eventually forms the layer I of the cerebral cortex while the neurons of the cortical plate (CP) and subplate form the remaining cortical layers. GABAergic cortical interneurons are not derived from the VZ but originate in the ganglionic eminences and preoptic area of the ventral telencephalon. From there, they migrate tangentially to the cortex in separate streams, followed by radial migration to reach their designated laminar location (Agirman et al., 2017; Kolk & Rakic, 2022; Lim et al., 2018). Interneurons from the medial ganglionic eminence (MGE) start to emerge around E9.5 with peak differentiation at E13.5 and distribute themselves into pre-designated locations within the cortical plate, occupying primarily deeper layers. Interneurons derived from caudal ganglionic eminence are born later, around E12.5, and tend to populate the superficial layers (Miyoshi & Fishell, 2011). The overall development and precise organization of the cerebral cortex is strongly dependent upon an interconnecting network of diverse transcription factors, gradients of morphogen signaling and electrical activity (Agirman et al., 2017; Chini & Hanganu-Opatz, 2021; Kolk & Rakic, 2022).

While there may not be much difference in the timing of early events such as laminar organization in the PFC from other cortical areas, the PFC is the last cortical region to reach maturity in terms of local microcircuits and afferent inputs (Caballero et al., 2016b).

1.4 Protracted maturation of PFC

In comparison to sensory and motor cortices, the PFC undergoes protracted functional and anatomical maturation process during postnatal development that continues through adolescence until early adulthood in mammals. Local microcircuits, consisting of different classes of inhibitory interneurons and excitatory projection neurons, along with afferent inputs, mature during this time **(Fig. 1)**. These developmental changes lead to calibrations of the excitatory-inhibitory balance in the neural networks of the PFC to acquire matured cognitive functions. Alteration in the developmental trajectory of inputs and the local microcircuits could contribute to susceptibility to psychiatric disorders such as schizophrenia, which usually first emerge during adolescence and present deficits in the domain of PFC-mediated executive functions (Caballero & Tseng, 2016a; Chini & Hanganu-Opatz, 2021; Schubert et al., 2015).

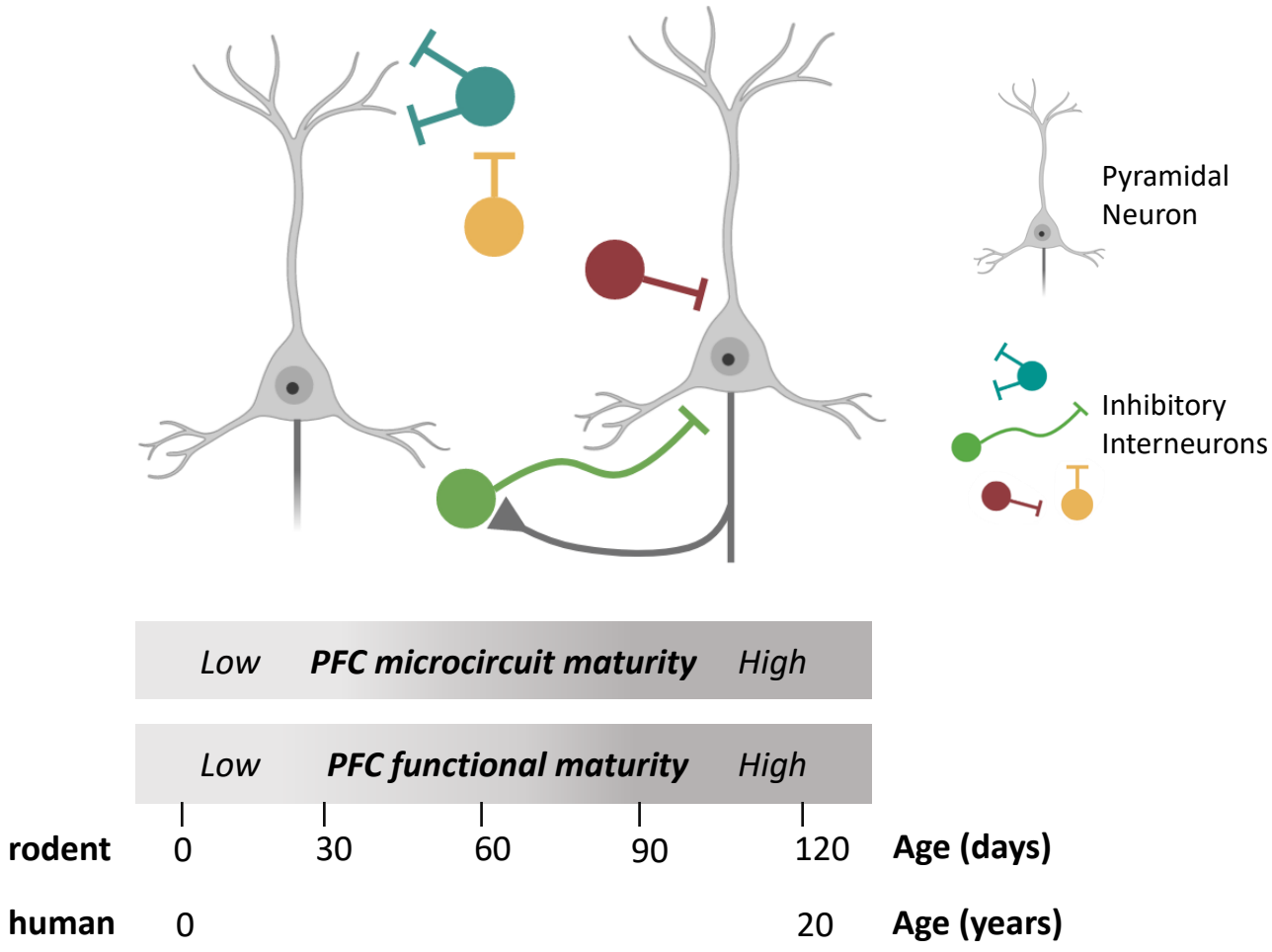

Figure 1. Protracted maturation of PFC and its local microcircuits. The PFC undergoes extensive functional remodeling during adolescence that continues into adulthood. The postnatal development of local microcircuits parallels the functional maturation of the PFC. The schematic shows the local microcircuits, consisting of excitatory pyramidal neurons and different classes of GABAergic interneurons providing strong inhibitory input on pyramidal cells. Created with BioRender.com.

1.4.1 Maturation of GABAergic inhibitory circuitry

The GABAergic system is a major player in prolonged PFC circuit maturation as it begins to go through significant functional changes at the onset of adolescence (Caballero & Tseng, 2016a). Appropriate expression of GAD65/67, the GABA synthesizing enzymes, reflects the capability of prefrontal interneurons to synthesize and release GABA. Although GABA is the major inhibitory neurotransmitter in adult PFC, $GABA_A$ receptor activation during embryonic and early postnatal stages is depolarizing. This promotes proliferation and migration of projection neurons and supports synapse maturation and circuit refinement (Le Magueresse & Monyer, 2013). $GABA_A$ receptor signaling at the dendrites of PFC pyramidal neurons switches from being depolarizing to hyperpolarizing over the first postnatal week, while the shift to hyperpolarization at the AIS occurs over a periadolescent period. Unlike dendritic

$GABA_A$ receptor signaling, GABAergic maturation at AIS is thus developmentally delayed into adolescence (Rinetti-Vargas et al., 2017).

Among the GABAergic interneurons, the most prominent phenotypic shift is observed in those expressing calcium-binding proteins PV and CR. Between adolescence and young adulthood, CR expression decreases while PV expression rises in both humans and rodents. There is also a modest increase in CB protein level in rodents between adolescence and young adulthood **(Fig. 2)**. Alongside increased PV level, a small increase in PV neuron population is also detected in rodent mPFC (Caballero et al., 2014; Caballero & Tseng, 2016a; Du et al., 2018). PV-expressing fast-spiking interneurons experience doubling of incoming excitatory post-synaptic currents frequency during this critical period, accompanied by a surge in inhibitory post-synaptic potentials onto the pyramidal neurons of layers V-VI. The strengthening of inhibitory transmission throughout adolescence, mediated largely by PV interneurons, facilitates regulation of pyramidal neuron activity, and refines the dynamics of neural network of PFC (Caballero & Tseng, 2016a; Ferguson & Gao, 2018; Larsen & Luna, 2018). Downregulation of PV expression in the PFC during postnatal day (P)34-(P)38

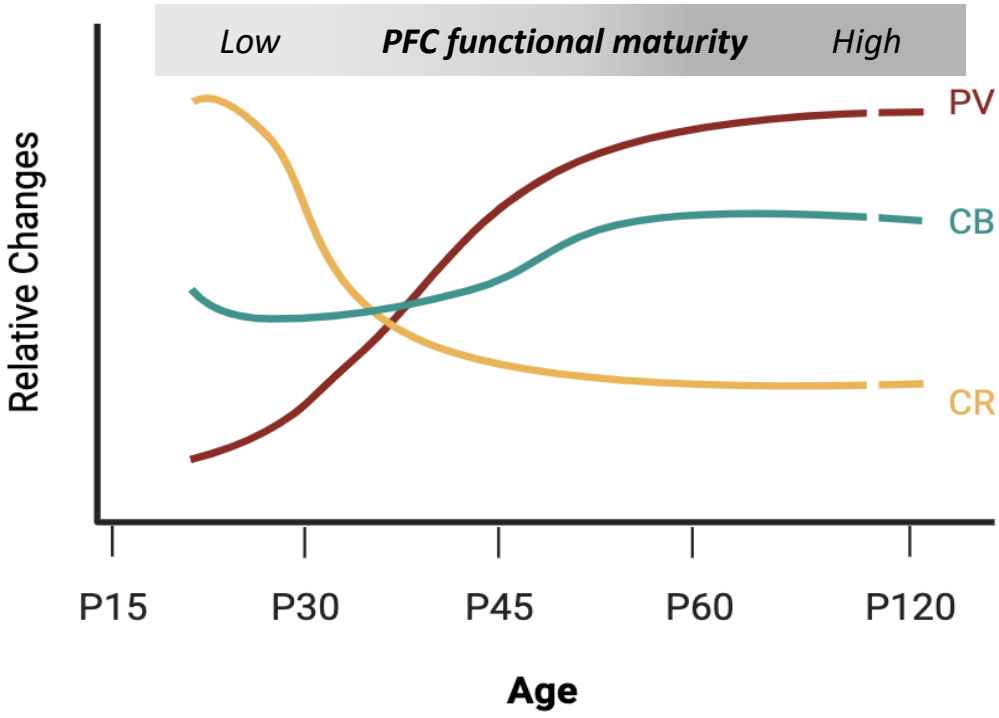

Figure 2. Developmental trajectory of expression of calcium-binding proteins in interneurons in rodent PFC. PV and CR protein expression levels show opposite developmental patterns during the transition from adolescence to adulthood, while CB protein expression increases slightly during the periadolescent period. Adapted from Caballero & Tseng, 2016a. Created with BioRender.com.

reduces the frequency of inhibitory presynaptic input onto layer V pyramidal neurons, resulting in long-lasting alteration in E/I balance (Caballero et al., 2020). Inhibition of PV interneurons

of the mPFC between P14-P50 generates a similar lasting deficit in the strength of local GABAergic transmission onto pyramidal neurons, paralleled by disruption of PFC network function and cognitive flexibility. In adulthood however, inhibition of PV neuron activity did not bring about similar alterations in network function and behavior (Canetta et al., 2022). Together, these findings support the aspect of a sensitive time window during which PV upregulation and activity are required for PFC circuit maturation to acquire adult-like executive functions.

1.4.2 Long-range input into the developing PFC

The PFC receives diverse inputs from cortical and subcortical structures that contribute to sustaining a multitude of PFC functions. The PFC receives cholinergic inputs from basal forebrain and glutamatergic afferents from hippocampus, mediodorsal thalamus, amygdala, and the ventral midbrain. Additionally, the PFC is innervated by monoaminergic neuromodulatory systems: serotonergic projections from dorsal raphe (DR) nuclei secreting serotonin (5-HT), noradrenergic projections from locus coeruleus (LC) producing noradrenaline (NA), and dopaminergic projections from the ventral tegmental area (VTA) releasing dopamine (DA). The development of dopaminergic projections in the PFC is of particular significance to the current study due to its association with the maturation of DA-modulated, PFC-dependent cognitive functions across adolescence. Since DA is intricately linked to the other monoamine neurotransmitters in the PFC, coordinately regulating PFC-dependent behaviors (Caballero et al., 2021; Chandler et al., 2014; Kolk & Rakic, 2022), the next section summarizes the contribution of the monoamine systems within the developing PFC and highlights their influence on each other.

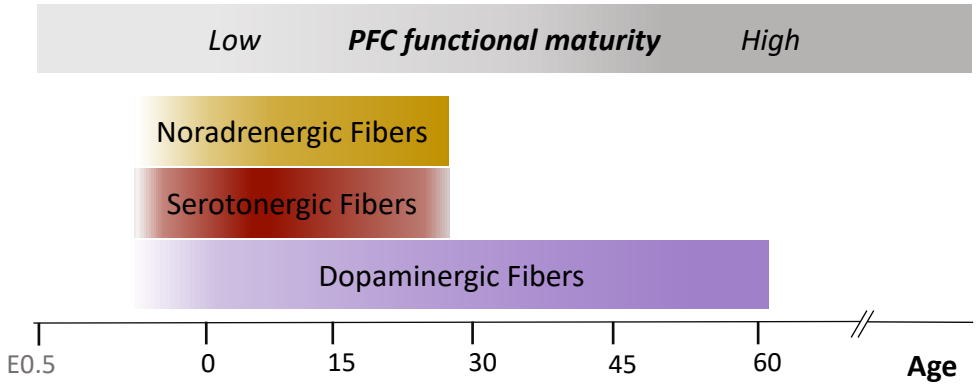

Figure 3. Timeline of monoaminergic innervation of PFC. The monoaminergic projections arrive in the PFC around E16-E18. By P28, the density and pattern of noradrenergic and serotonergic fibers in the PFC are similar to those in adult PFC, while dopaminergic fiber density continues to increase until adulthood, occurring in parallel with functional maturation of PFC. Based on Kalsbeek et al., 1988; Kolk & Rakic, 2022; Levitt & Moore, 1979; Maddaloni et al., 2017; Naneix et al., 2012.

1.4.2.1 Serotonergic innervation

Serotonergic projections from the medial part of the DR nuclei reach the PFC around E16/E17 in rodents and between 10-13 postnatal weeks in humans (Kolk and Rakic, 2021). Serotonergic fiber density in the PFC has been found to peak at P6 and stabilize by P28 **(Fig. 3)** (Maddaloni et al., 2017). The fibers first arrive in two bundles, in the SP and the MZ, establish contact with the Reelin-secreting Cajal Retzius cells of the MZ, and therefore possibly play an influential role on neuronal migration. Serotonergic transporter (5-HTT) knockout in mice results in a decrease in Reelin expressing cells and altered expression of layer markers in PFC during development, leading to modified prefrontal cytoarchitecture. 5-HTT knockout in mice is also found to alter the developing dopaminergic projections, increasing the number of dopaminergic axons in certain subdomains of PFC. The serotonergic system thus begins participating early on in modulating neurodevelopmental processes of proliferation, migration, and differentiation within the PFC (Garcia et al., 2019; Kolk & Rakic, 2022).

1.4.2.2 Noradrenergic innervation

NA release in the PFC is involved in functions such as selective attention, arousal, vigilance, salience of reward, and stress response (Chandler et al., 2014). Noradrenergic projections from the LC innervate the SP and MZ of the rodent frontal cortex around E17 and between 10-13 postnatal week in humans (Kolk & Rakic, 2022; Levitt & Moore, 1979). In rodents, the noradrenergic fibers have been found to develop swiftly, with the fiber pattern being comparable to that observed in adults by P6 **(Fig. 3)**. By the beginning of the fourth postnatal week, noradrenergic fiber density and morphology are similar to that in adult and remain steady further into adulthood (Levitt & Moore, 1979; Naneix et al., 2012). Noradrenergic innervation, like the serotonergic system, is also involved in neuronal migration and differentiation along with synaptogenesis, playing a role in PFC's development (Kolk & Rakic, 2022). While the interaction between noradrenergic and dopaminergic systems in the developing PFC is still unclear, the two pathways are strongly linked in adult PFC. Examples include DA uptake from extracellular spaces by noradrenergic/norepinephrine transporter (NET) due to low levels of DA transporter (DAT) in the PFC, DA signaling via adrenergic receptors in PFC astrocytes that triggers calcium mobilization and the ability of noradrenergic fibers to co-release DA along with NA in the PFC (Devoto et al., 2005, 2019; Morón et al., 2002; Pittolo et al., 2022).

1.4.2.3 Dopaminergic innervation

The dopaminergic input to the PFC is vital in modulating the performance of higher cognitive functions such as working memory, planning, decision making and behavioral flexibility. Mesoprefrontal projections arise, at least partially, from the midbrain dopaminergic (mDA) neurons that express the vesicular glutamate transporter 2 (vGLUT2) (see section 1.9) and have been shown to co-transmit glutamate (Pérez-López et al., 2018; Poulin et al., 2018). Similar to other monoaminergic projections, the dopaminergic innervation of the PFC begins during the embryonic phase **(Fig. 3)**. The fibers are sparse at prenatal stages and innervation density increases slowly during the postnatal phase to eventually stabilize in adulthood (Islam et al., 2021). This is in contrast to the serotonergic and noradrenergic innervations of the PFC, which reach adult density levels rapidly within the first few postnatal weeks (Levitt & Moore, 1979; Maddaloni et al., 2017; Naneix et al., 2012).

Experimental findings from the last couple of decades implicate the mesoprefrontal system in facilitating the formation of local microcircuit activity in the adolescent PFC. Recordings from PFC slices have shown that DA modulation of NMDA receptor transmission prompt recurrent depolarizing plateaus in pyramidal neurons, an effect that is observed from P45 onwards (Tseng & O'Donnell, 2005). PFC slice recordings have also shown DA receptors (DRDs)-mediated increase in excitability of interneurons. At juvenile stage, the excitatory effect is mediated by DRD1 but after P50, DA-dependent boost in excitability of fast-spiking interneurons is exerted not only via DRD1 but also through DRD2 (Tseng & O'Donnell, 2007). Collectively, these changes refine the circuitry responsible for excitation-inhibition balance and correlate with the maturation of executive functions (O'Donnell, 2010). Given that the maturation of the PFC microcircuits and development of dopaminergic innervation occur in parallel, input from mesoprefrontal fibers could play an important role in the maturation of PFC microcircuits. Indeed, altering DA input during early adolescence leads to neuroanatomical and functional changes in layer V pyramidal neurons of PFC in adulthood (Manitt et al., 2013). Moreover, there is evidence that DA neurotransmission in the striatum during a critical development period prompts maturation of spiny medium neuron of the direct pathway (Lieberman et al., 2018). To discern if a similar role is played by DA in the functional remodeling process of PFC, it is essential to understand how the dopaminergic innervation is established in the PFC. The next sections will describe the mDA system and its ontogeny, with a focus on the development of the mesoprefrontal system in rodents.

1.5 mDA neuronal groups and their targets

mDA neurons are located in the ventral midbrain where they form the A8, A9, and A10 group. The A8 neurons are located in the retrorubral field (RRF), the A9 neurons in the substantia nigra par compacta (SNpc) and substantia nigra pars lateralis (SNpr), while the A10 neurons form the ventral tegmental area (VTA) and linear nucleus (LiN). mDA neuronal projections run through the medial forebrain bundle (MFB) and then diverge into the various forebrain target areas. In rodents, SNpc mDA neurons project primarily to the striatum, forming the mesostriatal pathway, and are involved in regulating voluntary movement. The degeneration of SNpc neurons result in the motor symptoms of Parkinson's disease (Bentivoglio M & Morelli M, 2005; Björklund & Dunnett, 2007). mDA neurons of the RRF send out projections to the shell of nucleus accumbens (NAc) and are also involved in the mestostriatal pathway (Lammel et al., 2008). VTA mDA neurons project to various limbic and cortical regions: ventral striatum (olfactory tubercle, core and shell of NAc), basolateral amygdala and PFC (Björklund and Dunnett 2007a). VTA mDA neurons contributes to reward learning, motivation, aversion, salience signaling, working memory, decision making, and goal-directed behavior (Beier et al. 2015; Lammel et al., 2012; Morales and Margolis 2017). Their other targets include lateral septum, lateral habenula and hippocampus (Antonopoulos et al., 1997; Gasbarri et al., 1994; Stamatakis & Stuber, 2012; Tsetsenis et al., 2023)

1.6 Development of mDA neurons

The mDA neurons develop through a series of complex developmental steps, each defined by expression of a distinct set of transcription factors and signaling molecules**.** The mDA neurons emerge from progenitors in the floor plate along the ventral midline of the embryonic midbrain. Crossregulation between transcription factors such as orthodenticle homolog 2 (OTX2), engrailed 1/2 (EN1/2), forkhead box A1/2 (FOXA1/2) and the secreted factors sonic hedgehog (SHH), fibroblast growth factor 8 (FGF8) and wingless-related MMTV integration site 1 (WNT1) are essential for the induction of the ventral midbrain primordium. Early in neurodevelopment, anteroposterior patterning divides the neural tube into forebrain, midbrain, hindbrain and spinal cord while dorsoventral patterning subdivides it into floor plate, basal plate, alar plate, and roof plate. Starting at E7.5, OTX2 in the midbrain and gastrulation brain homeobox 2 (GBX2) in the hindbrain repress each other to determine the appropriate midbrain-hindbrain boundary called the isthmus. WNT1 is expressed at the isthmus and is needed for establishment of posterior midbrain and anterior hindbrain. These regions are also distinguished by expression of EN1 and EN2 and paired box transcription factors PAX2 and PAX5 (Arenas et al., 2015; Blaess & Ang, 2015; Veenvliet & Smidt, 2014). The isthmus

produces FGF8, which regulates patterning along the anteroposterior axis. The ventral neural tube is induced and patterned by the morphogen SHH. Initially, around E7.5/E8 in mice, SHH is secreted from the notochord, a mesodermal cord-like structure underlying the ventral neural tube. Cells in the midline of the developing neural tube respond to SHH signaling. This is evident from GLI1 expression, a transcription factor expressed in cells in response to high levels of SHH signaling and therefore acting as a readout of the activated SHH signaling pathway. SHH is crucial for the induction of the mDA progenitor domain and its subsequent maintenance in early development. Inactivation of SHH signaling in *Shh*-null mutant mice results in complete loss of mDA neurons, while conditional knockout of smoothened (SMO), a SHH receptor, around E9, inactivates SHH signaling and leads to severe depletion of mDA neurons (Blaess et al., 2006). SHH signaling induces expression of the transcription factors FOXA1/2 in the floor plate of the ventral midbrain. The *Foxa2*-positive floor plate cells then stop responding to SHH and by E8.5 start to secrete SHH themselves and induce floor plate fate in neighboring cells. The isthmus and the floor plate act as organizing centers in the development of midbrain and the intersection of the morphogen gradients along the anteroposterior and dorsoventral axes determines the region for establishment of mDA progenitor domain (Arenas et al., 2015; Blaess et al., 2011; Blaess & Ang, 2015; Smidt & Burbach, 2007). SHH, together with WNT, also induces expression of LIM homeobox transcription factor 1 alpha and beta (LMX1A/B). The medial area of the floor plate domain is found to express LMX1A at E9. This domain eventually gives rise to mDA neurons. Neurogenesis of mDA neurons commences around E10.5, regulated by the proneural genes Neurogenin 2 (NEUROG2) and mouse achaete-schute homolog 1 (MASH1/ ASCL1) (Arenas et al., 2015; Andersson et al., 2006). Basic helix-loop-helix transcription factors such as FERD3L and homeodomain transcription factors like MSX1 are also significantly involved in specification of mDA progenitor domain (Blaess & Ang, 2015). In mouse, cell cycle exit of mDA neurons starts at around E10.5 and continues until about E14.5. At E10.5, postmitotic mDA neurons begin to express the transcription factor nuclear receptor subfamily 4A2 (NR4A2)/nuclear receptor related 1 protein (NURR1). NURR1 regulates expression of proteins critical for the acquisition of mDA neuronal phenotype, including tyrosine hydroxylase (TH), the rate limiting enzyme in DA synthesis, DA transporter (DAT), and vesicular monoamine transporter-2 (VMAT2). The next step in the differentiation of mDA is marked by the expression of the transcription factor pituitary homeobox 3 (PITX3) and TH (Arenas et al., 2015; Blaess & Ang, 2015). TH expression is first detected in mice between E10 and 10.5 (Dumas & Wallén-Mackenzie, 2019). As the mDA neurons differentiate, they migrate from the VZ towards the mantle layer and form the three distinct mDA neuronal groups: A8, A9, and A10. Birthdating of ventral midbrain cells and/or TH immunostaining to trace the migration route have suggested that mDA neurons migrate radially from the VZ towards the pial surface

to form the VTA, while those forming the SNpc initially migrate radially and then tangentially from the midline. The extracellular matrix molecule Reelin and its receptors apolipoprotein E receptor 2 (APOER2) and very low density lipoprotein receptor (VLDLR), chemokine (C-X-C motif) ligand 12 (CXCL12) and its receptor chemokine (C-X-C motif) receptor 4 (CXCR4), L1 cell adhesion molecule (L1CAM) and L1CAM ligand protein tyrosine phosphatase, receptor type Z, polypeptide 1 (PTPRZ1) are some of the molecules and signaling pathways involved in regulating radial and tangential migration of the differentiating mDA neurons (Blaess & Ang, 2015; Bodea & Blaess, 2015).

While all mDA progenitors undergo dopaminergic fate specification, proliferation, differentiation and migration to form the mature neurons of the A8, A9, and A10 clusters, the molecular profiles of these mDA subpopulations are different from each other. For instance, SNpc and dorsolateral VTA subgroups are commonly identified by expression of G-protein-regulated inward-rectifier potassium channel 2 (GIRK2) and glycosylated active form of the dopamine transporter (glyco-DAT), while mDA neurons of VTA and dorsal tier of SNpc are characterized by their abundance of Calbindin 1 (CALB1) (Brignani & Pasterkamp, 2017). Panman and colleagues have shown that mDA neurons of SNpc are distinguishable by their selective expression of *Sox6*, while the markers OTX2 and NOLZ1 are expressed in a subset of mDA neurons within the VTA (Panman et al., 2014). By utilizing single-cell RNA sequencing strategy in recent past, various research groups have shown that mDA neurons of SNpc and VTA can be further categorized into distinctive subpopulations on the basis of their molecular profile (Brignani & Pasterkamp, 2017; Kamath et al., 2022; Poulin et al., 2020). Poulin and colleagues, for example, used this genetic tool to identify six subtypes of mDA neurons while Le Manno and colleagues, using the same technique, described five distinct subgroups of mDA neurons (La Manno et al., 2016; Poulin et al., 2014). Current evidence indicates that molecular heterogeneity among the subtypes of mDA neurons begins at progenitor stage. The question remains when and how during development the fate of these mDA neuron subsets is specified.

1.7 *Shh*-expressing progenitors contribute to different mDA neuron subpopulations over time

mDA neuron diversity could be partially predetermined in mDA progenitors. Subsets of mDA progenitors can be classified based on their gene expression profile and their disposition to SHH signaling. The expression of *Shh* in the midbrain floor plate is dynamic (Blaess et al., 2011; Hayes et al., 2011). As mentioned above, initially, between E7.5-E8, *Shh* is expressed only in the notochord but between E8-E8.5, the floor plate cells switch on *Shh* expression. As

SHH prompts floor plate fate in neighboring cells, the *Shh*-expressing domain continues to expand laterally from the ventral midline and *Gli1* expression continues to shift adjacent to the *Shh*-expressing domain until E10.5 (Blaess et al., 2011; Hayes et al., 2013). Within the floor plate domain, the *Lmx1a*-expressing region that gives rise to mDA neurons can be further divided into a medial and lateral domain based on expression profiles of transcription factors. For example, it has been shown that OTX2 and NOLZ1/ZNF503 are confined to the progenitors of lateral domain, while *Sox6* is expressed in medial progenitors (Panman et al., 2014). The spatiotemporal expression pattern of *Shh* has been utilized by several genetic inducible fate mapping (GIFM) studies to suggest that the medial progenitor domain is biased to give rise to neurons of the SNpc and dorsolateral VTA while the lateral progenitor domain preferentially gives rise to the medial VTA (Blaess et al., 2011; Hayes et al., 2011). SHH signaling is essential for induction of all mDA progenitors but the lateral progenitor domain requires it longer than the medial domain. GIFM studies demonstrate that progenitors of the ventral midline that responds to SHH before E9.5 preferentially generate mDA neurons of the SNpc. Medial VTA mDA neurons, on the other hand, are found to be derived from the lateral progenitor domain that continues to express *Gli1* in response to SHH after E9.5 (Blaess et al., 2006, 2011; Hayes et al., 2011). The GIFM studies therefore support that the duration for which a particular mDA progenitor domain is responsive to SHH signaling could influence its developmental potential into SNpc-mDA or VTA-mDA neuron.

1.7.1 SHH signaling pathway

SHH signal transduction is mediated by two cell surface receptors: patched (PTCH), a 12-transmembrane protein and SMO, a 7-transmembrane protein similar to the G-protein coupled receptor (GPCR). The primary cilium acts as the cellular location for many of the signaling components of the pathway. In absence of the glycoprotein SHH, PTCH, located at the base of PC, interacts with SMO and inhibits its activity. SHH binding to the PTCH receptor alters this interaction and terminates PTCH inhibition of SMO. SMO is translocated to the primary cilium and gets activated, initiating intracellular downstream signaling that regulates GLI family of zinc finger transcription factors. In mammals, there are three GLI transcription factors: GLI1, GLI2 and GLI3. GLI1 act as transcriptional activator while GLI2 and GLI3 act as positive or negative regulators of the pathway, respectively, after being processed as an activator or a repressor. In response to SHH signaling, the transcriptional activator form of GLI2 accumulates in the primary cilium, suppressing the negative regulation by GLI3 repressor. GLI2 is the main downstream activator of the SHH pathway and activates transcription of target genes involved in SHH signaling feedback, such as *Gli1* and *Ptch* (Carballo et al., 2018; Wu et al., 2017).

1.8 Distinct mDA progenitor domains give rise to discrete mDA neuron subsets – origins of mesoprefrontal neurons

SHH signaling between E8 and E10.5 is essential for generation of mDA neurons. Conditional inactivation studies of SHH signaling pathway show that SHH is required for induction and proliferation of progenitors and GIFM studies demonstrate the role of dynamic *Shh* expression in establishing mDA diversity at the progenitor stage. Conditional inactivation studies of pathway have also called attention to the roles of GLI2 activator and GLI3 repressor in the development of mDA progenitor domains (Blaess et al., 2006, 2011; Hayes et al., 2013). Conditional inactivation in the midbrain of transcription factor GLI2 around E9 inactivates SHH signaling activity in the ventral midbrain (*Gli2* conditional knockout mice). Since the medial progenitor domain by this time point ceases to require SHH for its induction, the domain is formed, although its size is reduced. The lateral mDA progenitor domain however is almost entirely missing. In the brain of adult *Gli2* conditional knockout mice (*Gli2* cKO), this results in a severe reduction of the number of mDA neurons in the medial VTA, accompanied by absence of mesoprefrontal projections, whereas the mDA projections to the caudoputamen complex, NAc, amygdala are not significantly reduced (see section 1.16) (Kabanova et al., 2015). An inverse effect is observed when the gene encoding cell adhesion molecule-related/downregulated by oncogenes (CDON), a PTCH co-receptor modulating SHH pathway activity, is inactivated. CDON is expressed in mDA progenitors and its inactivation leads to increased number of proliferating mDA progenitors as well as VTA-mDA neurons, while the number of SNpc neurons remains unaltered. Along with an increased number of VTA-mDA neurons, there is concomitant increase in DA and DA metabolites and higher number of DA presynaptic sites in the mPFC, an effect selective to this region and not observed in other target areas of VTA (Verwey et al., 2016). These data suggest that the spatiotemporal dynamics of SHH signaling generates distinct mDA progenitor domains and SHH signaling is required after E8.5 in the developing mouse brain to induce the lateral mDA progenitor domain that contains the progenitors fated to emerge as mesoprefrontal mDA neurons.

1.9 Mesoprefrontal mDA neurons in the adult brain

In the adult rodent brain, mesoprefrontal mDA neurons are located in the LiN and in the medial and ventral regions of VTA (Lammel et al., 2011; Yamaguchi et al., 2011). Although it is not known if mesoprefrontal mDA neurons can be characterized by a particular gene expression profile (Poulin et al., 2020), they have been segregated from other mDA neurons on the basis of their molecular profile such as low levels of *Dat* expression, and in terms of electrophysiological properties (Lammel et al., 2008). Mesoprefrontal mDA neurons, unlike

other mDA neurons, are also known to lack functionally active somatodendritic DRD2-autoreceptors (Lammel et al., 2008). A considerable number of mesoprefrontal mDA neurons have been reported to express *Slc17a6*, the gene encoding vGLUT2, indicating their ability to co-release the neurotransmitter glutamate. This is consistent with data showing that at least a subset of mesoprefrontal mDA neurons co-release glutamate in the PFC (Kabanova et al., 2015; Pérez-López et al., 2018). However, *Slc17a6* expression is not an exclusive marker of mesoprefrontal neurons, as its presence has also been detected in dorsolateral SNpc and NAc projecting VTA-mDA neurons (Yamaguchi et al., 2011; Poulin et al., 2018). Furthermore, *Slc17a6* is broadly expressed in mDA neurons during development and only gets restricted to the aforementioned mDA subpopulations postnatally (Steinkellner et al., 2018; Dumas and Wallén-Mackenzie, 2019; Kouwenhoven et al., 2020). Studies investigating electrophysiological properties of mesoprefrontal neurons in rats and mice have reported discrepant results. In rats, whole-cell patch-clamp recordings of mDA neurons that were retrogradely labeled by DiI injection from the mPFC or the NAc have shown that hyperpolarization-activated cation current (I_h) is larger in mesoprefrontal neurons compared to the NAc projecting neurons (Margolis et al., 2005). Results from a study in mice, however, indicated that retrogradely traced mesoprefrontal mDA neurons lack functional I_h currents (Lammel et al., 2008). Studies employing optogenetic techniques have revealed contributions of mesoprefrontal mDA neurons in neural circuits underlying motivated behaviors. Lammel and colleagues have shown that projections from lateral habenula preferentially terminate on a subpopulation of mDA neurons projecting to the mPFC and optogenetic stimulation of this pathway elicits aversive behavior (Lammel et al., 2012). In another study, optogenetic excitation of mesoprefrontal projections was shown to cause conditioned place aversion and anxiety-like effect in mice in a social behavior test (Gunaydin et al., 2014). Yet, the role of mesoprefrontal mDA neurons encoding aversion remains unclear since there have been contradicting reports. Ellwood and colleagues, for instance, have shown that neither phasic nor tonic activation of mesoprefrontal projections elicited conditioned place preference or aversion. Tonic stimulation and phasic burst protocols rather mediated other behavioral functions such as maintenance or deviation from already learnt behavioral rules (Ellwood et al., 2017).

1.10 Early development of mesoprefrontal projections

Classic rodent studies following the development of mDA projections and their innervation targets have utilized DA or TH antibody labeling as primary markers of DA neurons and axons. As discussed earlier, TH is the rate-limiting enzyme in DA synthesis and thus a marker for mDA neurons. Since DA is the substrate of the enzyme dopamine beta hydroxylase (DBH) in

the synthesis of NA, TH and DA are also present in NA neurons. Thus, TH and DA are markers for both DA and NA neurons and their projections to the PFC. This could be a methodological limitation in tracing specifically mDA axon growth. In humans, this disadvantage is irrelevant since TH immunoreactivity is primarily localized to the projections emerging from mDA neurons (Gaspar et al., 1989; Verney et al., 1993). In rodents, it is possible to discriminate NA and DA fibers from each other by the characteristics of fiber pattern. NA fibers are identified by their thick axonal projections with regularly spaced varicosities while DA fibers have thin axons with irregularly spaced varicosities (Miner et al., 2003). Their distribution patterns within the rodent mPFC are also distinct. Except for the caudal cingulate cortex where TH-positive fibers concentrate in layers I-III, in adult rodent mPFC, there is a dense input of TH-positive fibers to the deeper layers compared to the much sparser TH-positive innervation in the superficial layers. NA fibers, in contrast, spread more uniformly across all layers (Levitt and Moore, 1979; Kalsbeek et al., 1988; Naneix et al., 2012). Furthermore, the density of TH-positive fibers in mPFC increases relatively rapidly from early adolescence to adulthood, whereas the density of DBH-expressing NA fibers remains constant across the same period. Nevertheless, since TH expression is not exclusive to mDA projections in mice, it needs to be considered that NA fibers may also be labeled to a certain extent when performing immunostaining for TH.

TH immunoreactivity reveals that mDA neurons in the ventral midbrain of rodents start to extend axonal processes between E11 and E12 in the embryonic rodent brain. In mice, axons initially grow slightly dorsally, but by E13, almost all axons follow a rostral trajectory and by E13.5 form a TH-positive axon tract within the MFB, advancing towards their forebrain targets (Kolk et al., 2009; Nakamura et al., 2000). At E14.5, the TH-positive fiber tract can already be detected within the region ventral to the ganglionic eminences (Kolk et al., 2009). Analysis of DA-positive fiber bundles in rats show that they also require a similar amount of time to reach this region (Kalsbeek et al., 1988; Voorn et al., 1988). In mice, while most of the TH-positive axons from the MFB begin to move dorsally to innervate the maturing striatum, a small number of fibers follow a rostrocaudal route to course towards the frontal cortex. At this point, the TH-positive fibers diverge into two paths to reach the mPFC. The thicker bundle of TH-positive axons bends just when it is posterior to the olfactory bulb (OB) and extends toward the cortical subplate. The smaller subset of TH axons crosses the striatum and developing external capsule to reach the developing mPFC. The TH fibers enter the mPFC in two streams within the SP and the MZ around E15. The fibers continue to grow in the SP for the next two days without entering the CP, which also expands and develops to receive the incoming fibers. In mice, the first TH-positive axons are detected in the CP at E18.5. Tracing experiments with the lipophilic fluorescent dye DiI show that when DiI is microinjected into the rostromedial VTA,

rather than the more caudal aspects of medial VTA, DiI-stained, TH- positive axons are found in the subplate at E16 and in the cortical plate at E18.5. However, no DiI-labeled fibers are found in the MZ after rostromedial injections. Conversely, after DiI microinjection into the developing mPFC at E16.5 and P0, the presence of the dye is eventually observed in the rostral VTA. Together, these data suggest that one subset of mesoprefrontal projections in mice originates in the rostral medial VTA, while the origin of TH axons in the MZ is from mDA neurons in another ventral midbrain region (Kolk et al., 2009). In rats, the TH-positive axons within the MFB also arrive in the mPFC in two bundles. At E18, one of the axonal bundles is observed above the subplate while the other axonal trail can be detected within the MZ. The DA fibers in the future mPFC adopt a coiled structure and start innervating the thickening cortical plate from E20 onwards (Garcia et al., 2019; Kalsbeek et al., 1988; Kolk et al., 2009). In rats, DA-positive fibers are detected in the developing layer VI of mPFC, orbital cortex, and caudal cingulate cortex soon after birth. Within 24 hours, there is a spurt in fiber density in layer VI. Between P2 and P4, the DA axons change their morphology from thick, straight fibers to thin fibers with irregularly shaped varicosities. While this marks the beginning of postnatal maturation of DA-positive fibers in the mPFC, their development, unlike other projections of the VTA-mDA neurons, is protracted. By the end of the first postnatal week, only a few DA-positive fibers in layer I are detectable in most subregions of the mPFC but the IL subdomain by this time shows an adult-like pattern of DA innervation, with DA-positive fibers reaching up to the pial surface. As the projections continue to increase in the deeper layers in the second postnatal week, the DA-positive fibers also extend into the upper cortical layers II and I in the PrL. At P20, the DA- positive fibers in layer I of the anterior cingulate cortex of mPFC fade away, but the projections in the caudal cingulate cortex are found in layers II and III. The morphological characteristics of DA-positive fibers in the mPFC, with thin axons and multiple varicosities, do not change significantly after P35, but the density of fibers continues to increase until adulthood **(Fig. 3)**, with the deeper layers becoming more densely innervated than the upper layers (Kalsbeek et al., 1988). The delayed maturation profile displayed by prefrontal TH-positive axons is not influenced by sex or pubertal onset in rodents. The developmental trajectory of TH fibers is similar in male and female rats, even though pubertal onset is approximately 10 days earlier in female than in male rats (Willing et al., 2017).

1.11 Development of mesoprefrontal pathway in adolescence

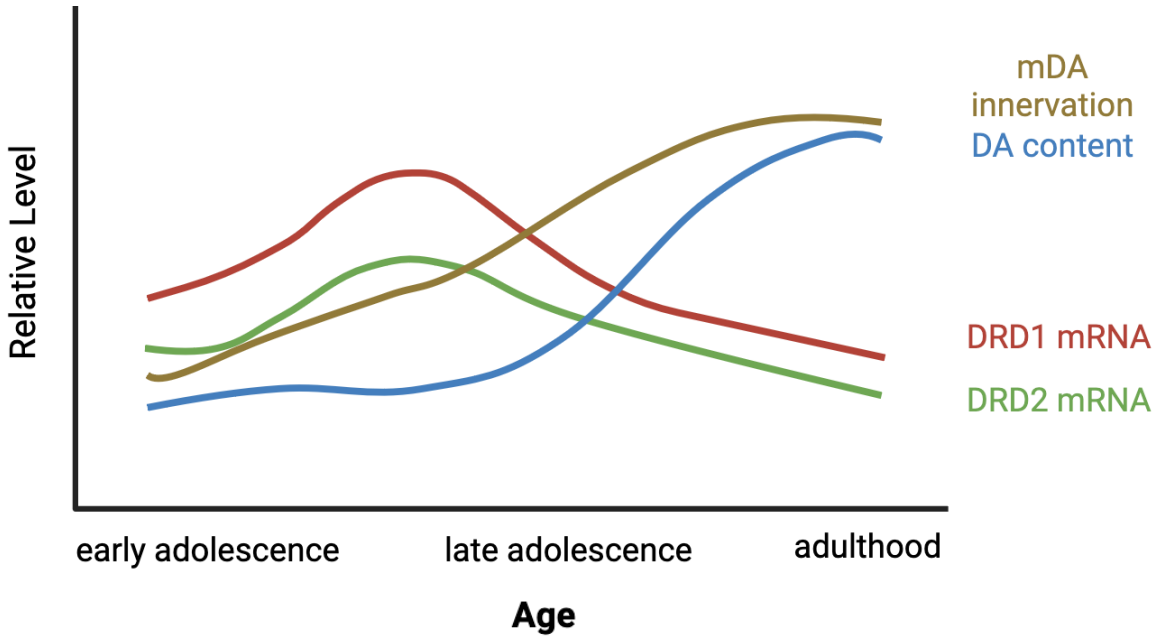

Figure 4. Development of the DA system in the rodent mPFC. Dopaminergic innervation (as shown in Figure 3) and DA content in the PFC increase throughout adolescence and stabilize in adulthood. The expression of *Drd1* and *Drd2* transcripts peaks during adolescence and is reported to decline with the transition into adulthood. Based on Islam et al., 2021. Created with BioRender.com.

Naneix and colleagues (Naneix et al., 2012) have shown that increase in TH-positive fibers in rat mPFC is relatively rapid during adolescence **(Fig. 4)**, whereas the density of DBH-expressing NA fibers in mPFC remains constant from early adolescence to adulthood. This suggest that the source of gain in TH-positive fiber density during adolescence is likely mesoprefrontal mDA neurons. In mice, the change in TH/DA fiber density in the mPFC during adolescence has not yet been studied in detail. To gain insight into potential mechanisms underlying protracted DA innervation of the mPFC, Reynolds and colleagues used an elegant virus-based approach to axon labeling. In this study, retrogradely transported canine adenovirus (CAV) expressing Cre recombinase was injected into the nucleus accumbens of mice at P21, which is considered juvenile/early adolescence in mice. Concurrently, a Cre-dependent virus expressing enhanced yellow fluorescent protein was injected into the VTA. CAV-Cre is preferentially taken up by axon terminals in the nucleus accumbens leading to axon-initiated, Cre-mediated recombination. As a result, only those VTA neurons whose axons have reached the nucleus accumbens around P21 were fluorescently labeled. The study, furthermore, showed that fluorescently labeled fibers are present in the CgL and PrL subdomains of mPFC in adult mice. These results indicate that the late maturation of DA fibers in the mPFC may be due to at least some of the fibers initially innervating the nucleus

accumbens and growing into the mPFC during later stages of adolescence (Reynolds et al., 2018).

1.12 Molecular mechanisms to guide mesoprefrontal axons

Directing the extending mDA axons to their proper targets requires precise coordination of extracellular axon guidance cues, receptor complexes, cell adhesion molecules, neurotrophic and growth factors (Hoops & Flores, 2017; Vosberg et al., 2020). Several guidance cue pathways involved in regulating the axonal pathfinding of mesoprefrontal mDA axons have been identified. For example, during early stages of mDA development, Semaphorin 3F acts via its receptor Neuropilin-2 to repel mDA axons away from the midbrain, while it changes its role into a chemoattractant to guide the DA axons towards the cortical plate of the mPFC at the prenatal stage (Kolk et al., 2009). The expression of axon guidance molecules SLIT1, SLIT2, SLIT3, which bind to roundabout (ROBO) receptors ROBO1 and ROBO2 are necessary for the initial rostral axon growth. The SLIT/ROBO signaling system repulses the early axons from mDA neurons, preventing ectopic development of projections and guiding them into the MFB bundle (Dugan et al., 2011; Gates et al., 2004; Hivert et al., 2002; Holmes et al., 1998; Van den Heuvel & Pasterkamp, 2008). The extracellular protein Netrin-1 and its receptors, uncoordinated 5 (UNC5) and deleted in colorectal cancer (DCC) play a critical role in mesoprefrontal/mesolimbic axon growth, target recognition, axon arborization, synapse formation and thus in establishing mDA neuronal circuitry. Binding of Netrin-1 to DCC receptors attracts growing axons while Netrin-1 and UNC5 binding mediate repulsion. DCC receptors levels are high in NAc targeting mesolimbic mDA axons while mesoprefrontal mDA axons express low levels of DCC. In turn, Netrin-1 expression is low in NAc in comparison to PFC. The DCC-rich mesolimbic projections identify NAc as their target and do not grow towards the PFC. Reduced DCC expression, as seen in in *Dcc* haplosufficient mice, results in increased ectopic mDA axon innervation and DA presynaptic sites in the mPFC. The fine-tuning of DCC-Netrin1 expression levels during adolescence is thus critical to help mDA axons find their final target (Hoops & Flores, 2017; Reynolds et al., 2018; Vosberg et al., 2020).

1.13 Dopamine release in the mPFC

Besides stabilization of fiber density, the formation of varicosities on mDA fibers, which act as potential DA release and uptake sites, is likely another important indicator of functional maturation of mDA fibers. DA immunoreactive varicosities have been found to form appositions with both pyramidal and nonpyramidal somata in the mPFC and the number of close appositions formed by GABA-positive cell bodies with DA varicosities show a steady postnatal increase from P5 to P60. This is especially noticeable in layer VI, where the density

of DA varicosities is higher and GABA-positive cell bodies are frequently found to be in close contact with DA varicosities. The number of varicosities closely interacting with each GABA-positive neuron exhibit a more rapid increase between early adolescence (P25) and adulthood (P60) (Benes et al., 1993; Benes et al., 1996).

Analysis of DA concentration and its metabolites, dihydroxyphenylacetic acid (DOPAC) and homovanillic acid (HVA), by high throughput liquid chromatography (HPLC) in rat mPFC tissue has shown that DA levels rise steadily between the juvenile (P25) and late adolescent (P45) stages with a sharp increase between the end of adolescence and adulthood **(Fig. 4)**. DA concentration is significantly higher in adults than in juveniles and adolescents. A decrease in DA turnover ratios was observed with increasing age, an effect that could contribute to the overall increase in DA availability in the mPFC (Naneix et al., 2012). Although half of all the appositions in layer VI in rat mPFC are non-synaptic in nature (Benes et al., 1996), the parallel increase in mDA fiber density and greater interaction between the mDA axons and the GABAergic cell bodies during adolescence coincide with increase in DA tissue content. Whether this increase in concentration correlates with active DA release has not been investigated in the developing PFC.

1.14 Changing distribution of dopamine receptors during postnatal development

In comparison to the striatum and the NAc that receive dense projections from mDA neurons and have high expression levels of DRDs, the expression levels of the DRDs in PFC are considerably lower. DA released from the axonal varicosities in the PFC signal by binding to DRDs of the D1-like or D2-like subfamily of seven-transmembrane GPCRs and modulates activity of pyramidal neurons and interneurons (Tseng & O'Donnell, 2007). DRD1 and DRD5 belong to the D1-like subfamily, while DRD2, DRD3, and DRD4 are subtypes of the D2-like subfamily. The receptors of D1-like subfamily consist of a single exon with no introns. Structurally, they contain a short third cytoplasmic loop and a long C-terminal stretch. In contrast to the D1-like subfamily, the D2-like subfamily has a bigger third intracellular loop, a short C-terminal stretch, and multiple exons and introns in their receptor genes. The existence of introns allows differential splicing of the transcripts of this subfamily to generate isoforms. *Drd2* comes in two alternatively spliced variants, *Drd2s* (short form) and *Drd2l* (long form). Isoforms of *Drd3* and *Drd4* have also been identified. DRD1 and DRD5 signal by coupling to G proteins G_{as} and G_{aolf}, which stimulate adenylyl cyclase, increase cyclic adenosine monophosphate (cAMP) production and lead to activation of protein kinase A (PKA). D2-like receptors stimulate G_{ai} and G_{ao} proteins, block adenylyl cyclase, consequently reducing

cAMP and inhibiting PKA activity (Missale et al., 1998; Tritsch & Sabatini, 2012). Other than the classical signaling pathways, DRDs can activate a signaling cascade by interacting with ß-arrestin (Beaulieu et al., 2005). They have also been proposed to induce phospholipase C-mediated increase of intracellular calcium levels (S. P. Lee et al., 2004), but the functioning of this signal transduction pathway remains unclear (Chun et al., 2013).

	Receptor / Gene	Rodent					
		L2/3	L5	L6	Species	Method	Reference
D1-like Family	DRD1 / *Drd1*	++	++	+++	Rats	*In situ*	*Santana & Artigas, 2017*
		++	+++	+++	Rats	Receptor binding	*Vincent et al., 1993*
		++	++	+++	Mice	Genetic labeling	*Wei et al., 2018*
	DRD5 / *Drd5*	++	++	++	Mice	Immuno histochemistry	*Lidow et al., 2003*
		+++	++	++	Rats	Immuno histochemistry	*Ciliax et al., 2000*
D2-like Family	DRD2 / *Drd2*	+	+++	++	Rats	*In situ*	*Santana & Artigas, 2017*
		++	+++	+++	Rats	Receptor binding	*Vincent et al., 1993*
		+	+++	++	Rats	Genetic labeling	*Yu et al., 2019*
		+++	++	++	Mice	Genetic labeling	*Wei et al., 2018*
	DRD3 / *Drd3*	?	?	++	Mice	Genetic labeling	*Li and Kuzhikandathil, 2012*
	DRD4 / *Drd4*	?	++	++	Mice	Genetic labeling	*Noain et al., 2006*

Table 1. Laminar distribution of *Drds*/DRDs across the prefrontal cortical layers of rodent PFC. *L, cortical layer; +++ highest expression; ++ intermediate expression; + low expression; (+) absent/very low expression.* Adapted from Islam et al., 2021

The distribution and expression of DRDs and their transcripts in rodent PFC **(Table 1)** have been studied using multiple histological methods such as autoradiographic experiments employing radiolabeled agonist or antagonist of DRDs (Boyson et al., 1986; Noisin & Thomas, 1988), immunohistochemical and immunoblotting approach targeting the receptor protein (Levey et al., 1993; Sesack et al., 1994), in-situ hybridization technique detecting *Drd* transcripts (Gaspar et al., 1995), real-time quantitative PCR, and in recent years, genetic tools

and single-cell transcriptome analysis. Cumulatively, these studies indicate that of the five DRD subtypes, DRD1 and its mRNA are most highly expressed in the adult rodent PFC, followed by DRD2/*Drd2*. In comparison, DRD3, 4 and 5 show limited expression (Araki et al., 2007; Lidow et al., 2003; Rajput et al., 2009; Santana et al., 2009; Tarazi & Baldessarini, 2000). RNA *in situ* hybridization methods have characterized the distribution of certain *Drd* mRNAs within the subregions of the PFC. These studies in adult rats display that *Drd1* mRNA expression is most prominent in layer VI, followed by a large number of positive cells in layer V and an additional thinner band of positive cells in layer II. *Drd2*-expressing cells have a less widespread laminar distribution and are mainly localized in layer V and VI, with very few positive cells detected in layer II and III (Gaspar et al., 1995; Santana et al., 2009; Santana & Artigas, 2017). DRD1 and DRD2 are expressed in both pyramidal neurons and interneurons of rodent PFC but are rarely colocalized (Santana et al., 2009; Z. W. Zhang et al., 2010). A recent study has delineated specific topographical organization of DRD1 and DRD2-expressing pyramidal neurons in the PFC, based on their projection targets. Using a retrograde adeno-associated virus approach in *Drd1*/*Drd2*-Cre mice (Gong et al., 2007), the study reported that DRD1-expressing pyramidal neurons that projected primarily to the dorsal striatum were organized in Cgl and PrL subregions of the mPFC, while DRD1-expressing, NAc-projecting pyramidal neurons were localized in the IL. Their data further disclosed that DRD2-expressing pyramidal neurons did not project to the dorsal striatum but those projecting to the NAc similarly occupied the IL region (Green et al., 2020). Genetic labeling studies with transgenic mice that accommodate a BAC (bacterial artificial chromosome) construct expressing enhanced green fluorescent protein (EGFP) under *Drd3* (*Drd3-Egfp* mice) or *Drd4* (*Drd4-Egfp* mice) regions have shown *Drd3*-positive fluorescent cells are present in the caudal cingulate cortex of layer VI (Li and Kuzhikandathil, 2012) and EGFP-labeled *Drd4* neurons in layer V and VI of prelimbic and cingulate cortices (Noaín et al., 2006). Immunostaining for DRD5 in the mPFC have shown that immunopositive cells are uniformly distributed across the cortical layers. In rats, immunolabeled DRD5 cells are also detected across the cortical layers of prelimbic and cingulate cortices, with a higher density of labeled cells in layer II and III (Ciliax et al., 2000; Lidow et al., 2003; Table 1). The distribution of DRDs in the rodent mPFC correlates largely with the innervation pattern of DA fibers, suggesting that DRD expression might be influenced by DA release in the mPFC.

The developmental time course of DRD expression however does not quite follow the steady innervation trajectory of mesoprefrontal fibers. Literature on postnatal changes in DRD levels comprises of conflicting reports. The inconsistent reports could stem from varying selectivity and sensitivity of the diverse techniques used in detection of DRDs. A further aspect to consider is whether transcript levels reliably correspond to the expression levels of DRD

protein. Araki and colleagues have used RT-qPCR approach to quantify the relative gene expression of the *Drd* subtypes in the PFC. Their analysis at P0, P21, and P60, both at rostral and caudal levels of the murine cingulate cortex, demonstrates there is not much developmental change between birth and adulthood. The only exception being *Drd4*, which has the highest expression at birth followed by a rapid postnatal decrease in expression (Araki et al., 2007). In situ hybridization signals for *Drd1* or *Drd2* transcripts have been reported to be maximal between P14 and P30 in one study (Schambra et al., 1994) while Naneix and colleagues have shown that *Drd1, Drd5, Drd4, Drd2l* (but not *Drd2s*) expression in the mPFC of rats reaches peak expression only at P45 and then decreases between P45 and P70 **(Fig. 4)** (Naneix et al., 2012). At the protein level, Andersen and colleagues describes a developmental pattern of expression comparable to that of Naneix and colleagues, reporting a marked decline of DRD1 and DRD2 density in PFC of rats between adolescence (P40) and adulthood (P120) (Andersen et al., 2000). Interestingly, another study shows similar differential expression across postnatal development in a certain population of DRD1 expressing pyramidal neurons. In retrogradely traced prelimbic pyramidal neurons projecting to the NAc core, the number of DRD1 immunoreactive cells were found to increase from juvenile phase (P27) to adolescence (P44), followed by a decline in adulthood (P105) (Brenhouse et al., 2008). Tarazi and Baldessarini, however, report a different temporal expression pattern in frontal cortex of rats. Their investigation exhibits that binding of radioligands to DRD1, DRD2 and DRD4 receptors gradually rises from P7 to maximal levels at P60 (Tarazi & Baldessarini, 2000). Overall, the data from various published studies do not deliver a conclusive picture on the time course and distribution of DRD/*Drd* expression in the developing mPFC **(Table 2).**

In addition to the dynamic DRD expression in the PFC, maturation of receptor function could could be in the foreground of changing impact of the mesoprefrontal system over time. As discussed earlier (see section 1.4.2.3), investigations into DRD function have shown that DRD1-mediated modulation of NMDA receptor can bring about prolonged depolarizations in mPFC slices of adolescent or adult, but not preadolescent rats (Tseng & O'Donnell, 2005). DRD modulation of interneurons also transforms during adolescence as DRD2-mediated increase in excitability of fast-spiking interneurons in PFC slices appears only in late adolescence (Tseng & O'Donnell, 2007). Thus, while the changes in postnatal expression levels of DRD/*Drd* are still unclear, there is indeed a change in activity of DRDs in the post-pubertal stage, hinting towards a conspicuous role of DA in refinement of excitation-inhibition

	Receptor / Gene	Rodent							
		0W	1W	3W	6W	9W	Species	Method	Ref
D1 – like Family	DRD1 / *Drd1*	+		↔		↔	Rats	RT-qPCR	*Araki et al., 2007*
				+	↑	↓*	Rats	*In situ*	*Naneix et al., 2012*
			+	↑*	↑	↑	Rats	Receptor Autoradiography	*Tarazi & Baldessarini, 2000*
			+	↑	↓		Rats	Receptor Autoradiography	*Leslie et al., 1991*
	DRD5 / *Drd5*	+		↔		↔	Rats	RT-qPCR	*Araki et al., 2007*
				+	↑	↓*	Rats	RT-qPCR	*Naneix et al., 2012*
D2 – like Family	DRD2 / *Drd2*	+		↔		↔	Rats	RT-qPCR	*Araki et al., 2007*
	Drd2l			+	↑	↓*	Rats	RT-qPCR	*Naneix et al., 2012*
	Drd2s			+	↔	↔	Rats	RT-qPCR	*Naneix et al., 2012*
			+	↑*	↑	↑	Rats	Receptor Autoradiography	*Tarazi & Baldessarini, 2000*
	DRD3 / *Drd3*	+		↔		↔	Rats	RT-qPCR	*Araki et al., 2007*
	DRD4 / *Drd4*	+		↓*		↔	Rats	RT-qPCR	*Araki et al., 2007*
				+	↑	↓*	Rats	RT-qPCR	*Naneix et al., 2012*
			+	↑*	↑	↑	Rats	Receptor Autoradiography	*Tarazi & Baldessarini, 2000*

Table 2: Relative changes in expression of *Drds*/DRDs in PFC throughout postnatal development. *+ first postnatal stage analyzed & expression detected. ↑ increase; ↓ decrease; ↔ no change in expression compared to previous timepoint; * indicates increase or decrease in expression compared to previous timepoint that were significant; empty cells: no data available. W: Week.* Adapted from Islam et al., 2021

balance in PFC microcircuits during the transition from adolescence to adulthood. Failure to regulate the excitatory and inhibitory transmission during this critical period could potentially alter circuit maturation, contributing to susceptibility to neuropsychiatric disorders.

1.15 Mesoprefrontal system in neurodevelopment disorders

DA input to the PFC modulates its local microcircuits and consequently a variety of PFC-dependent cognitive and affective behaviors. Dysfunction of local PFC networks concomitant with impaired PFC-dependent executive functions are hallmarks of many of the neurodevelopmental disorders such as schizophrenia, autism spectrum disorder (ASD) and attention deficit/hyperactivity disorder (ADHD). Due to the role of mesoprefrontal DA in cognition, aberrant dopaminergic signaling in the PFC has been linked to the cognitive deficits present in these neurodevelopmental disorders. It is however unclear whether altered developmental trajectory of mesoprefrontal DA system contributes to the pathoetiology of the diseases or if dysregulated mesoprefrontal DA system is an outcome of abnormal PFC maturation (Islam et al., 2021). This section briefly summarizes three disorders of altered neural development: schizophrenia, ASD and ADHD, in which the mesoprefrontal system is afflicted.

Schizophrenia is a severely debilitating neuropsychiatric disorder of neurodevelopmental origin that typically emerges during late adolescence and is associated with positive/psychotic symptoms such as hallucinations, negative symptoms like social withdrawal and cognitive dysfunction, especially in the domains of working memory and inhibitory control (Howes & Shatalina, 2022; van Os & Kapur, 2009). The DA hypothesis of schizophrenia postulates that there is an imbalance in mesoprefrontal and mesolimbic DA systems. It is proposed that elevated DA transmission in the striatum results in the positive clinical symptoms while hypoactive mesoprefrontal dopaminergic transmission is connected to negative symptoms and cognitive dysfunction (Abi-Dargham, 2017). Evidence gathered from preclinical and clinical studies indicates striatal DA release is regulated by PFC activity. Imbalanced E/I in frontal cortex could lead to disrupted cortical functioning, disinhibiting pyramidal neurons that regulate mesostriatal mDA neurons, prompting hyperdopaminergia in the striatum. While it is unclear what accounts for reduced DA release in PFC, disruption of corticothalamic or hippocampal networks could contribute to the changes in the inputs to the VTA leading to an overall dysregulated DA system and hypoactivity within various VTA targets, including the PFC. Whether atypical development of the mesoprefrontal system is a contributor to DA hypoactivity in schizophrenia have not been methodically investigated (Howes & Shatalina, 2022; Islam et al., 2021; Sonnenschein et al., 2020).

Another psychiatric disorder that presents overlapping clinical traits and shared risk factors with schizophrenia is ASD (Prata et al., 2017). ASD comprises a group of neurodevelopmental disorders characterized primarily by deficits in social interaction, and stereotyped, inflexible, repetitive behaviors. While many environmental and genetic risk factors have been suggested, the neurobiological basis of ASD is not well-defined. Since ASD shares some clinical components with schizophrenia and many of the brain regions implicated in ASD pathophysiology are projection targets of mDA neurons, it led to the theory that aberrant DA signaling at certain mDA projection targets could be related to ASD symptomatology. In its current state, the DA hypothesis of ASD proposes that alterations in the mesocorticolimbic pathway may contribute to social and reward-related behavioral deficits, while dysfunction of nigrostriatal circuit could lead to impairments in goal-directed motor behavior exhibited by individuals with ASD (Lord et al., 2018; Mandic-Maravic et al., 2022; Pavăl, 2017; Pavăl & Miclutia, 2021). Several lines of work have supported this hypothesis, including studies that show reduced DA levels in the PFC. Functional changes in DA signaling in the PFC of ASD patients could translate to cognitive inflexibility, but to probe into the potential role of mesoprefrontal DA system in ASD pathophysiology, investigations need to be directed deeper towards DA system-targeted studies in patients and ASD mouse models (Islam et al., 2021; Mandic-Maravic et al., 2022; Pavăl, 2017).

Neurodevelopmental disorders are sometimes characterized by concurrent presence of multiple clinical conditions. In people with ASD, one of the most prevalent diagnosed comorbiditie is ADHD (Lord et al., 2018), which is a highly heritable, early-onset psychiatric disorder that interferes with normal neurodevelopment. ADHD is characterized by symptoms of persistent inattention, hyperactivity and impulsiveness that may reflect impaired executive functioning of PFC. This in turn hint towards a dysregulated catecholamine system in the PFC of individuals with ADHD. Major evidence confirming altered catecholamine signaling in the PFC comes from human studies that report therapeutic benefits of methylphenidate and amphetamine in the treatment of ADHD. These drugs act by inhibiting DA and NA reuptake, consequently increasing DA and NA transmission in the PFC, indicative of a hypofunctional mesoprefrontal system. Low doses of methylphenidate have also been shown to improve PFC function in animals. Furthermore, a meta-analysis study showed that there is a close association between ADHD and polymorphism in the genes that encode DRD4, DRD5, and DAT. *DRD4* polymorphism, in particular, have been shown by multiple studies to elevate the risk of developing ADHD in children (Islam et al., 2021; Shaw et al., 2007; J. Wu et al., 2012). Although it remains challenging to separate the impact of altered DA versus NA signaling on PFC dysfunction in ADHD, these reports together indicate a critical role of mesoprefrontal system in the pathophysiology of ADHD.

In summary, alterations in mesoprefrontal DA system have been shown to be closely associated with the most common neuropsychiatric disorders of neurodevelopmental origin, although it remains unresolved whether disrupted mesoprefrontal development is the basis or consequence of defects in PFC development. The etiology of neurodevelopment disorders is multilayered, with both genetic background and contributions from environmental risk factors. In addition to the PFC, neuropsychiatric disorders almost always involve multiple affected brain regions with complex interaction of neurotransmitters distinctive to each region. Another important factor to consider is that mesoprefrontal mDA neurons can co-release glutamate in the PFC (Kabanova et al., 2015; Pérez-López et al., 2018) and changes in mDA innervation of PFC can influence both DA and glutamate release. These create a challenge in dissecting out the exact role of mesoprefrontal DA in these disorders. One approach to accomplish this feat could be with the aid of mouse models that interfere with the development of mesoprefrontal projections, such as the *Dcc* and *Netrin-1* haploinsufficient mice that elevate DA transmission in the mPFC (Vosberg et al., 2020) or mouse models that lack mesoprefrontal innervation (Kabanova et al., 2015). Further insights into a potential causative role of mesoprefrontal dysfunction in neurodevelopment will contribute to a neurobiological framework essential for understanding the etiology of neuropsychiatric and neurodevelopmental disorders.

1.16 *Gli2* cKO mouse model

This thesis presents the possibility to specifically study the mesoprefrontal system in mice during postnatal development by means of the *Gli2* cKO mouse model, in which the mDA projections to the PFC are lacking. The *Gli2* cKO was generated by conditional inactivation of the zinc finger transcription factor GLI2, the main mediator of SHH-mediated mDA progenitor induction. Inactivation of SHH signaling activity around E9, about a day before the lateral progenitor domain ceases to require SHH for its induction, severely reduced the lateral progenitor domain, but only partially affected the medial progenitor domain (see section 1.7). Since the lateral progenitor domain contributes preferentially to the establishment of mDA neurons of ventromedial VTA, this resulted in acute deficit in the number of mDA neurons in the medial VTA in *Gli2* cKO mice along with the failure to establish appropriate mesoprefrontal innervation (Blaess et al., 2011; Kabanova et al., 2015). The number of mDA neurons of SNpc in *Gli2* cKO were slightly reduced and localized to a more medial position, an area typically occupied by VTA neurons, but no significant changes were observed in mDA projections to the caudoputamen complex, NAc, and amygdala. In accordance with nearly absent mesoprefrontal innervation, *Gli2* cKO mice exhibited decreased DA content in the PFC. Evaluation of functional properties of mesoprefrontal mDA neurons using optogenetic

approach demonstrated that they establish a specific mPFC circuit capable of rapid inhibition of pyramidal neurons via glutamatergic excitation of preferentially fast-spiking interneurons. This feature was impaired in *Gli2* cKO mice. With respect to cognition, the *Gli2* cKO mice did not show any deficits in attention and impulse control in the 5-choice-serial-reaction-time-task (5-CSRTT). Their horizontal exploratory behavior in open-field as well as motivational level were comparable to controls. Recognition memory of Gli2 cKO mice in novel object recognition test also remained intact. Gli2 cKO mice however tended to adhere to a stimulus-response strategy they previously learnt when task contingencies were changed in 5-CSRTT, displaying a form of perseverative behavior (Kabanova et al., 2015).

2. Objectives of the Study

The proper development of long-range inputs to the PFC and the formation of PFC local microcircuits within precise time courses are crucial to PFC maturation. Our understanding of the mechanisms of functional maturation of PFC is however inadequate due to the complex dynamics of diverse inputs to the developing PFC. Mesoprefrontal DA has been implicated to be one of the key players of PFC remodeling during adolescence but its role is still evolving. The aim of this thesis was to examine how the absence of the mesoprefrontal DA system impacts mPFC circuit elements during postnatal development.

The first aim of the present study was to assess how absence of mesoprefrontal input might influence the developmental trajectory of the GABAergic component of the mPFC microcircuit. Using immunohistochemical methods, we analyzed the density of three major GABAergic interneuron subpopulations of PFC: PV, CB and CR in control and cKO mice, comparing their cell densities at multiple developmental stages from early postnatal phase (P12) to full adulthood (P120). Since PV interneurons are the most abundant in rodent PFC and often implicated in neurodevelopmental disorders, the development of their fluorescence intensity and changes in their expression level of *Gad1* gene during postnatal development were further investigated. Additionally, CB protein expression in the mPFC was quantified by Western blotting during late adolescence/young adulthood in control and cKO.

The second objective of this thesis was to determine whether the innervation pattern of the other monoaminergic projections in the mPFC of cKO mice was affected in the absence of DA input, as a potential compensatory mechanism for the lack of DA input. Immunostaining for the monoamine transporter proteins SERT and NET was used to label the serotonergic and noradrenergic fibers, respectively, and their occupancy density in the mPFC was analyzed at early postnatal stage and late adolescence/young adulthood (P60) to compare the development of fiber growth and pattern in control and cKO.

The third objective was to assess if the expression of dopamine receptors was modified in the mPFC in response to lack of DA input. Using a non-biased automated approach, *Drd1* and *Drd2* transcripts were detected and quantified in control and cKO of the mPFC between early postnatal phase and late adolescence.

The final aim was to investigate whether the absence of mesoprefrontal innervation and the changes in interneurons in the mPFC had an effect on the cognitive behavior of the cKO mice. To this end, the performance of cKO and control mice was compared in a spatial working memory task in a figure-of-eight maze that included a spatial delayed-response task.

3. Materials and Methods

3.1 Materials

3.1.1 Table 3: Equipment

Product	Model/ Cat. No	Manufacturer	Registered Office
Autoclave	DX-150 Benchtop	SysTec	Bergheim, DE
Balance	AC211S	Sartorius	Göttingen, DE
Balance	ATL-822-1	Sartorius	Göttingen, DE
Balance	SE 1202	VWR	Darmstadt, DE
Balance	Roma Silver 65856	Soehnle	Nassau, DE
Vortexer	Vortex Genius	IKA	Staufen, DE
Vortexer	Zx3	Velp Scientifica	Usmate Velate, IT
Waterbath	10679808	FGL	Burgwedel, DE
Steamer	5100	Braun	Melsungen, DE
Thermocycler	DANN Engine PTC-200	Bio-Rad	Hercules, USA
Thermocycler	BIometra TRIO	Analytik Jena	Jena, DE
Shaker	Nutation Mixer	VWR	Darmstadt, DE
Rocking Platform	4440148	VWR	Darmstadt, DE
Eight-maze	90cm x 80cm x 30cm		
RNAScope® Hybridization oven	HybEZ PN 321710/321720	Advanced Cell Diagonostic	Newark, USA
Humidity Control Tray	PN 310012	Advanced Cell Diagonostic	Newark, USA
EZ Batch Slide Holder	PN 321716	Advanced Cell Diagonostic	Newark, USA
Refrigerators & Freezers 4°C, -20°C, -80°C	G2013 Comfort HERAfreeze	Liebherr Kendro	Lindau Hanau, DE
Refrigerator, 4°C	LKUexv 1610	Liebherr	Ulm, DE
Freezer, -20°C	LGUex 1500	Liebherr	Ulm, DE
Magnetic Stirrer	AGE 1200 rpm	VELP Scientifica	Usmate Velate, IT
Hot Plate	SB162	Bibby Sterlin	Staffordshire, UK
Incubator (with shaker)	KS-15	Edmund Bühler GmbH	Bodelshausen, DE
pH Meter	FE20 FiveEasy	Mettler Toledo	Columbus, USA
Cryostat	Leica CM 3050S	Leica Biosystems	Wetzlar, DE
Gel Chamber	Model 40-1515	PeqLab	Erlangen, DE
Gel Chamber	Model 40-1525	PeqLab	Erlangen, DE
Power Supply Electophoresis	EV231	PeqLab	Erlangen, DE
Gel Imager	Gel Doc XR+	Bio-Rad	Feldkirchen, DE
Chemiluminescence Detector	ChemicDoc XRS+	Bio-Rad	Feldkirchen, DE
Ultrasonic Homogenizer	HD 2070	Bandelin Electronic	Berlin, DE
Compact Bead Mill	TissueLyser LT	Qiagen	Hilden, DE
Stainless Steel Beads	69989	Qiagen	Hilden, DE

Table 3 continued from page 39

Product	Model/ Cat. No	Manufacturer	Registered Office
Spectrophotometer	Nandodrop 2000c	Thermo Fischer Scientific	Schwerte, DE

3.1.2 Table 4: List of microscopes

Microscope/Equipment	Model/Cat. No.	Manufacturer	Registered Office
Epifluorescence Microscope	AxioObserver Z1	Carl Zeiss	Oberkochen, DE
10x objective	EC PlnN 10x/0.3 DIC I 1.11µm	Carl Zeiss	Oberkochen, DE
20x objective	EC PlnN 20x/0.5 DIC II 0.67 µm	Carl Zeiss	Oberkochen, DE
ApoTome	ApoTome.2	Carl Zeiss	Oberkochen, DE
Fluorescence Lamp	Illuminator HXP120C	Carl Zeiss	Oberkochen, DE
Microscope Camera	AxioCam MRm	Carl Zeiss	Oberkochen, DE
Power Unit	Power Supply 231	Carl Zeiss	Oberkochen, DE

Microscope/Equipment	Model/Cat. No.	Manufacturer	Registered Office
Widefield Epifluorescence Microscope	AxioScan.Z1 Slide scanner	Carl Zeiss	Oberkochen, DE
5x Objective	Fluar 5x/0.25	Carl Zeiss	Oberkochen, DE
20x Objective	PlanNeofluar 20x/0.5	Carl Zeiss	Oberkochen, DE
Microscope Camera (color)	Hitachi HV-F202SCL	Hitachi Kokusai Electric America	Neu-Isenburg, DE
Microscope Camera (monochrome)	Hamamatsu Orca Flash 4.0 v3	Hamamatsu Photonics	Herrsching am Ammersee, DE
LED Light Source	Colibri 7	Carl Zeiss	Oberkochen, DE

Microscope/Equipment	Model/Cat. No.	Manufacturer	Registered Office
Leica Confocal Microscope	Leica TCS SP8	Leica Microsystems	Wetzlar, DE
10x Objective	HCX PL APO 10x/ 0.40	Leica Microsystems	Wetzlar, DE
63x Objective	HC PL APO 63X/1.3 Gly	Leica Microsystems	Wetzlar, DE
405 nm laser line	Solid-State Laser	Leica Microsystems	Wetzlar, DE
552 nm laser line	Solid-State Laser	Leica Microsystems	Wetzlar, DE
Microscope Camera	DM6000	Leica Microsystems	Wetzlar, DE

Microscope/Equipment	Model/Cat. No.	Manufacturer	Registered Office
Spinning Disk Confocal Microscope	AxioObserver 7	Carl Zeiss	Oberkochen, DE
5x Objective	PlanNeofluar 5x/0.16	Carl Zeiss	Oberkochen, DE

Table 4 continued from page 40

Microscope/Equipment	Model/Cat. No.	Manufacturer	Registered Office
20x objective	PlanApochromat 20x/0.8	Carl Zeiss	Oberkochen, DE
40x objective	C-Apochromat, 40x/1.2 water	Carl Zeiss	Oberkochen, DE
63x objective	C-Apochromat, 63x/1.2 water	Carl Zeiss	Oberkochen, DE
405 nm laser line	VS-Laser Control	Visitron Systems	Puchheim, DE
488 nm laser line	VS-Laser Control	Visitron Systems	Puchheim, DE
561 nm laser line	VS-Laser Control	Visitron Systems	Puchheim, DE
561 nm laser line	VS-Laser Control	Visitron Systems	Puchheim, DE
VS-Homogenizer	13x13 sCMOS	Visitron Systems	Puchheim, DE
Microscope Camera	sCMOS pco.edge 4.2	PCO	Kelheim, DE
Spinning Disk Unit	CSU-W1	Yokogawa Electric Corporation	Tokyo, JP

3.1.3 Table 5: Data acquisition and analysis

Computing	Software	Manufacturer	Registered office
Gel Documentation	Quantity One	Bio-Rad	Feldkirchen, DE
Gel Documentation	Quantity One	Bio-Rad	Feldkirchen, DE
Immunoblot Documentation	Image Lab	Bio-Rad	Feldkirchen, DE
Image Acquisition	Zen 2 (blue edition)	Carl Zeiss	Oberkochen, DE
Image Acquisition	Leica Application Suite AF v3.x	Leica Microsystems	Wetzlar, DE
Image Acquisition	VisiView	Visitron Systems	Puchheim, DE
Image Processing	Affinity Photo 1.9.1	Serif	Nottingham, UK
Image Processing	Fiji/ ImageJ version 2.0.0	Wayne Rasband, National Institute of Health	Bethesda, USA
Image Processing	CellProfiler 3.1.9	Broad Institute of MIT and Harvard	Cambridge, USA
Statistical Analysis	GraphPad Prism version 9.0.2	GraphPad Software	San Diego, USA

3.1.4 Table 6: Consumables

Product	Model/Cat. No	Manufacturer	Registered office
12-well culture plate	353043	BD Biosciences	Heidelberg, DE
24-well culture plate	353047	BD Biosciences	Heidelberg, DE
96-well culture plate	781900	Brand	Wertheim, DE
Nitrocellulose Blotting Membrane	10600002	GE Healthcare Lifescience	Solingen, DE

Table 6 continued from page 41

Product	Model/Cat. No	Manufacturer	Registered office
Microscope Slides	Menzel-Gläser SuperFrost	Thermo Fischer Scientific	Schwerte, DE
Microscope Slides	SuperFrost	Carl Roth	Karlsruhe, DE
Adhesive Microscope Slides	Menzel-Gläser SuperFrost Plus	Thermo Fischer Scientific	Schwerte, DE
Adhesive Microscope Slides	Histobond 0810001	Paul Marienfeld	Lauda-Königshofen, DE
Microscope Cover Glass	60 x 24 mm 40990	Hecht Assistent	Sondheim vor der Rhön, DE
Microscope Cover Glass	60 x 24 mm 0101242	Paul Marienfeld	Lauda-Königshofen, DE
Slide Boxes	HS15994E	Carl Roth	Karlsruhe, DE
Autoclave Tape	SteriClin Sticky Tape	VP group	Feuchtwangen, DE
Disposable Blades	14035838382	Leica Biosystems	Wetzlar, DE
Embedding Molds	Peel-A-Way E-6032-1CS	Merck	Darmstadt, DE
Brain Matrix	1mm Steel RBMS-200C	World Precision Instruments	Friedberg, DE
Forceps Dumont (#5)	11252 – 30	Fine Science Tools	Heidelberg, DE
Graefe Forceps (0.8mm)	11050-10	Fine Science Tools	Heidelberg, DE
Student Anatomical Standard Pattern Forceps	91100-12	Fine Science Tools	Heidelberg, DE
Fine Scissors-Sharp	14060-11 14060-09	Fine Science Tools	Heidelberg, DE
Noyes Spring Scissors	15012-12	Fine Science Tools	Heidelberg, DE
Student Surgical scissor	91401-12	Fine Science Tools	Heidelberg, DE
Artery Scissors-Ball Tip	14080-11	Fine Science Tools	Heidelberg, DE
Extra Fine Bonn Scissors	14084-08 14085-08	Fine Science Tools	Heidelberg, DE
Needles	0.40x20 mm BL/LB 27Gx3/4''	Braun	Melsungen, DE
Winged Needle Infusion Set	P294A05	Venisystems	Hospira, USA
Winged Needle Infusion Set	P295A05	Venisystems	Hospira, USA
Winged Needle Infusion Set	P296A05	Venisystems	Hospira, USA
Winged Needle Infusion Set	Surflo SV*21BLK03	Terumo Europe	Leuven, BE
Perforated Spoon	Moria MC17BIS 10370-18	Fine Science Tools	Heidelberg, DE
Hydrophobic Barrier Pen	DakoPen S2002	Agilent Technologies	Glostrup, DK

Table 6 continued from page 42

Product	Model/Cat. No	Manufacturer	Registered office
Hydrophobic Barrier Pen	ImmEdge H-4000	Vector Laboratories	Newark, USA
DermaClean Gloves	PFC 4303971	Ansell	Munich, DE
Eppendorf tubes 1.5mL	72690	Eppendorf AG	Hamburg, DE
Eppendorf tubes 2mL	AM12425	Thermo Fisher Scientific	Schwerte, DE
Filter Tips	ART 100/200/1000	Thermo Fisher Scientific	Schwerte, DE
Pipettes (10, 20, 200, 1000 µL)	FA10002M FA10003M FA10005M FA10006M	Gilson	Middleton, USA
Lens Cleaning Tissue 105	2105841	Whatman	Dassel, DE
Tissue Wipes	05511	KimTech	Surrey, UK
Liquid Scintillation Vials	Z190527	Merck	Darmstadt, DE
Parafilm, PM996	P7793-1EA	Merck	Darmstadt, DE
PCR tubes	732-0551 732-0545	VWR	Darmstadt, DE
Petri Dishes (15 mm)	351029	BD Biosciences	Heidelberg, DE
Pipette-boy Accujet pro	26300	Brand	Wertheim, DE
Polypropylene conical tubes 15mL	352096	Fine Science Tools	Heidelberg, DE
Polypropylene Conical Tubes 50mL	352070	BD Biosciences	Heidelberg, DE
Serological Pipettes	4487 (5mL) 4488 (10mL) 4489 (25mL)	Corning Life Sciences	Kaiserslautern, DE
Syringes – 1mL	2-piece Fine Dosage/9166033V 3-piece Fine Dosage/9161465V	Braun	Melsungen, DE
Syringes – 50mL	Omnifix Solo 50ml	Braun	Melsungen, DE

3.1.5 Table 7: Chemical Reagents

Chemicals	Catalog No.	Manufacturer	Registered office
Ampuwa water	40676.00.00	Ampuwa, Fresenius	Bad Homburg, DE
Aqua-PolyMount	18606	Polysciences Inc.	Eppelheim, DE

Table 7 continued from page 43

Chemicals	**Catalog No.**	**Manufacturer**	**Registered office**
Agarose UltraPure™	11553277	Thermo Fisher Scientific	Schwerte, DE
DNA Ladder 100bp	15628019	Thermo Fisher Scientific	Schwerte, DE
DNA Ladder 1Kb Plus	10787-018	Thermo Fisher Scientific	Schwerte, DE
dNTPs (100mM)	28-4065-52	GE Healthcare	Dornstadt, DE
Taq DNA Polymerase Recombinant	10342-020	Thermo Fischer Scientific	Schwerte, DE
EDTA	E6511	Merck	Darmstadt, DE
Ethidium Bromide	2218.2	Carl Roth	Karlsruhe, DE
Ethylene Glycol	1009492500	Merck	Darmstadt, DE
Glacial Acetic Acid	A6283-1L	Merck	Darmstadt, DE
Glycerol	G5516	Merck	Darmstadt, DE
Hoechst 33258	ab228550	Abcam	Berlin, DE
Ketanest®	Ketanest® S 25 mg/ml	Pfizer	Berlin, DE
Rompun®	Rompun® 2%	Bayer	Leverkusen, DE
Normal Donkey Serum (NDS)	017-000-121	Jackson ImmunoResearch	Cambridgeshire, UK
Paraformaldehyde (PFA)	0335.2	Carl Roth	Karlsruhe, DE
Potassium Chloride (KCl)	26764.260	VWR	Darmstadt, DE
Potassium Phosphate Monobasic (KH_2PO_4)	P9791	Merck	Darmstadt, DE
RNAse away	13398800	Roche	Basel, CH
RNAScope® Hydrogen Peroxide Reagent	322330	Advanced Cell Diagnostic	Newark, USA
RNAScope®Protease III	322340	Advanced Cell Diagnostic	Newark, USA
RNAScope® Target Retrieval	322000	Advanced Cell Diagnostic	Newark, USA
RNAScope® Wash buffer	322000	Advanced Cell Diagnostic	Newark, USA
RNAscope Multiplex Fluorescent Detection Kit	323110	Advanced Cell Diagnostic	Newark, USA
TSA Buffer	322809	Advanced Cell Diagnostic	Newark, USA
TSA Fluorophore Cyanine3	FP1170012	PerkinElmer LAS	Rodgau, DE
TSA Fluorophore Cyanine5	FP1171024	PerkinElmer LAS	Rodgau, DE
Magnesium chloride ($MgCl_2$)	25108.260	VWR	Darmstadt, DE
Sodium bicarbonate ($NaHCO_3$)	27775.293	VWR	Darmstadt, DE
Sodium chloride (NaCl)	27788.297	VWR	Darmstadt, DE

Table 7 continued from page 44

Chemicals	Catalog No.	Manufacturer	Registered office
Sodium Dihydrogen Phosphate ($NaH_2PO_42H_2O$)	28013.264	VWR	Darmstadt, DE
Sodium Hydroxide (NaOH)	31627.290	VWR	Darmstadt, DE
Sodium Phosphate (Na_2HPO_4)	28028.298	VWR	Darmstadt, DE
Sucrose	27480.360	Merck	Darmstadt, DE
Sucrose Tablets 20mg	1811555 (5TUT)	TestDiet	Indiana, USA
Tissue Tek O.C.T.	4583	Sakura	Alphen aan den Rijn, NL
Protease Inhibitor Cocktail	05892791001	Merck	Darmstadt, DE
Tris	443864E	VWR	Darmstadt, DE
Tris-HCl	85827.297	VWR	Darmstadt, DE
Glycine	0167	VWR	Darmstadt, DE
Sodium Dodecyl Sulphate	44215HN	VWR	Darmstadt, DE
Methanol	4627.5	Carl Roth	Karlsruhe, DE
Pyronin Y	0207	VWR	Darmstadt, DE
Bromophenol Blue	A1120,0005	AppliChem	Darmstadt, DE
TEMED	0761	VWR	Darmstadt, DE
Acrylamide/Bisacrymalide 30%	Rotiphorese Gel 30 3029.2	Carl Roth	Karlsruhe, DE
Ammonium Peroxodisulfate	21300.260	VWR	Darmstadt, DE
2-Mercaptoethanol	M131	VWR	Darmstadt, DE
2-Propanol	20842.330	VWR	Darmstadt, DE
Milk Powder (Skimmed)	1.15363.9010	VWR	Darmstadt, DE
Prestained Protein Ladder	PageRuler 26617	Thermo Fischer Scientific	Schwerte, DE
Triton X-100	1.08219.1000	Merck	Darmstadt, DE
Tween-20	28829.183	VWR	Darmstadt, DE
Immobilon	WBLUC0020	Millipore	Darmstadt, DE

3.1.6 Table 8: Buffers and Solutions

Buffer/Solution	Content
Blocking solution for immunohistochemistry (IHC)	10% Normal donkey serum (NDS) in 0.3% PBT (PBS 1X plus 0.3% Triton X-100) OR 10% Normal donkey serum (NDS) in 0.5% PBT (PBS 1X plus 0.5% Triton X-100)
Loading buffer 10X (gel electrophoreses)	50% Glycerol 0.4% Bromphenol blue 0.4% Xylene Cyanol mixed stored at 4°C

Table 8 continued from page 45

Buffer/Solution	**Content**
Lysis buffer	333 µL 1.5 M Tris, pH 8.8 (50 mM) 20 µL 0.5 M EDTA (1 mM) 500 µL 10% Tween 9.1 mL dH_2O stored at -20°C
Phosphate buffer solution (PBS) 5X	40 g NaCl (137 mM) 1 g KCl (2,7 mM) 7.1 g Na_2HPO4 (10 mM) 1.36 g KH_2PO4 (2 mM) in ~1 L dH_2O stored at room temperature
Paraformaldehyde (PFA) 20%	500 g PFA in ~2.0 L dH2O 8.0 mL NaOH to adjust pH to 7.0 filtered through 0.4 µm filter and stored at -20°C
PFA 4% (fixation solution)	10 mL 20% PFA in 50mL PBS 1X
PBT 0.3% (IHC)	30 mL 10% Triton-X (0.3 %) 970 mL PBS 1X
PBT 0.5% (IHC)	50 mL 10% Triton-X (0.5 %) 950 mL PBS 1X
Tissue digestion buffer	1. NaOH solution: 25mM NaOH 0.2 mM EDTA 2. Tris solution: 40 mM Tris HCl calibrated to pH 5.5
TAE 50X (gel electrophoreses)	242g Tris-base 100mL 0.5M EDTA (pH 8.0) 57.1mL Glacial acetic acid in ~1L H_2O stored at room temperature
Tris-acetate-buffer (TAE) 1X (gel electrophoreses)	TAE 50X diluted 1:50 with dH_2O stored at room temperature
Saline sodium citrate (SSC) 20x	88.2 g Sodium citrate 174 g NaCl ~1L dH_2O calibrated to pH 5.5 stored at room temperature
Saline sodium citrate 5X	SSC 20X diluted 1:5 with dH_2O stored at room temperature
Walter´s antifreeze solution (for storage of adult cryosectioned tissue at -20°C)	400 mL Phosphate buffer 100 mM: 1.57 g Na2HPO4 5.45 g Na2HPO4 in ~400 mL dH2O 300 mL Ethylene glycol 300 mL Glycerol stored at room temperature

Table 8 continued from page 46

Buffer/Solution	**Content**
Western blot electrophoresis Buffer 10X	30.3 g Tris-base 144.2 g Glycine 10 g SDS in ~1 L dH_2O calibrated to pH 8.4 stored at room temperature
Western blot transfer buffer	3 g Tris 14.4 g Glycine 200 ml Methanol 3.75 ml 10% SDS in ~1 L dH_2O stored at 4°C
Laemmli buffer 4X	0.9 g Tris 1.2 g SDS 12 mg Pyronin 6 mg Bromophenol blue in ~30 ml dH_2O
Tris buffer for resolving gel	181.65 g Tris 2 g SDS in ~1 L dH_2O Calibrated to pH 8.8
Tris buffer for stacking Gel	181.65 g Tris 3 g SDS in ~1.5 L dH_2O Calibrated to pH 6.8
Blocking solution for blotted membranes	5% Milk in 0.1% PBT (PBS + 0.1% Tween-20)

3.1.7 Table 9: Gels

Gels	**Content**
Resolving gel 12% Gel volume 20 ml	6.6 ml dH_20 8 ml 30% Acrylamide/bis solution 0.2 ml 10% SDS 0.2 ml 10% APS 0.012 ml TEMED Tris 1M Buffer (pH 8.8) 5ml
Stacking gel 5% Gel volume 3 ml	2.1ml dH_20 0.5 ml 30% Acrylamide/bis solution 0.03 ml 10% SDS 0.03 ml 10% APS 0.003 ml TEMED Tris 1M Buffer (pH 6.8) 0.38ml

Table 9 continued from page 47

Gels	Content
Agarose gel 1.5% Gel volume 100 ml	1.5 g Agarose powder ~100 ml 1x TAE Buffer 2-3 µl 1% Ethidium bromide solution
Agarose gel 2% Gel volume 100 ml	2 g Agarose powder ~100 ml 1x TAE Buffer 2-3 µl 1% Ethidium bromide solution

3.1.8 Antibodies

3.1.8.1 Table 10: Primary Antibodies

Primary antibody	Dilution	Cat. No.	Manufacturer	Registered office
Rabbit Anti-Parvalbumin	1:1000	PV27	Swant	Burgdorf, CH
Rabbit Anti-Calbindin	1:2000	CB38a	Swant	Burgdorf, CH
Goat Anti-Calretinin	1:2000	CG1	Swant	Burgdorf, CH
Rat Anti-GFP	1:2000	04404-26	Nacalai Tesque	Kyoto, JP
Mouse Anti-TH	1:500	MAB318	Merck	Darmstadt, DE
Rabbit Anti-NET	1:2000	260003	Synaptic Systems	Göttingen, DE
Rabbit Anti-SERT	1:5000	24330	Immnostar	Hudson, USA
Rat Anti-CTIP2	1:500	ab18465	Abcam	Berlin, DE
Rabbit Anti-DRD2	1:500	AB5084P	Merck	Darmstadt, DE
Mouse Anti-beta Actin	1:10000	ab6276	Abcam	Berlin, DE

3.1.8.2 Table 11: Secondary Antibodies

Secondary antibody	Dilution	Cat. No.	Manufacturer	Registered office
Donkey Anti-Goat Biotin	1:500	706-065-147	Jackson ImmunoResearch	Cambridgeshire, UK
Donkey Anti-Rabbit Biotin	1:500	711-065-152	Jackson ImmunoResearch	Cambridgeshire, UK
Donkey Anti-Rat Cy3	1:200	712-165-153	Jackson ImmunoResearch	Cambridgeshire, UK
Cy3 Streptavidin	1:1000	016-160-084	Jackson ImmunoResearch	Cambridgeshire, UK
Alexa 647 Streptavidin	1:500	S32357	Thermo Fischer Scientific	Schwerte, DE
Donkey Anti-Mouse Alexa 488	1:500	A-21202	Thermo Fischer Scientific	Schwerte, DE

Table 11 continued from page 48

Secondary antibody	Dilution	Cat. No.	Manufacturer	Registered office
Donkey Anti-Mouse Alexa 488	1:500	A-21202	Thermo Fischer Scientific	Schwerte, DE
Donkey Anti-Rabbit Alexa 488	1:500	A-21206	Thermo Fischer Scientific	Schwerte, DE
Donkey Anti-Rat Alexa 488	1:500	A-21208	Thermo Fischer Scientific	Schwerte, DE
Donkey Anti-Rabbit Alexa 546	1:500	A10040	Thermo Fischer Scientific	Schwerte, DE
Donkey Anti-Rabbit Alexa 647	1:500	A-31573	Thermo Fischer Scientific	Schwerte, DE
HRP-linked Anti-Mouse	1:3000	7076	Cell Signaling Technology	Danvers, USA
HRP-linked Anti-Rabbit	1:3000	7074	Cell Signaling Technology	Danvers, USA

3.1.9 Table 12: RNAscope Probes

Probe	Cat. No.	Manufacturer	Registered office
Mm-Drd1	461901	Advanced Cell Diagnostic	Newark, USA
Mm-Drd2	406501	Advanced Cell Diagnostic	Newark, USA
Mm-Gad1	400951	Advanced Cell Diagnostic	Newark, USA

3.1.10 Table 13: Enzyme

Enzyme	Cat. No.	Manufacturer	Registered office
Proteinase K	03115879001	Roche	Basel, CH

3.1.11 Table 14: PCR Primers for genotyping mice

PCR	Primer	Sequence 5'-3'
Gli2zfd	Gli2-S Gli2-AS Gli2neo-pA	AAACAAAGCTCCTGTACACG CACCCCAAAGCA TGTGTTTT ATGCCTGCTCTTTACTGAAG
Gli2flox	Flox C Flox D	AGGTCCTCTTATTGTCAGGC GAGACTCCAAGGTACTTAGC
Cre	Cre F Cre R	TAAAGATATCTCACGTACTGACGGTG TCTCTGACCAGAGTCATCCTTAGC
CreLK	CreLK Fwd CreLK Rev	GCATTACCGGTCGATGCAACGAGG GAACGCTAGAGCCTGTTTTGCACC

Table 14 continued from page 49

PCR	Primer	Sequence 5'-3'
GFP	GFP MS5 GFP MS6	ATCCTGGTCGAGCTGGACGGCGAG GCTCAGGGCGGACTGGGTGCTCC

3.1.12 Table 15: List of Mouse Lines

Name	Genotype	Allele symbol	Provided by/purchased from	Reference
Gli2 flox	*Gli2$^{flox/+}$*	Gli2tm6Alj/J	Alex Joyner, MSKCC, New York	Corrales et al., 2006
En1-Cre, Gli2-zfd	*En1$^{Cre/+}$; Gli2$^{zfd/+}$*	En1tm2(cre)Wrst/ J x Gli2 – zfd	Alex Joyner, MSKCC, New York	Corrales et al., 2006
En1-Cre, Gli2 cKO	*En1$^{Cre/+}$; Gli2$^{zfd/flox}$*	En1tm2(cre)Wrst/ J x Gli2 – zfd/ Gli2tm6Alj/J	Generated in the laboratory of S.Blaess	Blaess et al., 2006; Kabanova et al., 2015
Gad67-GFP	*Gad67-GFP pos*	CB6 – Tg(Gad1 – EGFP)G42Zjh/J	The Jackson Laboratory JAX stock #007677	Chattopadh yaya et al., 2004
Gli2-flox, Gad67-GFP	*Gli2$^{flox/+}$; Gad67-GFP pos*	Gli2tm6Alj/J x CB6 – Tg(Gad1 – EGFP)G42Zjh/J	Generated in the laboratory of S. Blaess	
En1-Cre, Gli2-zfd, Gad67-GFP	*En1$^{Cre/+}$; Gli2$^{zfd/+}$; Gad67-GFP pos*	En1tm2(cre)Wrst/ J x Gli2 – zfd x CB6 –Tg(Gad1 – EGFP)G42Zjh/J	Generated in the laboratory of S. Blaess	
En1-Cre, Gli2 cKO, Gad67-GFP	*En1$^{Cre/+}$; Gli2$^{zfd/flox}$; Gad67-GFP pos*	En1tm2(cre)Wrst/ J x Gli2 – zfd/ Gli2tm6Alj/J x CB6 –Tg(Gad1 – EGFP)G42Zjh/J	Generated in the laboratory of S. Blaess	

3.2 Methods

3.2.1 Mice

3.2.1.1 Mouse Breeding and Maintenance

Mice were housed in a controlled environment, with 12 hr light/night cycles and had access to food and water ad libitum. The transgenic mouse lines were maintained on a CD1/

C57BL/6 mixed background. To maintain the lines and to obtain animals for experiments, breedings were set up by pairing two females, aged at least six weeks old, with a male, aged at least eight weeks old. Pups were weaned at postnatal day 21. All experiments were performed in compliance with the regulations for the welfare of animals issued by the Federal Government of Germany, European Union legislation and the regulations of the University of Bonn. The protocol was approved by the Landesamt für Natur, Umwelt und Verbraucherschutz Nordrhein-Westfalen (Permit Number: 84-02.04.2014.A436, 81-02.04.2019.A415, 84-02.04.2017.A436).

3.2.1.2 Generation of *Gli2* conditional knockout mice

The *En1*$^{Cre/+}$*; Gli2*$^{zfd/+}$ mice were generated in the laboratory of A. Joyner by crossing En1Cre/+ knock-in mice (Kimmel et al., 2000) with Gli2zfd/+ mice (Mo et al., 1997), whereby the alleles became linked by intrachromosomal recombination (Corrales et al., 2006). In Gli2zfd/+ mice, a targeting vector containing 2.5 kb of 5' and 5kb of 3' genomic sequences was constructed in such a way that homologous recombination leads to deletion of 2.4 kb region of *Gli2* that contain exons coding for zinc fingers 3-5. For the zinc finger deleted (zfd) allele, this creates an out-of-frame mutation to the sequences from the deletion to the 3' end, resulting in a shortened protein that is unable to bind to the DNA (Mo et al., 1997). In Gli2 flox/+ mice, exons 7 and 8, upstream of the zinc finger encoding exons, are flanked by loxP sequences. Following mRNA splicing, cre-mediated recombination between the loxP sites of the floxed allele results in a frameshift mutation from exons 6 to 9 (Corrales et al., 2006). To create viable conditional knockout mice in which the transcription factor Gli2 was inactivated in the midbrain after E8.5, the En1$^{Cre/+}$; Gli2$^{zfd/+}$ mice were crossed with Gli2 $^{flox/+}$ mice to generate En1$^{Cre/+}$; Gli2$^{zfd/flox}$ mice (Blaess et al., 2006). The Gli2 $^{flox/+}$ mice were bred with the *Gad67-GFP* mouse line to generate *Gli2*$^{flox/+}$*; Gad67-GFP pos* mice, which were then further crossed with the En1$^{Cre/+}$; Gli2$^{zfd/+}$ mice and the En1$^{Cre/+}$; Gli2$^{zfd/flox}$ mice to generate control mice with GFP transgene *En1*$^{Cre/+}$*; Gli2*$^{zfd/+}$*; Gad67-GFP pos* and conditional knockout mice with GFP transgene *En1*$^{Cre/+}$*; Gli2*$^{zfd/flox}$*; Gad67-GFP pos*.

3.2.2 Genotyping

3.2.2.1 Tissue Biopsy and Lysis

To determine the genotype of the mouse, polymerase chain reaction (PCR) was carried out on tissue samples from mice 14 days or older. The ear biopsies obtained from mice were digested in 100 µL of lysis buffer and 1 µL of proteinase K at 60°C for 8 hours. Proteinase K was subsequently inactivated with an additional step of heat inactivation at 95°C for 10 minutes. The digested samples were centrifuged and 1 µL of digest supernatant was used

to perform PCR. In an alternative protocol, the tissue samples were digested in 75 µL of NaOH solution and incubated at 96°C for 1 hr. This was followed by addition of 75 µL of Tris HCl solution. The digested solution was diluted with dH_2O 10-fold and 1 µL of diluted digest supernatant was used to perform PCR.

3.2.2.2 Table 16: List of PCR Protocols

Cre PCR			
Reaction mix (20 µL)	**Thermocycler program**		
1 µL Template DNA	Steps	Temp. (°C)	Time (min)
0.16 µl dNTPs (25 nM)	1) 1st Denaturing	95	2:00
1 µL Cre F Primer (10 µM)	2) Denaturing	95	0:40
1 µL Cre R Primer (10 µM)	3) Annealing	59	1:00
2 µL PCR rxn buffer (1X)	4) Extension	72	0:50
14.04 µl dH_2O	5) Last Extension	72	10:00
0.6 µL $MgCl_2$ (1.5 mM)	6) Incubation	8	hold
0.2 µl Taq Polymerase	Steps 2-4 are repeated for 30 cycles		
	1.5% Agarose gel		
	Mutant band: 300 bp		

Cre LK PCR			
Reaction mix (20 µL)	**Thermocycler program**		
1 µL Template DNA	Steps	Temp. (°C)	Time (min)
0.16 µl dNTPs (25 nM)	1) 1st Denaturing	95	2:00
1 µL CreLK Fwd Primer (10 µM)	2) Denaturing	95	0:40
1 µL CreLK Rev Primer (10 µM)	3) Annealing	59	1:00
2 µL PCR rxn buffer (1X)	4) Extension	72	0:50
14.04 µl dH_2O	5) Last Extension	72	10:00
0.6 µL $MgCl_2$ (1.5 mM)	6) Incubation	8	hold
0.2 µl Taq Polymerase	Steps 2-4 are repeated for 30 cycles		
	1.5% Agarose gel		
	Mutant band: 330 bp		

GFP PCR			
Reaction mix (20 µL)	**Thermocycler program**		
1 µL Template DNA	Steps	Temp. (°C)	Time (min)
0.16 µl dNTPs (25 nM)	1) 1st Denaturing	95	2:00
1 µL GFP MS5 Primer (10 µM)	2) Denaturing	95	0:40
1 µL GFP MS6 Primer (10 µM)	3) Annealing	59	1:00
2 µL PCR rxn buffer (1X)	4) Extension	72	0:50

Table 16 continued from page 52

GFP PCR			
Reaction mix (20 µL)	**Thermocycler program**		
14.04 µl dH_2O	5) Last Extension	72	10:00
0.6 µL $MgCl_2$ (1.5 mM)	6) Incubation	8	hold
0.2 µl Taq Polymerase	Steps 2-4 are repeated for 30 cycles		
	1.5% Agarose gel		
	Mutant band: 600 bp		

Gli2-zfd PCR			
Reaction mix (20 µL)	**Thermocycler program**		
1 µL Template DNA	Steps	Temp. (°C)	Time (min)
0.16 µl dNTPs (25 nM)	1) 1st Denaturing	94	5:00
1 µL Gli2-S Primer (10 µM)	2) Denaturing	94	1:00
1 µL Gli2-AS Primer (10 µM)	3) Annealing	58	1:00
1 µL Gli2 neo-pA Primer (10 µM)	4) Extension	72	1:30
2 µL PCR rxn buffer (1X)	5) Last Extension	72	10:00
13.04 µl dH_2O	6) Incubation	8	hold
0.6 µL $MgCl_2$ (1.5m M)	Steps 2-4 are repeated for 35 cycles		
0.2 µl Taq Polymerase			
	1.5% Agarose gel		
	Wildtype band: 300 bp; Mutant band: 550 bp		

Gli2-flox PCR			
Reaction mix (20 µL)	**Thermocycler program**		
1 µL Template DNA	Steps	Temp. (°C)	Time (min)
0.16 µl dNTPs (25 nM)	1) 1st Denaturing	94	5:00
1 µL Flox C Primer (10 µM)	2) Denaturing	94	1:00
1 µL Flox D Primer (10 µM)	3) Annealing	58	1:00
2 µL PCR rxn buffer (1X)	4) Extension	72	1:30
14.04 µl dH_2O	5) Last Extension	72	10:00
0.6 µL $MgCl_2$ (1.5 mM)	6) Incubation	8	hold
0.2 µl Taq Polymerase	Steps 2-4 are repeated for 30 cycles		
	2% Agarose gel		
	Wildtype band: 231 bp; Mutant band: 247 bp		

3.2.3 Histology

3.2.3.1 Tissue fixation and perfusion

Mice of all postnatal stages were perfused transcardially to preserve brain tissue for immunohistology and *in situ* hybridization. An intraperitoneal injection of Ketanest/Rompun was used to achieve anesthesia and absence of response to toe or tail pinches was checked before operating on the animal. Each mouse was first perfused with 30-50 mL PBS to flush

out the blood. Once the fluid flowing out of the right atrium was clear, PBS was switched to 4% PFA for tissue fixation. After perfusion with 50 mL of 4%PFA, the mouse was decapitated and the skin and muscles covering the cranium were removed. The skull bone was carefully chipped off from the caudal end to expose the brain. The nerve tracts on the ventral surface of the brain were cut off and the brain was scooped out and transferred to a liquid scintillation vial containing 4% PFA to post-fix overnight at 4°C on a shaker.

3.2.3.2 Cryopreservation

Following overnight fixation in 4% PFA, the brain was transferred to 15% sucrose in PBS solution and kept at 4°C on a shaker until it sank to the bottom of the vial. The brain was next transferred to a 30% sucrose in PBS solution and again kept at 4°C on a shaker until it sank to the bottom of the vial. The brain was embedded in a cryomold filled with OCT TissueTek, put on dry ice to freeze and then stored in a -80°C freezer.

3.2.3.3 Cryosectioning

The frozen OCT block containing the brain was cryosectioned with a Leica cryostat (CM 3050S). The temperature of the cryo-chamber, including the cryo-block and the blade, was maintained at -20°C. The brains were sectioned at 40 µm thickness and collected as free-floating sections in a 24-well plate or 96-well plate filled with Walter´s antifreeze solution and stored in a -20°C freezer.

3.2.3.4 Immunostaining

For immunostaining, 40µm free floating sections were first rinsed with PBS for 5 minutes and then with 0.3% PBT for 5 minutes. Then they were incubated in a blocking buffer solution of 10% NDS in 0.3% PBT for 1 hour. Sections were incubated in primary antibody solution overnight at 4°C. All primary antibodies were diluted in 3% NDS in 0.3% PBT. The following primary antibodies were used at dilutions stated herein: rabbit anti-parvalbumin (1:1000), rabbit anti-calbindin (1:2000), goat anti-calretinin (1:2000), rabbit anti-NET (1:2000), rabbit anti-SERT (1:5000), mouse anti-TH (1:500), rat anti-GFP (1:2000), rat anti-Ctip2 (1:500). For anti-SERT immunostaining, sections were incubated in blocking solution of 3% NDS in 0.5% PBT for 2 hours at room temperature.

Following primary antibody incubation, sections were washed 3 times (10 minutes each) with 0.3% PBT and incubated in secondary antibody solution for 2 hours at room temperature. All secondary antibodies were diluted in 3% NDS in 0.3% PBT. The following secondary

antibodies were used at dilutions stated herein: donkey anti-goat biotin (1:500), donkey anti-rabbit biotin (1:500), Cy3 Streptavidin (1:1000), Alexa 647 Streptavidin (1:500), donkey anti-rabbit Alexa 488 (1:500), donkey anti-mouse Alexa 488 (1:500), donkey anti-rat Alexa 488 (1:500), donkey anti-rabbit Alexa 546 (1:500), donkey anti-rat Cy3 (1:200), donkey anti-rabbit Alexa 647 (1:500) . Hoechst solution was diluted (1:10000) in the secondary antibody solution. Following secondary antibody incubation, sections were washed 3 times (5 minutes each) in 0.3% PBT. For biotinylated secondary antibodies, the sections were further incubated in fluorophore conjugated streptavidin solution for 1 hour and rinsed with 0.3% PBT 3 times (5 minutes each). All washing and incubation steps were carried out in a 24-well plate on a gently nutated platform.

After staining, sections were mounted on Superfrost slides (Menzel-Gläser) and allowed to air dry at room temperature for several minutes. The slides were then carefully coverslipped with Aqua Polymount to avoid trapping air bubbles, dried overnight, and stored at 4°C.

3.2.3.5 Multiplex-fluorescence *in situ* hybridization

RNAscope® Fluorescent Multiplex assay is an advanced approach of *in situ* hybridization (ISH) technique that permits single transcript detection with minimal or no background signal (Wang et al., 2012). RNAscope® assay was performed according to the instructions provided by the manufacturer for frozen tissue (User Manual: 323100-USM, Advanced Cell Diagnostics) and adapted for free-floating sections as described below.

Pretreatment. 40μm free-floating sections were removed from cryoprotectant, washed in DPBS and mounted on SuperFrost plus slides carefully to avoid bubbles and folds. Once mounted, the sections were dried at 40°C for 30 minutes. 4% PFA was freshly prepared with DBPS and the dried slides were incubated for 10 minutes. Following fixation, the slides were washed in DPBS thrice for 3 minutes and dehydrated in ethanol solutions of 50%, 70% and 100%, for 3 minutes each. 50% and 70% ethanol solutions were prepared with sterile water. The slides were dried at 40°C for 20 minutes. The sections were next incubated in RNAscope® hydrogen peroxide reagent for 10 minutes and washed in sterile water twice for 2 minutes.

Heat Induced Antigen Retrieval. RNAscope® Target Retrieval Reagent 1X was prepared with sterile water on the day of the assay. While the sections were incubated in hydrogen peroxide, the steamer was turned on and the HybEZ™ oven was set to 40°C. Once the target retrieval solution was heated up to at least 98°C, the slides were immersed in sterile water for a few seconds and then transferred to the target retrieval solution for 3 minutes in the

steamer. The slides were washed in sterile water twice for 2 minutes, dehydrated in 100% ethanol for 3 minutes and further dried in the oven at 40°C for 20 minutes.

Protease Induced Antigen Retrieval. Once dried, a barrier was drawn around the sections with a hydrophobic pen. The slides were loaded to the horizontal batch slide holder and placed in a pre-warmed humidity control tray. A wet absorbent paper was placed in the humidity control tray and the tray was always kept inside the oven, when not in use. The sections were covered with adequate drops of RNAscope® Protease III Reagent and incubated for 15 minutes at 40°C in the HybEZ™ oven. The slides were washed in sterile water twice for 2 minutes.

Probe Hybridization. The probe solution was prepared during incubation of protease treatment. The probes and probe diluent were heated at 40°C for 15 minutes in a water bath. The probes were briefly spinned down and mixed with RNAscope® probe diluent at a concentration of 1:50. The sections were covered with probe solution and incubated for 2 hours at 40°C in the humidity control tray in the HybEZ™ oven. The slides were washed in RNAscope® Wash Buffer Reagent 1X twice for 2 minutes and stored overnight at room temperature in SSC 5X.

Signal Amplification. The slides were washed in wash buffer twice for 2 minutes and the residual wash buffer on the slide was flicked away gently. The sections were incubated sequentially with RNAscope® Multiplex FL v2 Amp 1 for 30 minutes, RNAscope® Multiplex FL v2 Amp 2 for 30 minutes and RNAscope® Multiplex FL v2 Amp 3 for 15 minutes in the humidified tray in the HybEZ™ oven at 40°C. After each amplification step, the slides were washed in wash buffer twice for 2 minutes. The assay was continued further to develop signal for each probe channel separately and the HRP specific to the probe channel was chosen accordingly. TSA fluorophores were diluted in TSA buffer at a concentration of 1:3000. The sections were incubated with RNAscope® Multiplex FL v2 HRP-C2 or RNAscope® Multiplex FL v2 HRP-C3 for 15 minutes and then with TSA Cyanine3 or TSA Cyanine5 for 30 minutes and finally with RNAscope® Multiplex FL v2 HRP blocker for 15 minutes in the HybEZ™ oven at 40°C. After each incubation step, the slides were washed in wash buffer twice for 2 minutes.

Cell nuclei were counterstained by adding a few drops of DAPI solution to the sections and incubating for 30 seconds at room temperature. Excess DAPI solution was gently flicked off the slides. The slides were then carefully coverslipped with Aqua Polymount to avoid trapping air bubbles and dried overnight at room temperature in the dark.

For combined *in situ* hybridization and immunohistochemistry, free-floating 40μm sections were first immunostained according to the protocol earlier (see section 3.2.3.4). They were

then mounted on SuperFrost plus slides and the RNAscope® assay was performed as described above.

3.2.4 Gel Electrophoresis and Western Blotting

Tissue lysate preparation for immunoblotting involved performing all steps at low temperature and as quickly as possible to reduce protease activity and protein degradation. The mouse was sacrificed by cervical dislocation and decapitated immediately. The brain was removed from the cranium, washed with cold PBS and placed into a pre-chilled brain matrix. The prefrontal cortex was cautiously dissected out, transferred to a Eppendorf tube and snap-frozen in liquid nitrogen.

The protease inhibitor cocktail tablet was dissolved in 10 mL PBS 1X and added to the tissue (2 ml per 100 mg tissue) for homogenization in a bead mill homogenizer. The contents were then sonicated and centrifuged. The supernatant was collected in a fresh Eppendorf tube and the protein concentration was measured using a spectrophotometer. The volume of lysate was determined to ensure 60 µg protein in each well. Laemmli buffer 4X was added to the sample and boiled at 95°C for 5 minutes. Protein separation according to molecular weight was done by SDS-PAGE. A 12% resolving gel, overlaid with a 5% stacking gel, was used to separate calbindin and the DRD2 proteins (see section 3.1.7, Table 8 for more details on the gels). The gels were run at 60-80 V while proteins were stacked and at a higher voltage (100 V) when protein bands entered the resolving gel. Proteins were blotted on a nitrocellulose membrane in a wet blot chamber, at 45 mA overnight in a cooling room (4° C) or at 100 V for 90 minutes, set in ice. The membrane was blocked with 5% non-fat dry milk solution in 0.1% Tween-20 in PBS buffer and incubated in primary antibody solution overnight at 4°C. The following primary antibodies were used: rabbit anti-calbindin (1:2000), rabbit anti-DRD2 (1:500), mouse anti-ß-actin (1:10000). The membrane was washed three times for 10 minutes and incubated in secondary antibody solution for 1 hour at room temperature. The following secondary antibodies were used: HRP-linked anti-rabbit (1:3000) and HRP-linked anti-mouse (1:3000). The membranes were washed again three times for 10 minutes. 1% non-fat dry milk solution in 0.1% Tween-20 PBS buffer was used for all antibody dilution and washing. The blot was developed by incubating in HRP-substrate (100 µL per 1 cm^2) for 5 minutes in the dark and imaged at the chemiluminescence detector using Image Lab. Western blotting experiments were performed together with Antonia-Antigoni Sinani (Erasmus Mundus master student).

3.2.5 Behavioral test for assessing working memory

Male mice aged between P90-P100 were transferred to the behavioral testing facility a week prior to the training and handled daily. Each experimental animal was housed in a separate cage and put in a ventilated cabinet. During the training and testing period, the mice were kept under food restriction that maintained their weights at 85–90% of their free-feeding weight. The controlled feeding method was based on description by (Wahlsten, 2010) and detailed in the table below. This restricted diet schedule was maintained for a maximum of four weeks, which allowed for a sufficient number of sessions.

3.2.5.1 Table 17: Controlled Feeding of Experimental Animals

Friday	The animals are weighed. Excess but counted feed pellets are put in the feed trough.
Sunday	The animals are weighed, and unused feed counted. The mean body weight is calculated, and the daily food consumption is determined. The feed is removed.
Monday	The animals are weighed. The behavioral experiment is carried out. 50% of the previously determined daily consumption is put in the feed trough.
Tuesday	The animals are weighed. The behavioral experiment is carried out. 50% of the previously determined daily consumption is put in the feed trough.
Wednesday	The animals are weighed. The behavioral experiment is carried out. 50% of the previously determined daily consumption is put in the feed trough.
Thursday	The animals are weighed. The behavioral experiment is carried out. 50% of the previously determined daily consumption is put in the feed trough.
Friday	The animals are weighed. The behavioral experiment is carried out. Excess but counted feed pellets are put in the feed trough.

3.2.5.2 Forced-alternation, choice-alternation and delayed-alternation tasks

The behavioral sessions were carried out in a dimly lit room and the lighting was maintained at a constant level throughout all sessions. The maze (W 90 cm, L 80 cm; H 30 cm) consisted of a black PVC floor and transparent perspex walls. The animal was brought into the testing room at least 30 minutes before the first trial began. All the experiments were performed around the same time of the day, between 9:00 am and 2:00 pm.

The training period consisted of three phases. During habituation, the animals were allowed to freely explore the maze for 10 minutes with 9 sugar pellets sprinkled across the maze to encourage exploration. The maze was cleaned with 70% ethanol between animals. The mice

were next subjected to a forced-alternation task, where the animals were forced to alternate between the two reward arms by the experimenter for 30 laps. The food rewards were offered alternately in the corresponding reward area. Following the forced-alternation training phase, the animals moved onto the choice-alternation training phase. The first trial in this phase was always rewarded and marked as trial 0. The animals were then given 20 attempts so that they learned to turn left and right alternately at the decision-making junction. The rewards were offered accordingly in the alternating arms. To make a correct choice, the mouse had to remember the direction of the previous run and choose the other goal arm. The test phase started once the animals had reached the criterion of 80% correct decision in a session, on 2 out of 3 days, after 10 days of training. In the test phase, the animals first went through 10 attempts of choice runs and then further 10 trials consisting of the delayed-alternation task. For delay trials, the animals were confined within the center arm by two barriers for 30 seconds after each run. The animals were allowed to rest in their home cages for 30 minutes after each session before being returned to the incubator. The animals were sacrificed once the behavioral test was completed.

Training Phase								**Test Phase**
Day1	**Day2**	**Day3-Day5**	**Day6-Day7**	**Day8-Day12**	**Day13-Day14**	**Day15-Day19**	**Day20-Day21**	**Day22-26**
Habituation		Forced Alternation	*Break*	Choice Alternation	*Break*	Choice Alternation	*Break*	Choice Alternation & Delayed Alternation

Table 18. Timeline of the experimental design for assessment of spatial working memory in mice in an eight-maze.

3.2.6 Image Acquisition

For fluorescent detection of calcium-binding proteins in the PFC, immunostained sections from P19, P26, P33 and P60 postnatal stages were imaged at an inverted Zeiss AxioObserver Z1 equipped with Zeiss AxioCam MRm (Carl Zeiss). Tile images were acquired with conventional epifluorescence using the 20X objective (EC PlnN 20x/0.5, Carl Zeiss) and stitched with Zen blue software (Zeiss, 2012). Immunostained sections of calcium binding proteins from P12 stage were imaged at Zeiss Axio Scan.Z1 slide scanner with 20X objective (PlanNeofluar 20x/0.5) using the Zen 2 software (Zeiss, 2014). Those from P90 and P120 postnatal stages were imaged at an inverted Zeiss AxioObserver equipped with a CSU-W1 confocal scanner unit (50 µm pinhole disk, Yokogawa). Z-stacks (8 stacks, z-step=2µm) were acquired at 20X (PlanApochromat 20x/0.8) magnification and tile images were stitched with VisiView software (Visitron Systems). For intensity analysis of interneurons, PFC sections from postnatal stages

P33 and P60 were also imaged at the inverted Zeiss AxioObserver equipped with a CSU-W1 confocal scanner unit at 20X (PlanApochromat 20x/0.8) magnification with the same settings.

Confocal images of monoaminergic innervation of the PFC were acquired at Leica TCS SP8 upright microscope with 63X objective (HC PL APO 63X/1.3 Gly, Leica Microsystems). Z-series of 67 stacks were acquired at 1024 × 1024 pixel resolution, with a z-step of 0.15 µm. Acquisition parameters were kept constant across controls and cKOs.

To visualize *in situ* hybridized signal, imaging was performed at Zeiss AxioObserver with CSU-W1 confocal scanner unit at 40X magnification (C- Apochromat, 40x/1.2 water, Zeiss) keeping identical microscope settings for control and cKO. Z-series of 12 stacks were acquired with a z-step of 1 µm and montage images were stitched with VisiView software. For all z-stack acquisitions, images were represented as maximum intensity projections (MIP) of z-series.

3.2.7 Data Analysis

Images were analyzed from sections containing all three subdivisions of the mPFC located between bregma level 1.78mm and 1.54mm. The exceptions include images analyzed for CB cell density (located between bregma level 2.1mm and 1.98mm) and those selected for measurement of prefrontal cortical thickness (located between bregma level 2.34mm and 2.1mm).

3.2.7.1 Cell density analyses

Using ImageJ software (Schneider et al., 2012), the mPFC was traced on each image by overlaying the matching Bregma level from the mouse brain atlas (Paxinos and Franklin, 2004). The mPFC was divided into upper and deeper layers for all analyses. The mean gray value of each image was deducted to help differentiate between labeled cells and background. For CB cell density analysis, subtraction of 25% mean gray value allowed better demarcation of the immunopositive cells from background. For densiometric quantification, fluorescently labeled cells having intensity above the mean gray value were counted manually, aided by the ‘Cell Counter’ plugin and normalized to their respective area.

3.2.7.2 PV intensity analysis

For PV intensity analysis, acquisition settings were set during imaging P120 control sections. These acquisition settings were duplicated for control and cKO sections across all analyzed ages. The soma of the immunolabeled PV neuron was marked at the spot exhibiting optimal

staining. The intensity values were recorded with the 'Cell Counter' plugin in ImageJ software. White matter value obtained from corpus callosum within the same image was subtracted from each intensity value for background correction.

3.2.7.3 Quantification of monoaminergic fibers

Projections were analyzed in the upper and deeper layers of the mPFC. Anatomical regions of interest were verified at 10X magnification by referencing to the mouse brain atlas before acquiring images with a 63X objective. Each acquisition area (175.74 µm X 175.74 µm) was processed using the Digital Enhancement of Fibers with Noise Elimination (DEFiNE) macro for Fiji (Powell et al., 2019). The workflow involved first the 'Clean Images' function, which converted the stacked image into a binary mask and removed big non-axonal particles. The processed z-stacks were then converted to MIP and other smaller fluorescent artifacts were removed. Once the background noise was removed, ten 12 × 12 μm^2 regions with no labeled fibers were manually set to measure mean pixel intensity and standard deviations of the selected regions. A threshold of 4 standard deviations was set above the mean background pixel intensity and labeled axonal fibers with intensity above the defined threshold were recorded to compute the total area occupied by the fibers (in μm^2).

3.2.7.4 Analysis of ISH signal

The image analysis software CellProfiler (Stirling et al., 2021) was used for a non-biased automated analysis of fluorescent signal from RNAscope assay. The pipelines used for analysis were based on 'Speckle Counting' (http://cellprofiler.org/examples/#Speckles), adjusted and optimized for individual experiments. For the *Gad1* target mRNA, a threshold was set at 2 standard deviations above mean pixel intensity. Signal dots or puncta with diameter between 3 and 20 pixels that were located within the PV cells (diameter between 50-130 pixels) were recorded. For *Drd1* and *Drd2* target genes, the threshold was set at 3 standard deviations above mean pixel intensity. The area, within which the signal dots were quantified, was expanded from the nuclear outline to include cell cytoplasm. Puncta with diameter between 3 and 20 pixels that were located within 20 pixels of the DAPI-positive nuclei (diameter between 35-135 pixels) were recorded. Since each signal punctum corresponded to a single molecule of target mRNA, quantification of the number of puncta per cell determined the expression level of the gene of interest.

3.2.7.5 Densitometric analysis of immunoblots

After image acquisition with Image Lab software (Bio-rad), protein bands were quantified using ImageJ software and normalized to that of β-actin, the loading control. The quantification of protein bands was performed by Antonia-Antigoni Sinani.

3.2.8 Statistical Analysis

Statistical analyses were performed with GraphPad Prism 9 (GraphPad Softwares) and data are reported as mean ± standard error of the mean (s.e.m) where applicable. Two-way analysis of variance (ANOVA) with age and genotype as the two main factors was used to analyze the cell densities and noradrenergic innervation in control and cKO. If significant effects of age or genotype were found, it was followed by Šídák's *post-hoc* multiple comparisons test. Statistical analysis of CB:PV cell density ratio and serotonergic innervation in control and cKO was done using Mann Whitney test. Data sets of *Gad1*, *Drd1, Drd2* gene expression were tested for normal distribution and then statistically analyzed using Kolmogorov-Smirnov test. Performance of mice in a spatial working memory task was evaluated using two-way ANOVA, followed by either Šídák's multiple comparisons or Fisher's least significant difference (LSD) *post-hoc* tests. P values of less than 0.05 were considered statistically significant.

4. Results

4.1 Developmental changes in CR, CB and PV interneuron population in the mPFC

Density analysis of cells expressing calcium binding proteins in the mFPC was performed at multiple developmental stages, spanning from early postnatal phase (P12, P19) to full adulthood (P120), with juvenile stage (P26), early adolescence (P33), late adolescence/young adulthood (P60) and adulthood (P90) in between. The mPFC was segmented into upper and deeper layers for analysis **(Fig. 5A, 6A, 7A)** to isolate any impact of denser input of TH-positive fibers to the deeper layers compared to the upper layers.

4.1.1 The density of CR interneurons in the mPFC remains unaltered throughout development

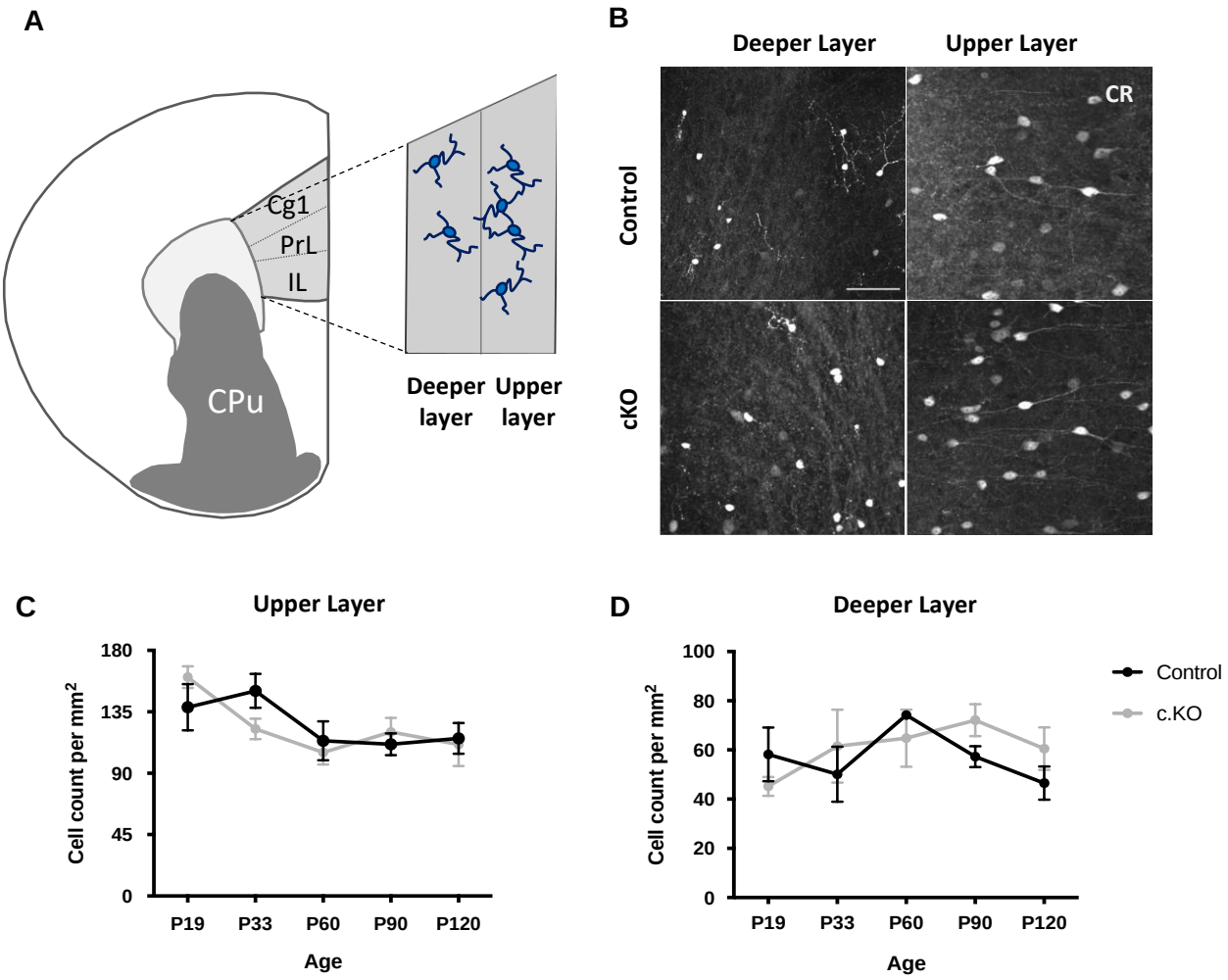

Figure 5. CR cell density in the mPFC throughout postnatal development. (A) The diagram shows the mPFC and its subregions. The subregions are further divided into upper and deeper layers and the relative distribution of CR cells in these layers is shown. (B) Representative images (20x magnification) of immunofluorescent staining for CR from PrL cortex on P90 coronal sections show that CR cell density in control and cKO is similar. (Figure legend continued on next page)

continued from Figure 5. (C, D) There is no significant change in cell density during development in the upper layers (C) and deeper layers (D) of control and cKO mPFC. (P19-P60 cell count was performed by Emmy Raafat Nabil Sedky). n=3-5 mice per group. Error bars indicate mean +/- SEM. Scale bar: 50 µm.

Analysis of developmental trajectory of CR immunostained cells **(Fig. 5C)** revealed no significant difference between early postnatal phase and full adulthood in control and cKO mice (**Fig. 5C, D,** P19-P60 cell count was performed by Emmy Raafat Nabil Sedky). Two-way ANOVA showed that there was also no significant effect of genotype and no genotype x age interaction in either layers. In the upper layer, there was a significant effect of age ($F_{(4, 35)}$ = 8.898, p = 0.0113) but no significant post-hoc differences were found upon further analysis. The CR expressing cells are relatively scattered in the deeper layer **(Fig. 5B)** and neither control nor cKO mice showed any changes across the analyzed age groups **(Fig. 5D)**.

These findings are similar to previous description of CR cell count at P25-35, P45-P55 and P65-75 in rats, which report no significant differences in cell count among the three age groups studied but a trend towards decreased CR fluorescence between P25-35 and P45-55 (Caballero et al., 2014).

4.1.2 CB cell density in the upper layer fluctuates in cKO mice between juvenile stage and late adolescence

CB immunostaining showed that CB expressing cells are present across the layers II-VI but most prominent in layer II and III **(Fig. 6B)**. The CB positive neurons of layer II are however weakly stained and it was particularly challenging to distinguish them from background. A further technical limitation of CB immunohistochemistry in this study included CB immunostained layer II/III pyramidal neurons, which were not possible to be discriminated from interneurons during analysis. Immunohistochemical analysis of CB positive cells (P12-P60 cell count was performed by Bianca Broske) in upper layer presented no apparent alterations in cell density across postnatal development in control mice. Caballero and colleagues have earlier likewise shown that CB immunoreactivity remained constant across development in rats (Caballero et al., 2014). In contrast, the cell density was found to vary considerably between P26 and P60 in cKO mice **(Fig. 6C)**. There was a significant effect of age ($F_{(6, 53)}$ = 8.898, p < 0.0003) in the upper layer and post-hoc analysis revealed that in cKO, the CB cell density at P33 is significantly lower compared to P60 (t=5.331, p<0.0001). There was also a trend for reduced CB cell density in cKO at P33 compared to P26 (t=3.174, p=0.09). No differences were detected in post-hoc analysis across ages in control mice. These data indicate that CB expression is not properly regulated during the adolescent period in cKO mice. In the deeper layer, the CB cell density remained stable until P33 and then increased

significantly between P60 and P90, both in control (t = 4.413, p=0.002) and cKO (t = 4.146, p=0.005) mice **(Fig. 6D)**.

4.1.3 CB protein level in the mPFC of control and cKO during late adolescence

Since CB cell density exhibited significant fluctuation during adolescence, in particular in cKO mice, immunoblotting analysis was performed at P60 to determine whether the expression of CB in cKO varied from that in control (experiments and analysis were performed by Antonia-Antigoni Sinani). However, unpaired t-test showed that there was no detectable difference in CB protein levels in the mPFC of control and cKO animals (p=0.39) **(Fig. 6E)**.

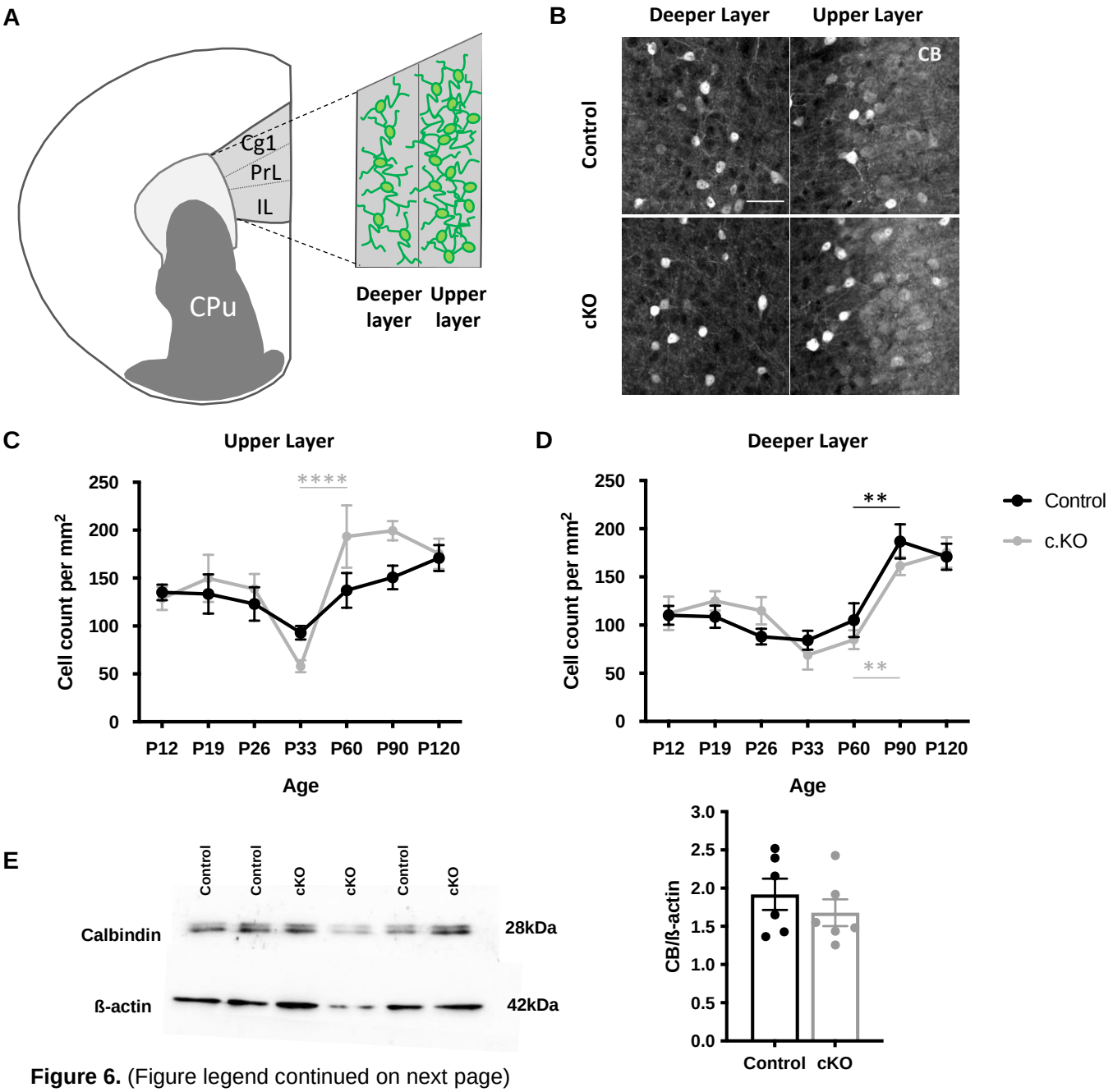

Figure 6. (Figure legend continued on next page)

Figure 6. CB cell density in the mPFC of cKO mice fluctuates during postnatal development. (A) The diagram shows the mPFC and its subregions. The subregions are further divided into upper and deeper layers and the relative distribution of CB cells in these layers is shown. (B) Representative images (20x magnification) of immunofluorescent staining for CB from PrL cortex on P90 coronal sections show a dense band of CB positive cells in the upper layers. (C) While there is no marked variation in cell density across postnatal development in the upper layer of control animals, cell density in cKO animals shows a significant change between early adolescence and late adolescence. (D) The cell density remained relatively constant throughout development in deeper layers for control and cKO (P12-P60 cell count analysis was performed by Bianca Broske). (E) Western blots on mPFC tissue from P60 control and cKO brains show no change in relative protein levels of CB (experiments and analysis were performed by Antonia-Antigoni Sinani). Two-way ANOVA; Šídák's multiple comparisons *post-hoc* test. **p<0.01, ****p<0.0001. n=4-6 mice per group. Error bars indicate mean +/- SEM. Scale bar: 50 µm.

4.1.4 PV neuron density in deeper layer is altered in cKO mice during late adolescence

Visual inspection of PV immunoreactivity in the mPFC revealed that PV positive cells can be detected across the layers II-VI, with noticeably more PV expressing cells in the deeper layers than the upper layers **(Fig. 7B)**. In the upper layer, the PV cell density did not show any marked changes across development **(Fig. 7C)**. Consistent with previous reports in rodents (Caballero et al., 2014; Du et al., 2018), both groups of mice showed a developmental increase in PV cell density in deeper layers between early postnatal phase and early adolescence **(Fig. 7D)**. Two-way ANOVA reported a significant effect of age ($F_{(6, 65)}$ = 21.6, p < 0.0001) and post-hoc analysis revealed that the surge in cell density between P12 and P33 was significant in mice of both genotypes. Two-way ANOVA also detected an effect of genotype ($F_{(1, 65)}$ = 5.76, p = 0.0193) and a significant difference between control and cKO mice was identified at P60 (t=3.410, p=0.0078). To examine if the divergence was indeed due to the genotype, a region where mDA projections are negligible in mice was examined. In the somatosensory cortex, PV cell densities in cKO mice and control mice were comparable at P60 **(Fig. 7E)**, indicating that the reduction in PV density in cKO mice may have resulted from altered maturation of mDA projections in the mPFC. The developmental course followed by PV interneurons was very similar in control and cKO mice until it reached peak cell density at P33 **(Fig. 7D)**. As the control mice transitioned from adolescence into adulthood, there were no further significant changes in cell density. The cKO mice, on the other hand, showed a marked decline in cell density between P33 and P60 (t=3.829 p=0.0121). The cell density in cKO mice is eventually comparable to the controls as the mice reach adulthood. Together, these data imply that in absence of mesoprefrontal innervation, the developmental trajectory of PV interneurons in the mPFC is disrupted during adolescence.

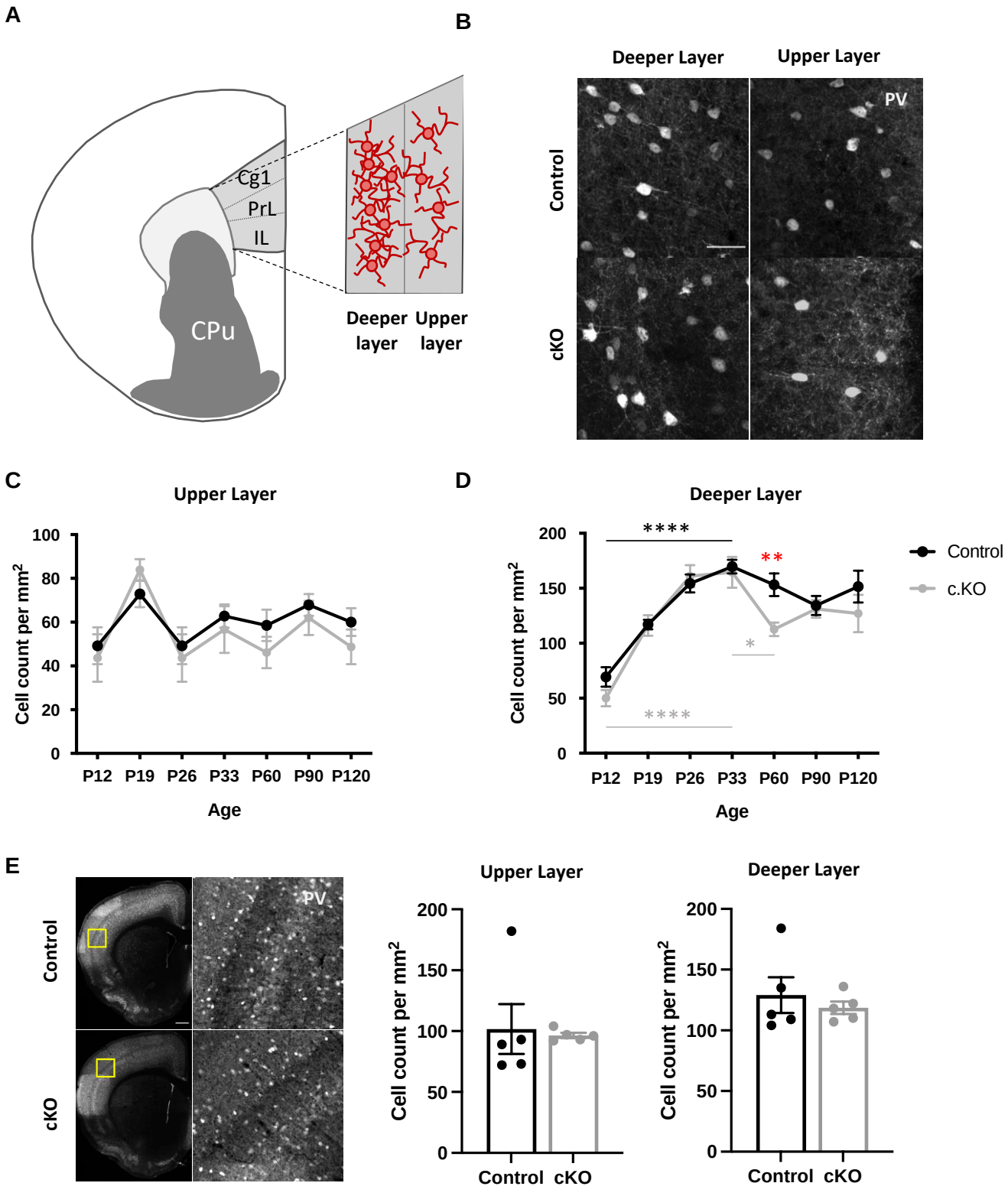

Figure 7. Postnatal development of PV cell density in the mPFC and SSC. (A) The diagram shows the mPFC and its subregions. The subregions are further divided into upper and deeper layers and the relative distribution of PV cells in the two layers. (B) Representative images (20x magnification) of immunofluorescent staining for PV from PrL cortex on P90 coronal sections show that PV cell density is higher in deeper layers. (C) Neither cKO nor control animals show a change in cell density in the upper layer during postnatal development. (D) Control and cKO mice exhibit peak PV density at P33. This is followed by a significant reduction in cell density in cKO at P60. (Figure legend continued on next page)

continued from Figure 7. (E) PV interneuron densities in the SSC of control and cKO mice at P60 are similar. The left panel of the image shows coronal sections from control and cKO mice displaying the upper and deeper layers of the SSC within the boxed area. The right panel images are enlargements of the boxed areas. n=4-9 mice per group. Error bars indicate mean +/- SEM. Two-way ANOVA; Šídák's multiple comparisons *post-hoc* test. *p<0.05, **p<0.01, ****p<0.0001. Red asterisk denotes significant difference between control and cKO. Scale bars: 50 µm (B) and 500 µm (E).

4.1.5 The ratio of CB to PV cell density is comparable between control and cKO mice

Since the density of CB and PV interneurons in cKO mice deviated from the developmental trajectory observed in control mice, especially during adolescence, the proportions of CB positive neurons and PV expressing neurons at P60 were examined further. The ratios of CB to PV cell densities for individual animals were determined at first to calculate the mean ratio of PV to CB cell density for each group. The CB:PV density ratio in cKO mice and control mice is comparable in deeper layers **(Fig. 8B)**. While a slight variation in the ratio between the groups is visible in upper layers **(Fig. 8A)**, the Mann-Whitney test revealed that the difference between control and cKO did not reach any statistical significance (p=0.11 for both upper and deeper layers).

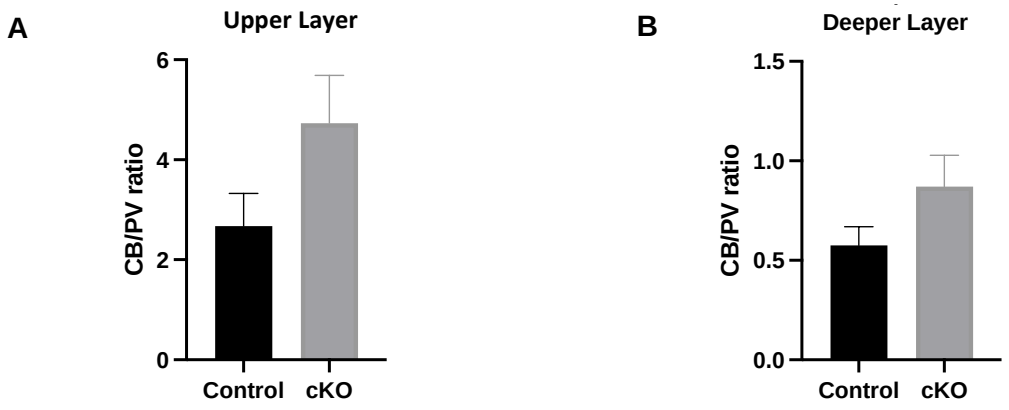

Figure 8. Ratio of CB cell density to PV cell density in the (A) upper and (B) deeper layers in mPFC of cKO and control mice is comparable at P60. Error bars indicate mean +/- SEM.

4.1.6 Fluorescence intensity of PV neurons differ between control and cKO at multiple developmental stages

To assess if the observed changes in PV cell density during late adolescence was accompanied with changes in PV expression level, the fluorescence intensity of PV immunostained cells was analyzed during adolescence and adulthood in the deeper layers. The highest intensity value of individual PV neurons was recorded from control and cKO groups and after subtracting the white matter value for background correction, fluorescence

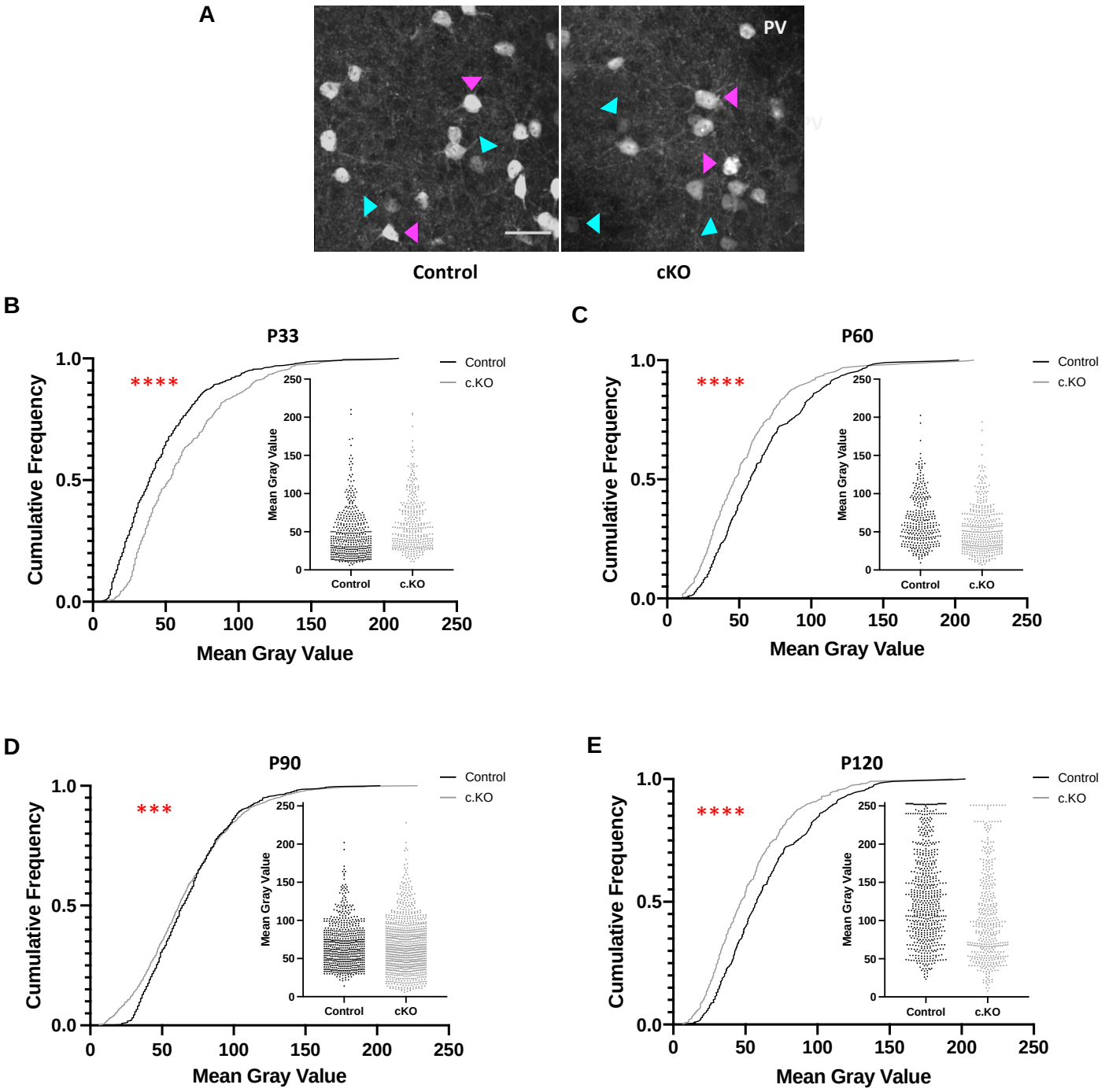

Figure 9. Fluorescence intensity of PV interneurons in the mPFC across different stages of development. (A) Representative images (20x magnification) of immunofluorescent staining for PV on P90 coronal sections from PrL cortex show that control animals have a higher percentage of high PV-expressing cells (magenta arrowheads) than cKO animal in the deeper layer. Low PV-expressing cells are indicated by cyan arrowheads. (B-E) Cumulative frequency plots and scatterplots (inset figures) of the recorded fluorescent intensities of individual PV interneuron at (B) P33, (C) P60, (D) P90 and (E) P120 show the range of fluorescence intensity of PV interneuron population in control and cKO. While the cKO mice contained less low-expressing PV neurons than control mice at P33 (B), the proportion of low-expressing PV interneurons was more in cKO mice compared to control mice at P60 (C) and P120 (E). Kolmogorov-Smirnov test. ***p<0.001, ****p<0.0001. n=3-9 animals per group. Number of cells, N=423 (control), N=333 (cKO) at P33; N=309 (control), N=407 (cKO) at P60; N=624 (control), N=944 (cKO) at P90; N=629 (control), N=429 (cKO) at P120. Scale bar: 50 µm.

intensity values of the two groups were compared. At P33, the cumulative frequency distribution of PV fluorescence intensity recorded in cKO mice was shifted toward higher intensity values relative to the control mice **(Fig. 9B)** but at P60, the cumulative probability plot of PV fluorescence intensity in cKO mice showed a marked leftward shift relative to the control mice **(Fig. 9C)**. A similar shift toward lower intensity values in cKO mice was also observed at P120 **(Fig. 9E)**. Intensity distribution scatterplots further illustrated that in cKO mice, the PV interneuron population at P60 and P120 consisted of a higher proportion of low-expressing PV interneurons relative to the control **(Fig. 9C,E)**. This also corresponds to the differences observed in PV densities at the indicated stages. In the cKO at P60, the proportion of low-expressing PV interneurons was higher (**Fig. 9C**) and the PV cell density was significantly lower (**Fig. 7D**) than the control, signifying an association between PV signal intensity and cell count.

4.2 GAD67 gene expression in mPFC PV neurons tends to be reduced in fully adult cKO mice

As altered GAD67 levels with concomitant PV deficits have been reported in various neuropsychiatric disorders and their animal models, the GAD67 gene (*Gad1*) expression was assessed by RNAscope® fluorescent multiplex assay, a multiplex fluorescence *in situ* hybridization technique. The number of *Gad1* signal dots within the PV interneurons, with diameter between 3 and 20 pixels and above the defined threshold, were calculated using the CellProfiler software (Stirling et al., 2021). Since each signal dot is assumed to correspond to a single molecule of *Gad1* mRNA, the number of puncta per cell were used to determine the expression level of the transcript. At P26, the cumulative frequency distribution and the scatterplot show that although the cKO mice had lower proportion of PV cells with reduced *Gad1* puncta compared to the control mice, they also consisted of fewer PV neurons with enhanced *Gad1* gene expression unlike the control **(Fig. 10B)** At P90, the *Gad1* gene expression was comparable in control and cKO **(Fig. 10C)** while at P120, the cumulative frequency distribution curve in cKO was significantly shifted towards lower number of *Gad1* puncta relative to the control group **(Fig. 10D)**. These results imply that reduced *Gad1* gene expression in PV interneuron at P120 in cKO mice could be correlated with higher proportion of low-expressing PV neurons observed at the same postnatal stages **(Fig. 9E)**.

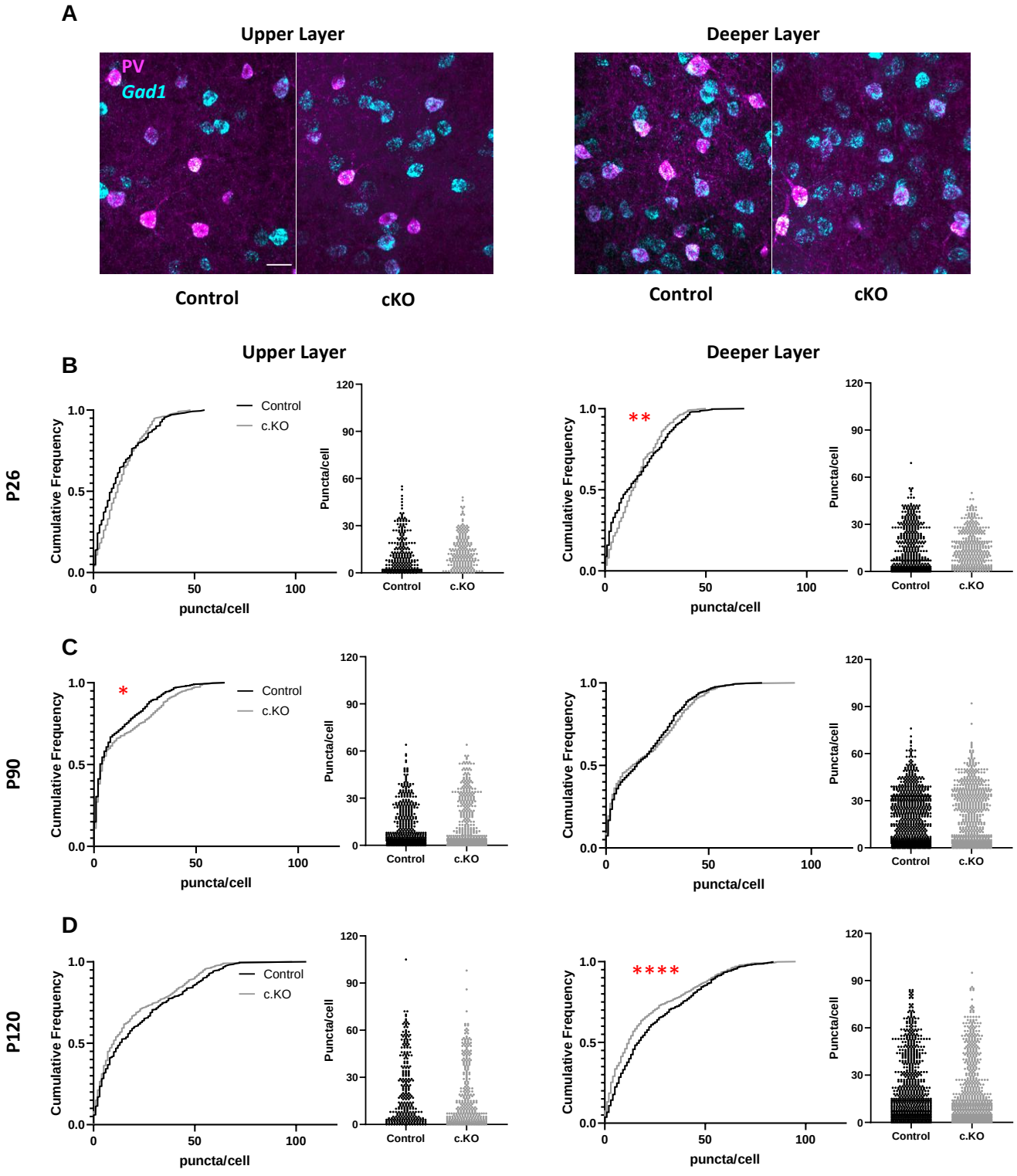

Figure 10. Gad67 gene expression in PV interneurons of the mPFC across at three different ages. (A) Representative images (40x magnification) show multiplex fluorescent *in situ* hybridization for *Gad1* mRNA and immunofluorescent staining for PV on P120 coronal sections of control and cKO animals. (B,D) Cumulative frequency plots and scatterplots of the recorded cells at (B) P26, (C) P90, and (D) P120 show the relative expression of *Gad1* in each group. Kolmogorov-Smirnov test. *p<0.05, **p<0.01, ****p<0.0001. n=3-5 animals per group. Number of cells, control: N=240 (upper layer), 457 (deeper layer), cKO: N=228 (upper layer), 382 (deeper layer) at P26; N=593 (upper layer), 876 (deeper layer), cKO: N=514 (upper layer), 788 (deep layer) at P90; N=278 (upper layer), 705 (deeper layer), cKO: N=321 (upper layer), 701 (deeper layer) at P120. Scale bar: 25 µm.

4.3 Prefrontal cortical layer thickness is unaffected by absence of mesoprefrontal input

The changes in densities of PV and CB interneurons in cKO during adolescence made us contemplate if absence of mesoprefrontal input affected mPFC layer build-up and the laminar location of interneurons in the cortical layers. To determine if mPFC cortical layers were altered in cKO mice, the thickness of the layers was measured in both groups at P12 (experiment and analysis were performed by Wencke Trein). To be able to distinguish upper from deeper layers, the antibody anti-CTIP2 was used. The transcription factor CTIP2 is not expressed in layer II/III but strongly expressed in layer V and less intensely in layer VI **(Fig. 11A)**. Its variation in expression and subsequently the extent of immunofluorescent labeling helped to demarcate the different cortical layers while the neuron-sparse layer I could be easily identified by Hoechst staining. Layer thickness was measured at three levels **(Fig. 11A)** for each cortical layer. Two-way ANOVA revealed that there was no statistically significant difference in layer thickness between control and the cKO group at P12. This suggested that prefrontal layer development was not impacted by lack of DA input and the irregularities in interneuron densities did not stem from altered laminar arrangement of the neurons **(Fig. 11B).**

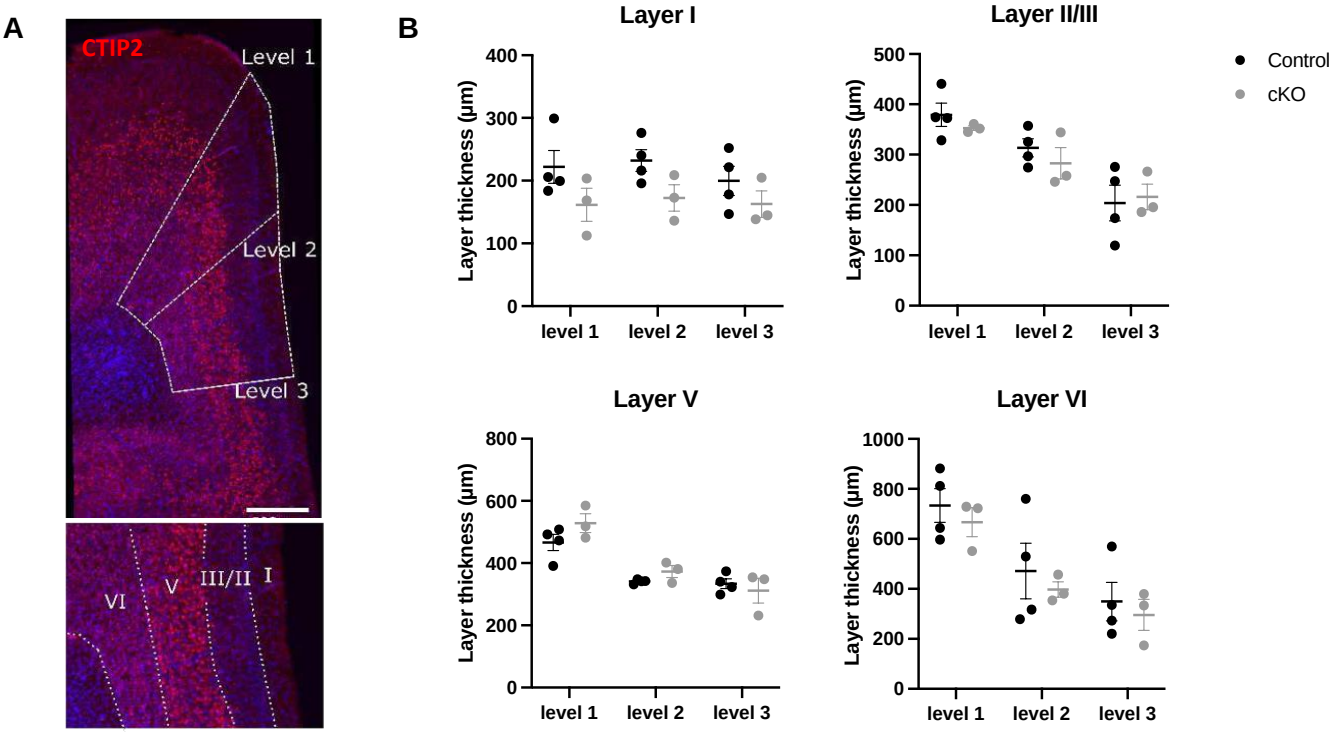

Figure 11. Measurement of cortical layer thickness in the mPFC at P12. (A) Representative images (20x magnification) show immunofluorescent staining for CTIP2 and Hoechst staining on P12 coronal sections. The variation in expression intensity of CTIP2 helps to define the cortical layers (lower panel). (B) There was no effect of genotype on the thickness of the layers (experiment and analysis were performed by Wencke Trein). n=3-4 animals per group. Error bars indicate mean +/- SEM. Scale bar: 500 µm.

4.4 Postnatal development of noradrenergic and serotonergic fibers in the mPFC of cKO and control mice

Since the monoaminergic systems in the mPFC interact and influence each other during development, it was investigated whether the absence of mesoprefrontal input elicited compensatory changes from serotonergic and noradrenergic projections or altered their development. The serotonergic and noradrenergic fibers within the region of interest were quantified automatically using the DEFiNE macro for Fiji (Powell et al., 2019). This image analysis pipeline allowed to calculate the total area occupied by NET/SERT-immunostained axons.

4.4.1 There is no significant difference in serotonergic innervation pattern of the mPFC at P60 in control and cKO mice

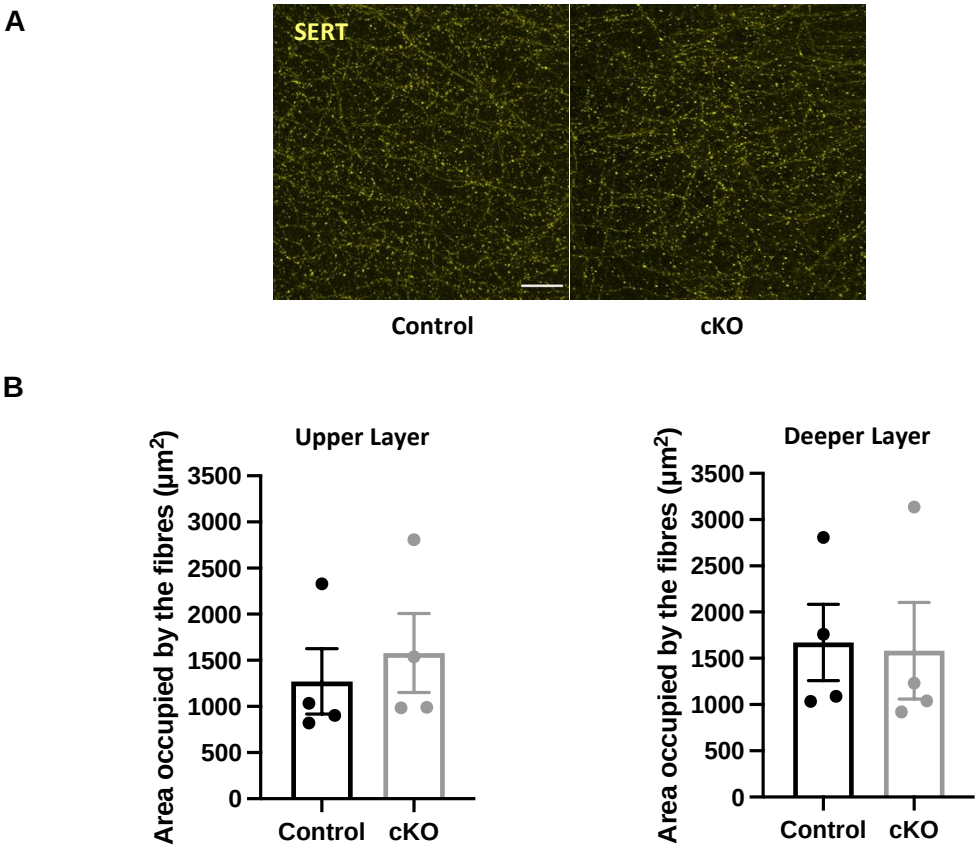

Figure 12. Serotonergic innervation of the mPFC in control and cKO groups is similar at P60. (A) Representative images (63x magnification) show immunofluorescent staining for SERT on P60 coronal sections from deeper layers of PrL cortex. (B) The serotonergic fiber occupancy in upper and deeper layers of mPFC show no significant differences between control and cKO. Acquisition area: 175.74 x 175.74 µm^2. n=4 mice per group. Error bars indicate mean +/- SEM. Scale bar: 25 µm.

SERT-immunostaining was performed at two developmental stages: P12 and P60. However, due to poor immunostaining quality at P12, the fibers were not easily detectable and

consequently the P12 immunostained sections were excluded during analysis. At P60, the axons appeared thick, long, continuous, and uniform **(Fig. 12A).** The morphological features of the fibers did not differ between control and cKO mice. Mann Whitney test did not report any difference between genotype at P60 in either layers **(Fig. 12B).**

4.4.2 Innervation pattern of noradrenergic fibers in the mPFC follows the same developmental trajectory in control and cKO mice

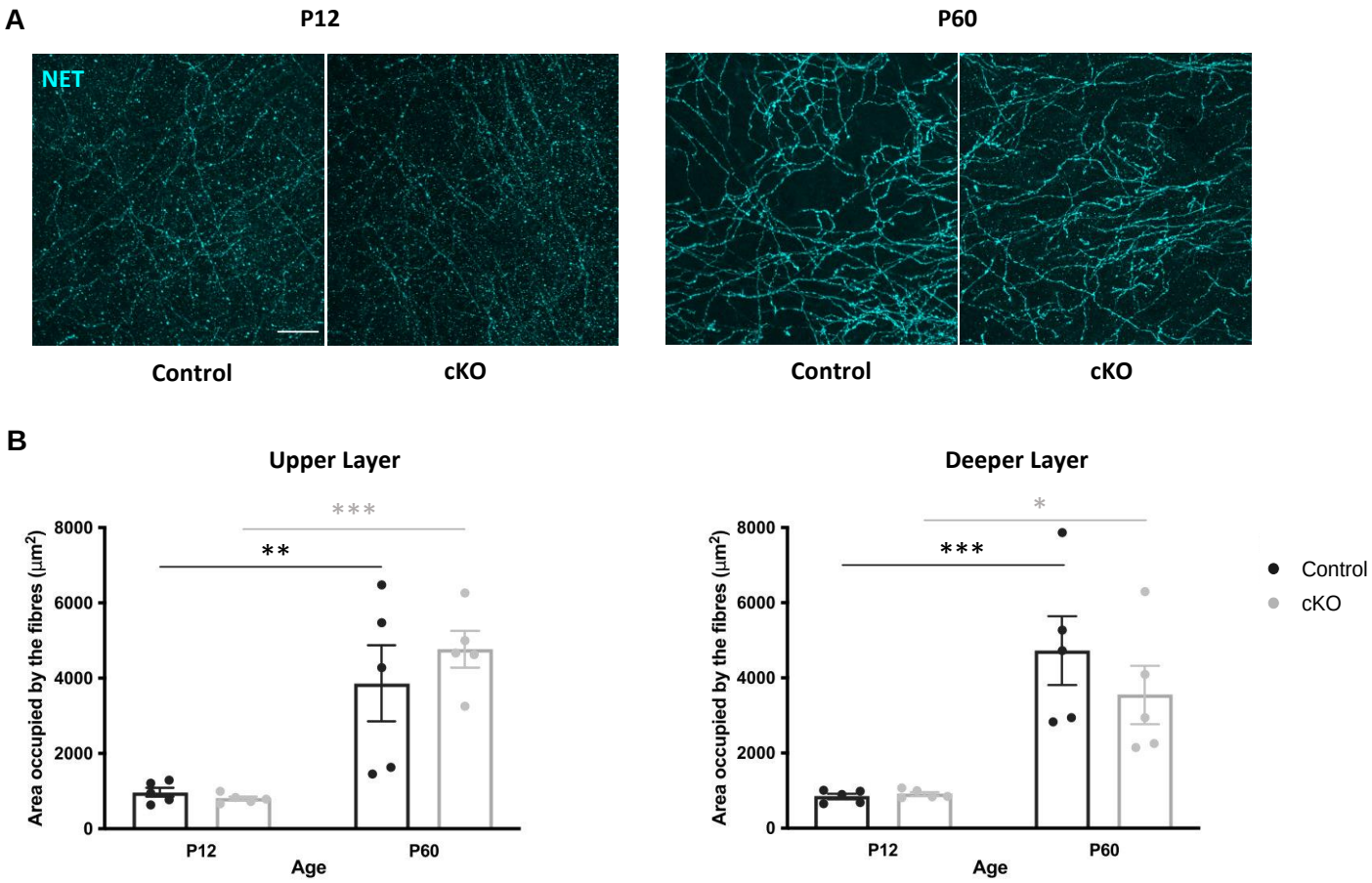

Figure 13. The increase in noradrenergic fiber density from P12 to P60 in the mPFC is almost identical in control and cKO mice. (A) Representative images (63x magnification) show immunofluorescent staining for NET on P12 and P60 coronal sections. (A, B) There is a significant increase in fluorescence intensity and occupancy of fibers between P12 and P60. Acquisition area: 175.74 x 175.74 µm^2. n=5 mice per group. Error bars indicate mean +/- SEM. Two-way ANOVA; Šídák's multiple comparisons *post-hoc* test. *p<0.05, **p<0.01, ***p<0.001. Scale bar: 25 µm.

The NET-immunoreactive fibers in the mPFC at P12 appeared thin, with intermittent varicosities along the axon. The innervation pattern at P60 was similar to that observed at P12, but the axons were smoother, more uniform, and appeared to be more branched **(Fig. 13A)**. When P12 and P60 imaged sections were visually compared, the fluorescent intensity of the axons was found to be noticeably augmented at P60 relative to P12 in both control and ckO brains. However, no morphological differences could be identified between the control

and cKO mice at either stage. Two-way ANOVA reported no effect of genotype but a significant effect of age in both upper ($F_{(1, 16)}$ = 37.05, p < 0.0001) and deeper layer ($F_{(1, 16)}$ = 30.29, p < 0.0001). Post-hoc analysis revealed that between P12 and P60, the increase in area occupied by noradrenergic fibers was significant in both control (p=0.0045 for upper layer, p=0.0006 for deeper layer) and cKO (p=0.0003 for upper layer, p=0.01 for deeper layer) mice **(Fig. 13B)**, following the temporal innervation pattern described by others (Levitt and Moore, 1979).

4.5 *Drd1* and *Drd2* expression in control mice tends to decrease between early postnatal phase and late adolescence but shows no developmental change in cKO mice

The loss of DA input to the striatum in Parkinson's disease patients or in animal models of the disease leads to compensatory upregulation of DRDs (Hisahara & Shimohama, 2011). To determine if such a compensative change occurs in cKO mice, the expression of *Drd1* and *Drd2* transcripts was assessed by RNAscope® fluorescent multiplex assay. The RNAscope® signal appeared as punctate dots **(Fig. 14A,B)** and *Drd1 and Drd2* signal puncta that were above the defined threshold, had a diameter between 3 and 20 pixels, and were located within 20 pixels distance of DAPI-positive nuclei, were quantified by the CellProfiler software (Stirling et al., 2021). The number of puncta per cell for each transcript was evaluated in the upper and deeper layers of the mPFC of control and cKO mice at two developmental stages to determine whether they demonstrated any changes in their postnatal expression levels. Kolmogorov-Smirnov test revealed significant differences (p<0.0001) between control and cKO for *Drd1* and *Drd2* transcripts, at both developmental stages, in the upper and deeper layers of mPFC **(Fig. 14C,D,E,F)**. However, since the expression level of the transcripts varied considerably between animals, the results could not be interpreted conclusively.

The scatterplots show that there is an overall decrease in expression of *Drd1* and *Drd2* transcripts in the control group at P60 in comparison to P12 **(Fig. 14D,F)**. This is consistent with qPCR and quantitative autoradiography studies that have reported that *Drd1*/*Drd2* transcript levels and DRD1/DRD2 receptor binding density declined after P40 (Islam et al., 2021). The cKO group on the whole, however, did not exhibit such reduction in expression for either of the transcripts between P12 and P60, and displayed an expression level at late adolescence similar to that of early postnatal phase **(Fig. 14D,F)**. This might be an indication of adaptive response to the absent DA input in cKO mice.

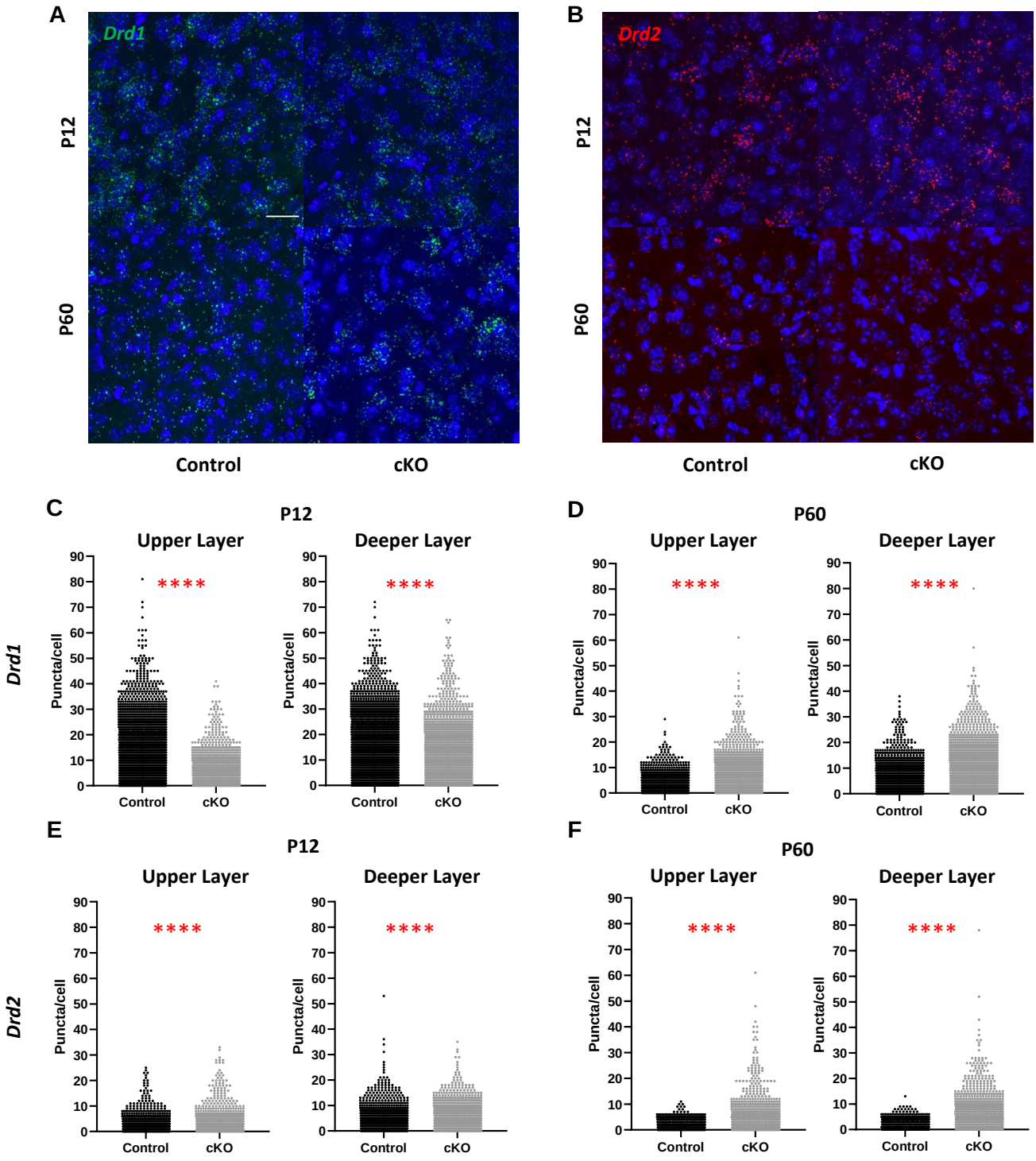

Figure 14. *Drd1* and *Drd2* expression does not change in cKO but is reduced in control between P12 and P60. (A,B) Representative images (40x magnification) show multiplex fluorescent *in situ* hybridization for (A) *Drd1* mRNA and (B) *Drd2* mRNA on P12 and P60 coronal sections of control and cKO animals. (C-F) Scatterplots show raw data of each recorded cell for *Drd1* signal puncta at (C) P12 and (D) P60, and *Drd2* signal puncta at (E) P12 and (F) P60. Kolmogorov-Smirnov test. ****p<0.0001. n=2-5 animals per group. Number of cells, control: N=10707 (upper layer), 11042 (deeper layer) for *Drd1* at P12, cKO: N=6351 (upper layer), 5930 (deeper layer) for *Drd1* at P12; N=16605 (upper layer), 19291 (deeper layer) for *Drd2* at P12, cKO: N=8993 (upper layer), 8695 (deeper layer) for *Drd2* at P12; control: N=8887 (upper layer), 10436 (deeper layer) for *Drd1* at P60, cKO: N=9824 (upper layer), 11125 (deeper layer) for *Drd1* at P60; N=5730 (upper layer), 5875 (deeper layer) for *Drd2* at P60, cKO: N=7814 (upper layer), 7754 (deeper layer) for *Drd2* at P60. Scale bar: 25 µm.

4.6 cKO mice displayed learning deficits during choice alternation training

DA neurotransmission in the PFC is critical for modulation of higher cognitive functions such as working memory. Disruption in DA signaling has been found to impair mPFC-mediated cognitive performance (Floresco & Magyar, 2006; Neve et al., 2004). At the circuit level, intact PV neuron functioning has been shown to be fundamental for working memory accuracy (Murray et al., 2015). Since the cKO mice lack DA input from mDA neurons and their PV interneuron population shows an altered developmental trajectory, we suspected that the cKO mice may have cognitive deficits. To determine if cKO mice specifically exhibited impairments related to working memory capacity, control and cKO mice aged between P90-P100 were trained to perform a delayed alternation task in an figure-eight-maze (modified T-maze) that allows continuous alternation **(Fig. 15A)**. Once the mice learned the task of alternately visiting the two goal arms through forced-alternation, they were given 20 attempts of choice alternation runs per session **(Fig. 15B)**. Due to the innate tendency of rodents to explore and switch between the arms, the mice were expected to spontaneously alternate between the two goal arms in this phase. Successful continuous alternation requires the mice to remember the visited arm in the previous trial, reflecting an intact spatial working memory (d'Isa et al., 2021; Wenk, 1998). Once the mice showed 80% or above accuracy in choosing the goal arm in 2 out of 3 sessions, they could move on to the test phase. Two-way ANOVA reported significant differences between control and cKO ($F_{(1, 140)} = 67.15$, $p < 0.0001$) and also between two groups of cKO that could and could not reach performance criterion respectively ($F_{(1, 60)} = 51.96$, $p < 0.0001$) **(Fig. 15C)**. While all control mice reached the criterion of 80% correct decisions by the end of choice-alternation training phase, only 3 out of 8 cKO mice could successfully move to the test-phase. The other 5 cKO mice showed significantly reduced spontaneous alternation and hence decreased number of correct choices. Their performance remained mostly at chance level, showing an inability to learn the task **(Fig. 15C)**. These mice were consequently removed from the test-phase **(Fig. 15D)**. When the working memory load was increased with introduction of a delay-period of 30s, the overall performance dropped but there was no notable difference between the control mice and cKO mice in the delayed alternation task in the test-phase **(Fig. 15D)**. These results indicate that while a subset of cKO mice did not achieve criterion, the mice that learned the choice alternation task had no delay-dependent working memory impairment.

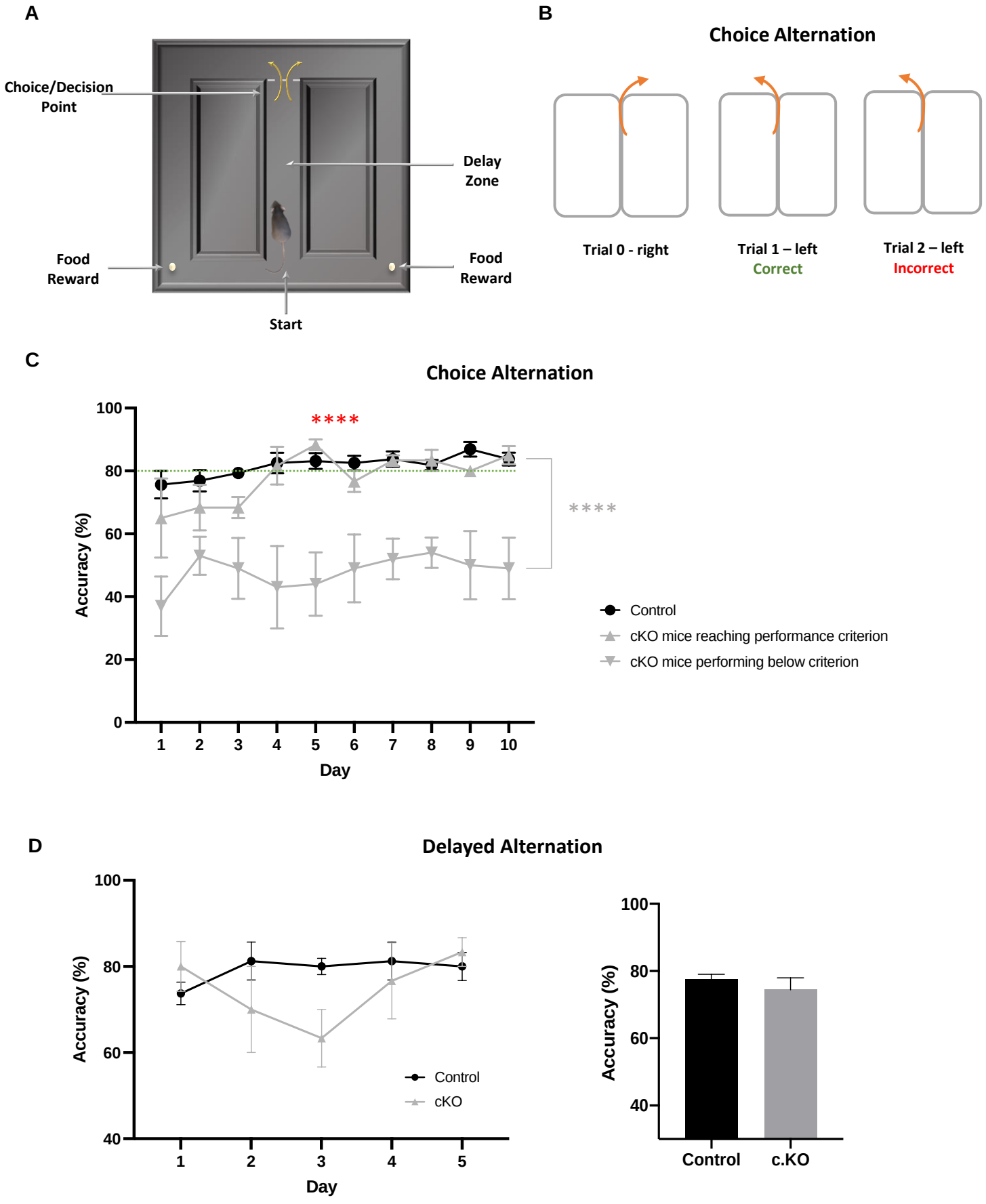

Figure 15. (Figure legend continued on next page)

Figure 15. Performance of control and cKO mice in a spatial working memory task involving continuous choice alternation training and delayed alternation testing. (A) Schematic illustration of the figure-eight-maze, indicating the goal arms, decision point and the delay zone. (B) Schematic illustration of the continuous choice alternation task in which the mice are rewarded only if they enter the goal arm not chosen on previous trial. (C) 5 out of 8 cKO mice failed to acquire the continuous choice alternation task (80% accuracy level indicated by the green dotted line). All control mice (n=8) performed at or above 80% accuracy level during the second training week. Only 3 cKO mice reached the criterion and only during the last four sessions of the training. The performance of rest of the cKO mice was consistently below or at chance level and significantly weaker than the control mice. (D) The performance of the control and the criterion-reaching cKO mice remained comparable over the five testing sessions with delay period (left) with no significant difference in overall performance between the two groups of mice (right). Two-way ANOVA. Uncorrected Fisher's LSD *post-hoc* test for continuous alternation. Šídák's multiple comparisons *post-hoc* test for delayed alternation. ****p<0.0001. n=8 controls and 3 cKO. Error bars indicate mean +/- SEM.

5. Discussion

5.1 PV and CB GABAergic interneurons in mice developmentally lacking mesoprefrontal innervation demonstrate aberrant developmental trajectory

This thesis examined the development of three subpopulations of GABAergic interneurons within the mPFC of control mice with an unperturbed mDA system, and the variation in their development in the absence of mesoprefrontal innervation. Using immunohistochemical analysis, this study has shown that in controls, CR and CB cell densities remained relatively stable postnatally, while PV cell density increased during postnatal development, peaking during early adolescence and then reaching a plateau as the mice entered adulthood. Visual inspection of PV immunostaining revealed an age-dependent enhancement of PV fluorescence intensity, suggesting that the surge in PV signaling in individual cells likely resulted in a higher number of identifiable PV positive cells with time. Results in this study lend further support to reports from earlier studies that have shown developmental upregulation of PV mRNA expression in the dorsolateral PFC of humans (Fung et al., 2010) and increase in PV protein level, PV immunofluorescence, and PV cell density in rats and mice during adolescence (Caballero et al., 2014; Du et al., 2018). The boost in adolescent PV expression is associated with an increase in excitatory glutamatergic transmission onto fast-spiking PV neurons and a DA-dependent facilitation of fast-spiking PV neuronal activity during late adolescence (Tseng & O'Donnell, 2005, 2007).

Identical to control mice, *Gli2* cKO mice reached peak PV density at P33 but then showed a prominent decrease in PV interneuron density at P60. Alongside lack of mesoprefrontal DA input to mPFC, mesoprefrontal glutamatergic excitation of fast-spiking interneurons has also been found to be impaired in adult *Gli2* cKO mice (Kabanova et al., 2015). Since PV expression is strongly correlated with afferent drive, especially during adolescence, a deficit in mesoprefrontal assisted activity of the fast-spiking interneurons could have led to downregulation of PV expression and subsequently PV immunoreactivity during late adolescence in *Gli2* cKO mice. Since only cells above a specified intensity were labelled in this study, the reduction in cell count observed at P60 therefore possibly resulted from an imbalance in PV signal intensity rather than loss of PV cells.

Indeed, when fluorescence signal intensities of PV immunoreactive neurons were analyzed, *Gli2* cKO mice had an increased proportion of low intensity PV neurons, i.e PV interneurons with low-level expression of PV and a decreased proportion of high intensity PV neurons, i.e. PV interneuron with high-level expression of PV, at P60 than control mice. At P90, the mPFC

of *Gli2* cKO mice contained more high intensity PV interneurons compared to the mPFC of control mice. This was also evident from PV cell density in *Gli2* cKO mice at P90, which was similar to control mice. Yet, the proportion of low intensity PV neurons was higher in *Gli2* cKO mice relative to control. And although the difference in PV cell density at P120 did not reach statistical significance, a detailed inspection of signal intensities of PV cells revealed that *Gli2* cKO mice maintained a greater proportion of low intensity PV neurons and fewer high intensity ones in the mPFC than control mice. This suggests that despite initial recovery of PV expression post adolescence, an inability to express adequate level of PV likely persists into adulthood. It is also interesting to note that the change in PV density and variation in signal intensity observed was specific to the deeper layer of mPFC, which contains the highest density of PV cells and is more densely innervated by mDA projections than the upper layers between early adolescence and adulthood (Kalsbeek et al., 1988; Naneix et al., 2012).

Caballero and colleagues found relatively stable CB expression in their study, with a trend toward augmented CB signal and slightly elevated periadolescent CB protein level (Caballero et al., 2014). Consistent with these observations in the aforementioned study, the present investigation found that in control mice, the CB cell density was stable throughout postnatal development in the upper layers of the mPFC. There was a deeper layer specific increase between P60 and P90, which was possibly a late representation of increase in CB protein expression throughout adolescence in control. We hypothesized that the aberrant CB cell density levels in *Gli2* cKO mice in the upper layer during adolescence at P60 could reflect compensatory increase in CB expression in response to decreased PV signal intensity observed at that stage. Western blotting however did not reveal any difference in CB protein level between control and *Gli2* cKO mice at P60. Since CB is expressed by a diverse group of interneurons (Kubota & Kawaguchi, 1994), another possibility could be a temporary shift of subpopulations of interneurons towards CB expression in response to PV downregulation, resulting in increased cell count. To this end, the ratio of CB to PV cell density at P60 was analyzed between control and cKO, but the result was inconclusive. Nevertheless, the prospect remains that the compensatory measure adapted by a specific subgroup of CB positive cells was masked as various groups of CB expressing neurons counterbalanced each other. To address this issue, a detailed analysis of different CB co-expressing interneuron groups of the mPFC is needed to identify if a specific CB co-expressing interneuron subpopulation in cKO show changes in cell density and CB expression level compared to control. In summary, the irregularities illustrated by PV and CB expressing interneurons in *Gli2* cKO further support the notion of adolescence being a vulnerable period for maturation of GABAergic transmission in the mPFC and suggest that the unavailability of mesoprefrontal

input during this critical period disrupts the maturation trajectory of PV and CB interneurons as observed in controls.

MGE is the source of PV immunopositive neurons and certain populations of CB expressing interneurons while CR interneurons originate from caudal ganglionic eminence (CGE) (Wonders & Anderson, 2006). The results of this thesis show that in absence of DA input, the MGE derived PV and CB interneurons are afflicted while the developmental trajectory of CGE derived CR interneurons remained unaffected. Since DA has been shown to stimulate the migration of cortical interneurons derived from MGE (Ohira, 2019), an additional potential cause of atypical interneuron density in cKO may be altered cortical interneuron migration. We concluded this to be not the case in *Gli2* cKO mice since the developmental pattern of the analyzed interneuron populations in control and cKO remained comparable until adolescence. If neuronal migration was affected in cKO, the developmental discrepancy would have been reflected in a change in thickness of cortical layers. The results from measurement of mPFC layer thickness with the help of CTIP2 immunostaining at P12 showed that cortical integrity was maintained. Visual examination of PV and CB immunostaining at P12 and P60 also did not expose any observable discrepancy between control and cKO in distribution and position of interneurons along the cortical layers of mPFC, suggesting no apparent migratory defect.

5.2 Reduced GAD67 mRNA in PV interneurons may contribute to impaired inhibition of pyramidal neuron in local PFC microcircuits of *Gli2* cKO

Alterations in PV interneurons in the PFC have been associated with multiple neuropsychiatric disorders such as schizophrenia, ASD, bipolar disorder (Hashemi et al., 2017; Kaar et al., 2019; Perlman et al., 2021). Lower level of gene or protein expression of the GABA synthesizing enzyme, GAD67, has also been associated with some of these diseases (Akbarian et al., 1995; Guidotti et al., 2000). In schizophrenic patients particularly, postmortem analysis of brain tissue has uncovered that along with decreased expression of PV mRNA, there was a selective deficit of GAD67 mRNA in about half of PV positive neurons (Hashimoto et al., 2003). Intriguingly, this phenomenon has also been reported in both neurodevelopmental and genetic models of schizophrenia (Behrens et al., 2007; F. H. Lee et al., 2013; Y. Zhang et al., 2008). Since PV interneurons were identified here to be the population most vulnerable to absence of mesoprefrontal input, we hypothesized that another marker of GABAergic transmission, namely GAD67 mRNA, could be altered in PV interneurons. Characterization of *Gad1* gene expression in PV immunopositive cells revealed an association between PV immunoreactivity and the GABAergic marker. Similar to the developmental trend observed with PV fluorescence intensity level, the pre-adolescent *Gad1*

transcript level was lower relative to post-adolescent levels of the mRNA in PV neurons. And although the difference was subtle, the proportion of low *Gad1* expressing PV neurons was higher in *Gli2* cKO mice compared to controls at P120, parallel to more low intensity PV neurons in cKO mice at this age. An intricate link between degree of PV expression and GABA neurotransmission has been demonstrated earlier. Injection of a short hairpin RNA against PV into the mPFC between P34 to P38 caused a 25% downregulation of PV expression, which was enough to result in a deficit in GABA neurotransmission and an increase in the E/I balance that lasted into adulthood and prevented the acquisition of matured inhibitory control (Caballero et al., 2020). Lazarus and colleagues have likewise shown that decreased *Gad 1* levels in PV interneurons of juvenile mice resulted in deficits in inhibitory transmission from PV interneurons to pyramidal neurons, disinhibiting them, and disrupting the E/I balance of the microcircuit (Lazarus et al., 2015). The *Gli2* cKO mice too have been reported to exhibit deficient mPFC pyramidal neuron inhibition by fast-spiking interneurons due to reduced mesoprefrontal glutamatergic excitation of the interneurons (Kabanova et al., 2015). It is possible that the concomitant reduction of PV and GAD67 mRNA expression in P120 *Gli2* cKO mice acted as a supplementary cause of deficient synaptic inhibition to pyramidal neurons, but it is difficult to infer without further experimental support whether the decline in *Gad 1* expression directly impacted GABA synthesis and conductance in the mPFC of *Gli2* cKO mice.

5.3 Interaction between DA, 5-HT and NA systems in *Gli2* cKO mouse model

Due to their robust interactions with each other, we presumed that serotonergic and noradrenergic projections would be developmentally influenced in *Gli2* cKO mice. An interaction between different monoaminergic systems during development has been demonstrated previously. The DA system within the PFC has been found to be particularly sensitive to manipulation of the 5-HT system. 5-HTT knockout in mice increased not only serotonergic but also dopaminergic fiber length in IL and PL subregions of mPFC (Garcia et al., 2019). Interestingly, 5,7-DHT lesion of serotonergic neurons in P5 rats increased innervation of TH-positive fibers in layer V and VI of the mPFC (Taylor et al., 1998), while 6-OHDA lesion of mDA neurons in P5 rats decreased serotonergic fiber density in layer II and III of mPFC (Cunningham et al., 2005). In contrast, the serotonergic innervation density of mPFC in *Gli2* cKO mice remained unaffected. While the lack of effect on serotonergic projections in current study was unexpected, it is necessary to note that in the aforementioned lesion studies, 5-HT immunopositive neurons of the DR and TH immunopositive neurons of VTA and SN were almost completely ablated. Cunningham and colleagues proposed that lesioning of the mDA neurons decreased trophic support for DR neurons, decreasing 5-HT

projections to PFC, whereas lesioning of DR nucleus eliminated its suppression on VTA mDA neurons, enhancing neurotrophic influence and mesoprefrontal innervation. The lesioned models discussed above are acute in nature and ablation of VTA and SN neurons affected both cortical and subcortical dopaminergic innervation. In contrast, in the *Gli2* cKO genetic mouse model, severe reduction of lateral mDA progenitors resulted in loss of primarily medial VTA mDA neurons that project to the PFC and subsequently mesoprefrontal innervation, while DA input to striatum and limbic system remained relatively unaffected. The selective loss of a mDA neuronal subpopulation may not have been sufficient to trigger the trophic response suggested in lesioned systems, which involve gross degeneration of mDA neurons.

Nevertheless, the stabilization of CB immunoreactivity post-adolescence and transient recovery of PV and GAD67 mRNA expression at P90 suggested involvement of compensatory mechanisms. We hypothesized noradrenergic innervation of mPFC to be a potential source of DA in *Gli2* cKO mice since both pharmacological activation of LC neurons and their electrical stimulation have been shown to increase extracellular DA in the mPFC (Cunningham et al., 2005). Although the postnatal innervation density of noradrenergic fibers in *Gli2* cKO mice was similar to control, it is still possible that the supply of DA originating from the neurons of LC aided the cKO mice to cope with diminished mesoprefrontal DA. Reduced reuptake of DA by NET too could have helped to boost cortical DA output. These theories however require further investigation that provide better spatial and temporal perspective of DA release from noradrenergic and remaining dopaminergic terminals in the PFC of ckO mice. DA content in the PFC in *Gli2* cKO mice has previously been measured by HPLC (Kabanova et al., 2015) but the recent development of genetically encoded DA biosensors coupled with fiber photometry present the possibility to resolve DA release dynamics in real-time in cKO mice in the future (Labouesse et al., 2020; Nakamoto et al., 2021). DA sensor photometry, for example, has already been used to study DA signaling in the PFC (Pittolo et al., 2022; M. Wu et al., 2024).

5.4 Adaptive response of *Drd* transcripts to offset limited DA input

Within the developing rodent PFC, *in situ* hybridization technique and radioligand binding autoradiography assays have detected *Drd1* and *Drd2* mRNA and DRD1 receptor protein respectively, prior to the arrival of the first TH positive fibers from VTA (Schambra et al., 1994). This indicates that the early expression of DRDs in rodent PFC is independent of mesoprefrontal innervation. The expression of *Drd1* and *Drd2* mRNA in *Gli2* cKO mice at P12 is consistent with this observation. A review of published research on the trajectory of DRD expression in PFC divulged mainly two discrepant developmental pathways of the receptors in rodents. Studies utilizing *in situ* hybridization technique and quantitative autoradiography

have shown a gradual increase in expression level of the *Drd1* and *Drd2* transcripts and their receptor protein in the frontal cortex of rats. Others with similar assay methods on rodent PFC have reported a peak expression of the transcripts around adolescence followed by a decline in adulthood and at the protein level, a decrease in receptor binding density of the radioligands between adolescence and adulthood (Islam et al., 2021). The results of *Drd1* and *Drd2* expression pattern from control mice in the present study are more consistent with the latter trend, implying receptor pruning. Naneix and colleagues noted that DA content in the mPFC exhibited a conspicuous surge between P45 and P70, while the expression level of the *Drds* decreased during this period after peak expression at P45 (Naneix et al., 2012). This suggests that expression of DRDs in PFC might be influenced by DA release in the mPFC. Just as drug-induced DA increase in the NAc leads to reduced expression of DRDs to adapt to the elevated DA in the system (Naneix et al., 2012; Volkow & Morales, 2015), increased DA levels in mPFC around adolescence may trigger downregulation of *Drds*. This course was not followed by the transcripts in *Gli2* cKO mouse model in this study. In comparison to the striatum, the interrelationship between DA content and DRD expression in mPFC has not been studied in detail, but the apparent lack of *Drd1* and *Drd2* downregulation between P12 and P60 in cKO could suggest a compensatory mechanism, similar to upregulation of DRDs following loss of striatal DA input in Parkinson's disease (Hisahara & Shimohama, 2011). It is however difficult to make an inference based on the results of the current study, since certain animals displayed particularly high or low expression of the transcripts, which could have skewed the collective result, as mentioned in section 4.5.

One study, however, has shown that depletion of DA projections in rats by intracisternal injection of 6-OHDA at P5 had no effects on postnatal expression of DRD1 in mPFC, striatum and NAc. Using quantitative autoradiography that employs binding of radiolabeled ligands to determine receptor expression levels, this investigation found that receptor binding density in lesioned animals reached its peak by the 2nd week and declined after 4th week (Leslie et al., 1991). This was likely due to the lesion protocol, which did not deplete DA sufficiently, and more drastic DA reduction was probably needed to bring about alteration of postnatal DRD expression level. The abovementioned study also supported the complementary relationship between DRDs and DA levels, showing that a rise in DA content in the frontal cortex between 4th and 6th postnatal week was accompanied by a decrease in DRD1 receptor binding (Leslie et al., 1991). It is nevertheless important to be cautious while interpreting the results since mRNA expression levels of the receptor do not always reliably correspond to the expression levels of receptor protein. Schambra and colleagues for example registered that mRNA signal of DRD1 and DRD2 did not accurately correlate with receptor binding signal during early postnatal days (Schambra et al., 1994). Furthermore, it remains unknown in what way

maturation of receptor function or downstream signaling cascade is influenced in *Gli2* cKO mice.

5.5 Functional implications of altered PV maturation in *Gli2* cKO mice

GABAergic interneurons in inhibitory microcircuits gate long-range inputs and generate cortical oscillatory activity and neural synchrony that underlie emotional and cognitive behavior (Le Magueresse & Monyer, 2013; Murray et al., 2015; Sohal et al., 2009; Uhlhaas & Singer, 2011) and thus, any alteration in their function can lead to network deficits and behavioral impairment. Supporting this notion, previous work has demonstrated that inhibiting PV upregulation or suppression of PV neuron activity during adolescence leads to ineffective inhibition of pyramidal neurons, network dysfunction and behavioral deficits such as impairments in extinction learning and extradimensional set-shifting behavior (Caballero et al., 2020; Canetta et al., 2022). Mukherjee and colleagues also found that chronic low-PV and low-GAD67 expression in PV interneurons in a genetic mouse model of schizophrenia altered network activity and set-shifting behavior (Mukherjee et al., 2019). The activity of PV neurons are important for generation of the gamma-frequency oscillations, which are associated with higher cognitive functions, for instance working memory. Parallel to PV downregulation, some of the aforementioned studies also showed that poor performance in cognitive task was associated with network deficit in gamma range or deficient task-induced gamma oscillation (Canetta et al., 2022; Mukherjee et al., 2019). These corroborate PV neuron activity and network function to be strongly linked processes in cognitive control. While *Gli2* cKO mouse model has already shown reduced inhibition of pyramidal neurons (Kabanova et al., 2015), it remains unknown if reduced PV signal intensity observed in *Gli2* cKO mice affects network functions. Given the altered trajectory of PV maturation, there is a strong possibility that it might have contributed to impaired gamma band activity and subsequently to the (Buzśaki & Wang, 2012; Murray et al., 2015; Sohal et al., 2009) behavioral deficits of this model.

Synchronous activity between the hippocampus and the PFC is another important factor in successful execution of certain cognitive tasks such as spatial working memory ((Kabanova et al., 2015). Downregulation of PV expression in the mPFC has been shown to disrupt the ability of mPFC to process ventral hippocampal input (Caballero et al., 2020). Impaired spontaneous alterations in T-maze tasks have also been linked to hippocampal dysfunction (Pioli et al., 2014). Thus, disrupted signal transmission via ventral hippocampal-mPFC pathway could be at the root of deficient performance of *Gli2* cKO mice in the choice-alternation task. Close monitoring of the trials disclosed that while control mice tried to rectify their mistakes once they visited the incorrect goal arm, cKO mice persisted towards one

particular goal arm and displayed an inability to break out of the behavior. This finding is interestingly reminiscent of their perseverant behavior in response to the change in task contingency in the 5-CSRTT task (Kabanova et al., 2015). Since cognitive flexibility is dependent upon intact PV signaling (Cho et al., 2015; Murray et al., 2015), these observations direct towards altered PV maturation in *Gli2* cKO mice. The cKO mice showed no deficits when tested for motor function, motivational factor and other PFC-dependent cognitive tasks such as attention and impulsivity, suggesting that their deficient spatial working memory performance was independent of these factors (Kabanova et al., 2015). In the present study, it is noteworthy that in the delayed-alternation task during the test phase, the performance of the cKO mice that were able to acquire the choice-alternation task was similar to the controls. It is difficult to provide a conclusive explanation on why some cKO mice were able to learn the task within the scheduled period while others showed severe limitation in task acquisition. One possibility is that the PFC circuitry was more strongly impacted in cKO mice that demonstrated response perseveration. We conjecture from our results that downregulation of PV expression during adolescence may contribute to gamma frequency synchrony deficits in the PFC, which subsequently affected the capacity to process afferent input, leading to behavioral impairments in adult mice.

5.6 Functional relevance of perturbed mesoprefrontal DA signaling on working memory

In both primates and rodents, inhibition of DA transmission in the PFC, modulated primarily via DRD1 receptor, results in impaired spatial working memory. The working memory performance is dependent on optimal level of DA activity, and inadequate or excessive DRD1 activation hampers working (Bubser & Schmidt, 1990; Floresco, 2013; Mizoguchi et al., 2009; Murphy et al., 1996; Sawaguchi & Goldman-Rakic, 1991; Seamans et al., 1998). Most experiments in this field have shown that prefrontal dopaminergic dysfunction is linked to delay-associated working memory defect, indicating a crucial role of DA in active maintenance of information during the brief delay period. In fact, DA has been indicated to be influential only for delayed working memory performance since non-delayed memory task or spontaneous alternation remained unaffected following DA manipulation (Bubser & Schmidt, 1990; Seamans et al., 1998). DA release has been shown to increase during maintenance of delay period and decrease with the length of the delay interval, with parallel decrease in spatial working memory task accuracy (Floresco & Phillips, 2001; Phillips et al., 2004). The competent performance of three *Gli2* cKO mice in the delayed alternation task was therefore a surprise, and again hints towards some form of compensation, possibly from neuromodulatory innervation and intact DRD1 function, for delay-dependent working memory performance.

A recent study using genetic mouse models however has shown that the role of DA in memory-guided choice may not be limited to delay-periods: in *Arc* and *Disc1* mutant mice, both of which have hypofunctional mesofrontal DA system, spontaneous alternation in a Y-maze was significantly reduced compared with wild-type animals. Further examination of the secondary motor area (M2) of the frontal cortex disclosed that the proportion of neurons in M2 that showed peak activation when mice were at the decision-making point of the maze was much larger in wild-type than *Arc* mutants. The deficit in coordinated activation of M2 neurons and alternation behavior was restored by stimulation of mDA neurons in adolescence, signifying the contribution of mesofrontal DA circuit in memory-dependent choice-alternation behavior (Mastwal et al., 2023). The dopaminergic innervation of M2 in *Gli2* cKO has not been examined and whether task-dependent neuronal activity in M2 was impacted in *Gli2* cKO mice remains undetermined. Hypodopaminergic PFC has also been attributed to inflexible cognitive behavior in schizophrenia and ADHD (Floresco & Magyar, 2006), but the behavioral deficit during choice-alternation task observed in *Gli2* cKO mice is likely a readout of the overall phenotype, as described in the previous section, and probably not a direct effect of the absence of mesoprefrontal dopaminergic innervation.

An aspect that has not been investigated in this study is the impact of deficient mesoprefrontal system on pyramidal neurons. Dysregulated mesoprefrontal DA circuit has been shown to contribute to synaptic alteration of layer II/III pyramidal neurons in the PFC. It has been observed that enhanced intrinsic excitability of mesoprefrontal neurons in early-life stress experienced mice potentially increased DA release in PFC and resulted in increased excitatory synapse on its layer II/III pyramidal neurons via upregulation of DRD2 signaling (Oh et al., 2021). Acute sleep loss provoked elevated DA release has also been shown to promote the development of dendritic spines in the mPFC (M. Wu et al., 2024). Under normal conditions, PFC pyramidal neurons are active during all phases of spatial working memory task (Vogel et al., 2022) DRD1-mediated modulation of NMDA receptor is capable of driving persistent activity in pyramidal neurons that facilitates repeated excitation of prefrontal neural network mediating working memory (Oh et al., 2021). It remains unknown whether and how absence of such modulation in *Gli2* cKO mouse model alters the contribution of pyramidal neurons in working memory.

5.7 Implications for neurodevelopmental disorders of the PFC

Disrupted maturation of PFC interneurons leads to dysregulated local microcircuits that have been associated with deficits in social, affective and cognitive behavior typically encountered in neurodevelopmental disorders such as schizophrenia, ADHD and ASD (Islam et al., 2021).

The results from *Gli2* cKO mouse model has implications for neurodevelopmental disorders with aberrant PV and GAD67 expression, such as schizophrenia (Hashimoto et al., 2003) and autism (Filice et al., 2020). In schizophrenia, reduced GAD67 expression in PV neurons has been suggested to underlie downstream pathophysiology of network dysfunction and consequent behavioral changes relevant to the disease (Chung et al., 2016). In the *Gli2* cKO mouse model, deficits in PV neurons and their corresponding decreased *Gad1* expression likely contribute to deficient inhibition of pyramidal neurons by fast-spiking PV neurons (Kabanova et al., 2015), which in turn may be responsible for the observed cognitive symptoms of the model. Both human studies and various animal models of schizophrenia have signified prefrontal PV neuron dysfunction as a common process involved in the pathophysiology of the disease (Hashimoto et al., 2003; F. H. Lee et al., 2013; Mukherjee et al., 2019; Volk et al., 2000). This could serve not only as a tool to better understand the mechanism of PFC-dependent cognitive deficits of schizophrenia but also to explore recovery of behavioral phenotypes. It has been recently shown that while PV neurons are especially vulnerable to insults during the periadolescent period that can alter their developmental trajectory and impact PFC maturation, their function along with prefrontal network dysfunction and associated behavioral deficits can be rescued (Canetta et al., 2022). Enhancing PV neuron activity in a genetic mouse model of schizophrenia also restored network function and related cognitive impairments (Mukherjee et al., 2019) and restoration of deficient mesofrontal circuit in mutant mice models during a critical developmental window has been shown to lead to lasting improvement of cortical functional activity and rescue of memory-dependent decision making behavior (Mastwal et al., 2023). The *Gli2* cKO mouse model, despite severe deficits in mesoprefrontal DA input, suggest involvement of compensation and prospect of restoration of GABAergic function. Together, this suggests a huge potential in the future for functional recovery of PV interneurons following a developmental insult in neurodevelopmental disorders.

6. Conclusions and Outlook

The results of this thesis demonstrate that absence of mesoprefrontal innervation in *Gli2* cKO mice leads to aberrations during the periadolescent maturation process of PV and CB interneurons in the mPFC. Our study identified the PV interneuron population to be particularly vulnerable to lack of mesoprefrontal input as cKO mice exhibited an inability to maintain adequate PV expression level during late adolescence that persisted into adulthood, and showed comparatively decreased expression of *Gad1* transcript in adulthood relative to control mice. Additionally, the *Gli2* mouse model presented deficits in spatial working memory along with evidence of perseverant behavior, adding to the works exploring the role of deficient mesoprefrontal circuit in neurodevelopmental deficits. The innervation pattern of serotonergic and noradrenergic fibers in the mPFC, which are intricately linked to the mesoprefrontal DA system, remained unaltered in cKO mice, but transient recovery of PV and *Gad1* expression in cKO suggest the possibility of their contribution in compensatory mechanisms. The lack of decline in expression levels of *Drd1* and *Drd2* transcripts between P12 and P60 in cKO mice also indicates a form of compensation in the model to counterbalance DA scarcity in the PFC. The findings of this thesis are, to our knowledge, the first to describe irregularities in the maturation trajectory of PV and CB interneurons in absence of mDA innervation of the mPFC. Our results confirm and complement previous studies, supporting the hypothesis that adolescence is a critical period during which mesoprefrontal input plays a crucial role in promoting postnatal maturation of these interneurons.

One of the unresolved questions of this thesis is the extent of DA neurotransmission in the PFC of the cKO mice. Further analysis needs to be performed to detect possible DA release from noradrenergic terminals as discussed in section 5.3. Moving forward, future studies can focus on analysis of network activity in the mPFC of *Gli2* cKO mice and development of functional connectivity within the local microcircuit. To assess task specific oscillatory synchronization between mPFC and ventral hippocampus, local field potentials from the mPFC and ventral hippocampus can be recorded simultaneously as the mice perform spatial working memory task in the figure-eight-maze (Liu et al., 2018; Xia et al., 2019). Postnatal development of microcircuits in cKO and control mice can be compared using electrophysiology methods. Paired whole cell recordings from fast-spiking interneurons and pyramidal neurons in pre- and post-adolescent PFC slices from control and cKO can demonstrate how connectivity in the local microcircuit change during adolescence in presence and absence of mesoprefrontal input (J. M. Yang et al., 2014). At cellular level, it will be interesting to see if morphological properties such as dendritic architecture of pyramidal neurons are affected by deficient inhibition of fast-spiking interneurons and if decreased PV

expression during late adolescence is related to deficit in excitatory recruitment of mPFC PV interneuron (see section 5.1). The latter can be achieved by examining the density of excitatory synapses on PV interneurons during late adolescence (Chung et al., 2016). In addition to cognitive impairment, deficits in social interaction and/or sensorimotor gating are often present in animal models with dysregulated mesoprefrontal system and imbalanced prefrontal PV levels. Further experiments, such as social interaction of juvenile mice and prepulse inhibition of startle response can be performed to investigate these behavioral features in *Gli2* cKO mice (Sotoyama et al., 2022; Tapias-Espinosa et al., 2023; Wöhr et al., 2015). Altogether, these additional experiments with the *Gli2* cKO mouse model would provide further insights into the processes that underlie altered PFC maturation in neurodevelopmental disorders with mesoprefrontal dysfunction.

7. References

Agirman, G., Broix, L., & Nguyen, L. (2017). Cerebral cortex development: an outside-in perspective. In *FEBS Letters* (Vol. 591, Issue 24, pp. 3978–3992). Wiley Blackwell. https://doi.org/10.1002/1873-3468.12924

Akbarian, S., Kim, J. J., Potkin, S. G., Hagman, J. O., Tafazzoli, A., Bunney, W. E., & Jones, E. G. (1995). Gene Expression for Glutamic Acid Decarboxylase is Reduced without Loss of Neurons in Prefrontal Cortex of Schizophrenics. *Archives of General Psychiatry*, *52*(4). https://doi.org/10.1001/archpsyc.1995.03950160008002

Andersen, S. L., Thompson, A. T., Rutstein, M., Hostetter, J. C., & Teicher, M. H. (2000). *Dopamine Receptor Pruning in Prefrontal Cortex During the Periadolescent Period in Rats*.

Antonopoulos, J., Dinopoulos, A., Dori, I., & Parnavelas, J. G. (1997). Distribution and synaptology of dopaminergic fibers in the mature and developing lateral septum of the rat. *Developmental Brain Research*, *102*(1). https://doi.org/10.1016/S0165-3806(97)00088-6

Araki, K. Y., Sims, J. R., & Bhide, P. G. (2007). Dopamine receptor mRNA and protein expression in the mouse corpus striatum and cerebral cortex during pre- and postnatal development. *Brain Research*, *1156*(1), 31–45. https://doi.org/10.1016/j.brainres.2007.04.043

Arenas, E., Denham, M., & Villaescusa, J. C. (2015). How to make a midbrain dopaminergic neuron. *Development (Cambridge)*, *142*(11), 1918–1936. https://doi.org/10.1242/dev.097394

Beaulieu, J. M., Sotnikova, T. D., Marion, S., Lefkowitz, R. J., Gainetdinov, R. R., & Caron, M. G. (2005). An Akt/β-arrestin 2/PP2A signaling complex mediates dopaminergic neurotransmission and behavior. *Cell*, *122*(2), 261–273. https://doi.org/10.1016/j.cell.2005.05.012

Behrens, M. M., Ali, S. S., Dao, D. N., Lucero, J., Shekhtman, G., Quick, K. L., & Dugan, L. L. (2007). Ketamine-induced loss of phenotype of fast-spiking interneurons is mediated by NADPH-oxidase. *Science*, *318*(5856). https://doi.org/10.1126/science.1148045

Bentivoglio M, & Morelli M. (2005). *"The organisation and circuits of mesencephalic dopaminergic neurons and the distribution of dopamine receptors in the brain," in Handbook of Chemical Neuroanatomy. (Dopamine)* (Dunnett S. B., Bentivoglio M., Bjorklund A., & Hokfelt T., Eds.). https://doi.org/10.1016/s0924-8196(05)80001-6

Björklund, A., & Dunnett, S. B. (2007). Dopamine neuron systems in the brain: an update. *Trends in Neurosciences*, *30*(5), 194–202. https://doi.org/10.1016/j.tins.2007.03.006

Black, J. E., Kodish, I. M., Grossman, A. W., Klintsova, A. Y., Orlovskaya, D., Vostrikov, V., Uranova, N., & Greenough, W. T. (2004). Pathology of Layer V Pyramidal Neurons in the Prefrontal Cortex of Patients with Schizophrenia. *American Journal of Psychiatry*, *161*(4). https://doi.org/10.1176/appi.ajp.161.4.742

Blaess, S., & Ang, S. L. (2015). Genetic control of midbrain dopaminergic neuron development. *Wiley Interdisciplinary Reviews: Developmental Biology*, *4*(2), 113–134. https://doi.org/10.1002/wdev.169

Blaess, S., Bodea, G. O., Kabanova, A., Chanet, S., Mugniery, E., Derouiche, A., Stephen, D., & Joyner, A. L. (2011). Temporal-spatial changes in Sonic Hedgehog expression and signaling reveal different potentials of ventral mesencephalic progenitors to populate distinct ventral midbrain nuclei. *Neural Development*, *6*(1). https://doi.org/10.1186/1749-8104-6-29

Blaess, S., Corrales, J. M. D., & Joyner, A. L. (2006). Sonic hedgehog regulates Gli activator and repressor functions with spatial and temporal precision in the mid/hindbrain region. *Development*, *133*(9), 1799–1809. https://doi.org/10.1242/dev.02339

Bodea, G. O., & Blaess, S. (2015). Establishing diversity in the dopaminergic system. In *FEBS Letters* (Vol. 589, Issue 24, pp. 3773–3785). Elsevier. https://doi.org/10.1016/j.febslet.2015.09.016

Boyson, S. J., Paul Mcgonigle, J., & Molinoff, P. B. (1986). Quantitative Autoradiographic Localization of the D, and D, Subtypes of Dopamine Receptors in Rat Brain. In *The Journal of Neurosci*.

Brenhouse, H. C., Sonntag, K. C., & Andersen, S. L. (2008). Transient D1 dopamine receptor expression on prefrontal cortex projection neurons: Relationship to enhanced motivational salience of drug cues in adolescence. *Journal of Neuroscience*, *28*(10), 2375–2382. https://doi.org/10.1523/JNEUROSCI.5064-07.2008

Brignani, S., & Pasterkamp, R. J. (2017). Neuronal subset-specific migration and axonal wiring mechanisms in the developing midbrain dopamine system. In *Frontiers in Neuroanatomy* (Vol. 11). Frontiers Media S.A. https://doi.org/10.3389/fnana.2017.00055

Bubser, M., & Schmidt, W. J. (1990). 6-Hydroxydopamine lesion of the rat prefrontal cortex increases locomotor activity, impairs acquisition of delayed alternation tasks, but does not affect uninterrupted tasks in the radial maze. *Behavioural Brain Research*, *37*(2). https://doi.org/10.1016/0166-4328(90)90091-R

Buzśaki, G., & Wang, X. J. (2012). Mechanisms of gamma oscillations. In *Annual Review of Neuroscience* (Vol. 35, pp. 203–225). https://doi.org/10.1146/annurev-neuro-062111-150444

Caballero, A., Flores-Barrera, E., Cass, D. K., & Tseng, K. Y. (2014). Differential regulation of parvalbumin and calretinin interneurons in the prefrontal cortex during adolescence. *Brain Structure and Function*, *219*(1), 395–406. https://doi.org/10.1007/s00429-013-0508-8

Caballero, A., Flores-Barrera, E., Thomases, D. R., & Tseng, K. Y. (2020). Downregulation of parvalbumin expression in the prefrontal cortex during adolescence causes enduring prefrontal disinhibition in adulthood. *Neuropsychopharmacology*, *45*(9), 1527–1535. https://doi.org/10.1038/s41386-020-0709-9

Caballero, A., Granberg, R., & Tseng, K. Y. (2016). Mechanisms contributing to prefrontal cortex maturation during adolescence. *Neuroscience and Biobehavioral Reviews*, *70*, 4–12. https://doi.org/10.1016/j.neubiorev.2016.05.013

Caballero, A., Orozco, A., & Tseng, K. Y. (2021). Developmental regulation of excitatory-inhibitory synaptic balance in the prefrontal cortex during adolescence. *Seminars in Cell and Developmental Biology*, *118*, 60–63. https://doi.org/10.1016/j.semcdb.2021.02.008

Caballero, A., & Tseng, K. Y. (2016). GABAergic Function as a Limiting Factor for Prefrontal Maturation during Adolescence. *Trends in Neurosciences*, *39*(7), 441–448. https://doi.org/10.1016/j.tins.2016.04.010

Canetta, S. E., Holt, E. S., Benoit, L. J., Teboul, E., Sahyoun, G. M., Ogden, R. T., Harris, A. Z., & Kellendonk, C. (2022). Mature parvalbumin interneuron function in prefrontal cortex requires activity during a postnatal sensitive period. *ELife*, *11*. https://doi.org/10.7554/ELIFE.80324

Caputi, A., Rozov, A., Blatow, M., & Monyer, H. (2009). Two calretinin-positive gabaergic cell types in layer 2/3 of the mouse neocortex provide different forms of inhibition. *Cerebral Cortex*, *19*(6), 1345–1359. https://doi.org/10.1093/cercor/bhn175

Chandler, D. J., Waterhouse, B. D., & Gao, W. J. (2014). New perspectives on catecholaminergic regulation of executive circuits: Evidence for independent modulation of prefrontal functions by midbrain dopaminergic and noradrenergic neurons. *Frontiers in Neural Circuits*, *8*(MAY), 1–10. https://doi.org/10.3389/fncir.2014.00053

Chini, M., & Hanganu-Opatz, I. L. (2021). Prefrontal Cortex Development in Health and Disease: Lessons from Rodents and Humans. In *Trends in Neurosciences* (Vol. 44, Issue 3, pp. 227–240). Elsevier Ltd. https://doi.org/10.1016/j.tins.2020.10.017

Cho, K. K. A., Hoch, R., Lee, A. T., Patel, T., Rubenstein, J. L. R., & Sohal, V. S. (2015). Gamma rhythms link prefrontal interneuron dysfunction with cognitive inflexibility in dlx5/6+/- mice. *Neuron*, *85*(6), 1332–1343. https://doi.org/10.1016/j.neuron.2015.02.019

Chun, L. S., Free, R. B., Doyle, T. B., Huang, X. P., Rankin, M. L., & Sibley, D. R. (2013). D1-D2 dopamine receptor synergy promotes calcium signaling via multiple mechanisms. *Molecular Pharmacology*, *84*(2), 190–200. https://doi.org/10.1124/mol.113.085175

Chung, D. W., Fish, K. N., & Lewis, D. A. (2016). Pathological basis for deficient excitatory drive to cortical parvalbumin interneurons in schizophrenia. *American Journal of Psychiatry*, *173*(11). https://doi.org/10.1176/appi.ajp.2016.16010025

Ciliax, B. J., Nash, N., Heilman, C., Sunahara, R., Hartney, A., Tiberi, M., Rye, D. B., Caron, M. G., Niznik, H. B., & Levey, A. I. (2000). Dopamine D 5 Receptor Immunolocalization in Rat and Monkey Brain. In *Synapse* (Vol. 37).

Corrales, J. M. D., Blaess, S., Mahoney, E. M., & Joyner, A. L. (2006). The level of sonic hedgehog signaling regulates the complexity of cerebellar foliation. *Development*, *133*(9). https://doi.org/10.1242/dev.02351

Cunningham, M. G., Connor, C. M., Zhang, K., & Benes, F. M. (2005). Diminished serotonergic innervation of adult medial prefrontal cortex after 6-OHDA lesions in the newborn rat. *Developmental Brain Research*, *157*(2), 124–131. https://doi.org/10.1016/j.devbrainres.2005.02.020

Devoto, P., Flore, G., Saba, P., Fà, M., & Gessa, G. L. (2005). Stimulation of the locus coeruleus elicits noradrenaline and dopamine release in the medial prefrontal and parietal cortex. *Journal of Neurochemistry*, *92*(2), 368–374. https://doi.org/10.1111/j.1471-4159.2004.02866.x

Devoto, P., Flore, G., Saba, P., Scheggi, S., Mulas, G., Gambarana, C., Spiga, S., & Gessa, G. L. (2019). Noradrenergic terminals are the primary source of α 2 -adrenoceptor mediated dopamine release in the medial prefrontal cortex. *Progress in Neuro-Psychopharmacology and Biological Psychiatry*, *90*, 97–103. https://doi.org/10.1016/j.pnpbp.2018.11.015

d'Isa, R., Comi, G., & Leocani, L. (2021). Apparatus design and behavioural testing protocol for the evaluation of spatial working memory in mice through the spontaneous alternation T-maze. *Scientific Reports*, *11*(1). https://doi.org/10.1038/s41598-021-00402-7

Du, X., Serena, K., Hwang, W., Grech, A. M., Wu, Y. W. C., Schroeder, A., & Hill, R. A. (2018). Prefrontal cortical parvalbumin and somatostatin expression and cell density increase during adolescence and are modified by BDNF and sex. *Molecular and Cellular Neuroscience*, *88*, 177–188. https://doi.org/10.1016/j.mcn.2018.02.001

Dugan, J. P., Stratton, A., Riley, H. P., Farmer, W. T., & Mastick, G. S. (2011). Midbrain dopaminergic axons are guided longitudinally through the diencephalon by Slit/Robo signals. *Molecular and Cellular Neuroscience*, *46*(1), 347–356. https://doi.org/10.1016/j.mcn.2010.11.003

Dumas, S., & Wallén-Mackenzie, Å. (2019). Developmental Co-expression of Vglut2 and Nurr1 in a Mes-Di-Encephalic Continuum Preceeds Dopamine and Glutamate Neuron Specification. *Frontiers in Cell and Developmental Biology*, *7*. https://doi.org/10.3389/fcell.2019.00307

Ellwood, I. T., Patel, T., Wadia, V., Lee, A. T., Liptak, A. T., Bender, K. J., & Sohal, V. S. (2017). Tonic or phasic stimulation of dopaminergic projections to prefrontal cortex causes mice to maintain or deviate from previously learned behavioral strategies. *Journal of Neuroscience*, *37*(35), 8315–8329. https://doi.org/10.1523/JNEUROSCI.1221-17.2017

Ferguson, B. R., & Gao, W. J. (2018). Pv interneurons: critical regulators of E/I balance for prefrontal cortex-dependent behavior and psychiatric disorders. *Frontiers in Neural Circuits*, *12*(May), 1–13. https://doi.org/10.3389/fncir.2018.00037

Filice, F., Janickova, L., Henzi, T., Bilella, A., & Schwaller, B. (2020). The Parvalbumin Hypothesis of Autism Spectrum Disorder. *Frontiers in Cellular Neuroscience*, *14*. https://doi.org/10.3389/fncel.2020.577525

Filice, F., Vörckel, K. J., Sungur, A. Ö., Wöhr, M., & Schwaller, B. (2016). Reduction in parvalbumin expression not loss of the parvalbumin-expressing GABA interneuron subpopulation in genetic parvalbumin and shank mouse models of autism. *Molecular Brain*, *9*(1), 1–17. https://doi.org/10.1186/s13041-016-0192-8

Floresco, S. B. (2013). Prefrontal dopamine and behavioral flexibility: Shifting from an "inverted-U" toward a family of functions. In *Frontiers in Neuroscience* (Issue 7 APR). https://doi.org/10.3389/fnins.2013.00062

Floresco, S. B., & Magyar, O. (2006). Mesocortical dopamine modulation of executive functions: Beyond working memory. In *Psychopharmacology* (Vol. 188, Issue 4, pp. 567–585). https://doi.org/10.1007/s00213-006-0404-5

Floresco, S. B., & Phillips, A. G. (2001). Delay-dependent modulation of memory retrieval by infusion of a dopamine D1 agonist into the rat medial prefrontal cortex. *Behavioral Neuroscience*, *115*(4). https://doi.org/10.1037/0735-7044.115.4.934

Fung, S. J., Webster, M. J., Sivagnanasundaram, S., Duncan, C., Elashoff, M., & Weickert, C. S. (2010). Expression of interneuron markers in the dorsolateral prefrontal cortex of the developing human and in schizophrenia. *American Journal of Psychiatry*, *167*(12), 1479–1488. https://doi.org/10.1176/appi.ajp.2010.09060784

Fuster, J. M. (2001). many of the principles discussed below apply also to the PFC of nonprimate species. In *Neuron* (Vol. 30).

Gabbott, P. L. A., Dickie, B. G. M., Vaid, R. R., Headlam, A. J. N., & Bacon, S. J. (1997). Local-Circuit Neurones in the Medial Prefrontal Cortex (Areas 25, 32 and 24b) in the Rat: Morphology and Quantitative Distribution Indexing terms: calcium-binding proteins; GABA; NADPH diaphorase; cortical modules; limbic system. In *J. Comp. Neurol* (Vol. 377). Wiley-Liss, Inc.

Garcia, L. P., Witteveen, J. S., Middelman, A., van Hulten, J. A., Martens, G. J. M., Homberg, J. R., & Kolk, S. M. (2019). Perturbed Developmental Serotonin Signaling Affects Prefrontal Catecholaminergic Innervation and Cortical Integrity. *Molecular Neurobiology*, *56*(2), 1405–1420. https://doi.org/10.1007/s12035-018-1105-x

Gasbarri, A., Verney, C., Innocenzi, R., Campana, E., & Pacitti, C. (1994). Mesolimbic dopaminergic neurons innervating the hippocampal formation in the rat: a combined retrograde tracing and immunohistochemical study. *Brain Research*, *668*(1–2). https://doi.org/10.1016/0006-8993(94)90512-6

Gaspar', P., Bloch2, B., & Le Moine2, C. (1995). D1 and D2 Receptor Gene Expression in the Rat Frontal Cortex: Cellular Localization in Different Classes of Efferent N eu rons. In *European Journal of Neuroscience* (Vol. 7).

Gates, M. A., Coupe, V. M., Torres, E. M., Fricker-Gates, R. A., & Dunnett, S. B. (2004). Spatially and temporally restricted chemoattractive and chemorepulsive cues direct the formation of the nigro-striatal circuit. *European Journal of Neuroscience*, *19*(4), 831–844. https://doi.org/10.1111/j.1460-9568.2004.03213.x

Glantz, L. A., & Lewis, D. A. (2000). Decreased dendritic spine density on prefrontal cortical pyramidal neurons in schizophrenia. *Archives of General Psychiatry*, *57*(1). https://doi.org/10.1001/archpsyc.57.1.65

Gong, S., Doughty, M., Harbaugh, C. R., Cummins, A., Hatten, M. E., Heintz, N., & Gerfen, C. R. (2007). Targeting Cre recombinase to specific neuron populations with bacterial artificial chromosome constructs. In *Journal of Neuroscience* (Vol. 27, Issue 37, pp. 9817–9823). https://doi.org/10.1523/JNEUROSCI.2707-07.2007

Green, S. M., Nathani, S., Zimmerman, J., Fireman, D., & Urs, N. M. (2020). Retrograde labeling illuminates distinct topographical organization of d1 and d2 receptor-positive pyramidal neurons in the prefrontal cortex of mice. *ENeuro*, *7*(5). https://doi.org/10.1523/ENEURO.0194-20.2020

Guidotti, A., Auta, J., Davis, J. M., Gerevini, V. D., Dwivedi, Y., Grayson, D. R., Impagnatiello, F., Pandey, G., Pesold, C., Sharma, R., Uzunov, D., & Costa, E. (2000). Decrease in reelin and glutamic acid decarboxylase67 (GAD67) expression in schizophrenia and bipolar disorder: A postmortem brain study. *Archives of General Psychiatry*, *57*(11). https://doi.org/10.1001/archpsyc.57.11.1061

Hashemi, E., Ariza, J., Rogers, H., Noctor, S. C., & Martínez-Cerdeño, V. (2017). The number of parvalbumin-expressing interneurons is decreased in the prefrontal cortex in autism. *Cerebral Cortex*, *27*(3), 1931–1943. https://doi.org/10.1093/cercor/bhw021

Hashimoto, T., Volk, D. W., Eggan, S. M., Mirnics, K., Pierri, J. N., Sun, Z., Sampson, A. R., & Lewis, D. A. (2003). Gene expression deficits in a subclass of GABA neurons in the prefrontal cortex of subjects with schizophrenia. *Journal of Neuroscience*, *23*(15). https://doi.org/10.1523/jneurosci.23-15-06315.2003

Hayes, L., Ralls, S., Wang, H., & Ahn, S. (2013). Duration of Shh signaling contributes to mDA neuron diversity. *Developmental Biology*, *374*(1), 115–126. https://doi.org/10.1016/j.ydbio.2012.11.016

Hayes, L., Zhang, Z., Albert, P., Zervas, M., & Ahn, S. (2011). Timing of Sonic hedgehog and Gli1 expression segregates midbrain dopamine neurons. *Journal of Comparative Neurology*, *519*(15). https://doi.org/10.1002/cne.22711

Hisahara, S., & Shimohama, S. (2011). Dopamine Receptors and Parkinson's Disease. *International Journal of Medicinal Chemistry*, *2011*, 1–16. https://doi.org/10.1155/2011/403039

Hivert, B., Liu, Z., Chuang, C. Y., Doherty, P., & Sundaresan, V. (2002). Robo1 and Robo2 are homophilic binding molecules that promote axonal growth. *Molecular and Cellular Neuroscience*, *21*(4). https://doi.org/10.1006/mcne.2002.1193

Holmes, G. P., Negus, K., Burridge, L., Raman, S., Algar, E., Yamada, T., & Little, M. H. (1998). *Distinct but overlapping expression patterns of two vertebrate slit homologs implies functional roles in CNS development and organogenesis*. http://www.cmcb.uq.e-

Hoops, D., & Flores, C. (2017). Making Dopamine Connections in Adolescence. In *Trends in Neurosciences* (Vol. 40, Issue 12, pp. 709–719). Elsevier Ltd. https://doi.org/10.1016/j.tins.2017.09.004

Howes, O. D., & Shatalina, E. (2022). Integrating the Neurodevelopmental and Dopamine Hypotheses of Schizophrenia and the Role of Cortical Excitation-Inhibition Balance. In *Biological Psychiatry* (Vol. 92, Issue 6). https://doi.org/10.1016/j.biopsych.2022.06.017

Islam, K. U. S., Meli, N., & Blaess, S. (2021). The Development of the Mesoprefrontal Dopaminergic System in Health and Disease. In *Frontiers in Neural Circuits* (Vol. 15). Frontiers Media S.A. https://doi.org/10.3389/fncir.2021.746582

Kaar, S. J., Angelescu, I., Marques, T. R., & Howes, O. D. (2019). Pre-frontal parvalbumin interneurons in schizophrenia: a meta-analysis of post-mortem studies. *Journal of Neural Transmission*, *126*(12), 1637–1651. https://doi.org/10.1007/s00702-019-02080-2

Kabanova, A., Pabst, M., Lorkowski, M., Braganza, O., Boehlen, A., Nikbakht, N., Pothmann, L., Vaswani, A. R., Musgrove, R., Di Monte, D. A., Sauvage, M., Beck, H., & Blaess, S. (2015). Function and developmental origin of a mesocortical inhibitory circuit. *Nature Neuroscience*, *18*(6), 872–882. https://doi.org/10.1038/nn.4020

Kalsbeek, A., Voorn, P., Buijs, R. M., Pool, C. W., & Uylings, H. B. M. (1988). Development of the dopaminergic innervation in the prefrontal cortex of the rat. *Journal of Comparative Neurology*, *269*(1), 58–72. https://doi.org/10.1002/cne.902690105

Kamath, T., Abdulraouf, A., Burris, S. J., Langlieb, J., Gazestani, V., Nadaf, N. M., Balderrama, K., Vanderburg, C., & Macosko, E. Z. (2022). Single-cell genomic profiling of human dopamine neurons identifies a population that selectively degenerates in Parkinson's disease. *Nature Neuroscience*, *25*(5), 588–595. https://doi.org/10.1038/s41593-022-01061-1

Kimmel, R. A., Turnbull, D. H., Blanquet, V., Wurst, W., Loomis, C. A., & Joyner, A. L. (2000). Two lineage boundaries coordinate vertebrate apical ectodermal ridge formation. *Genes and Development*, *14*(11). https://doi.org/10.1101/gad.14.11.1377

Kolk, S. M., Gunput, R. A. F., Tran, T. S., Van Den Heuvel, D. M. A., Prasad, A. A., Hellemons, A. J. C. G. M., Adolfs, Y., Ginty, D. D., Kolodkin, A. L., Burbach, J. P. H., Smidt, M. P., & Pasterkamp, R. J. (2009). Semaphorin 3F is a bifunctional guidance cue for dopaminergic axons and controls their fasciculation, channeling, rostral growth, and intracortical targeting. *Journal of Neuroscience*, *29*(40), 12542–12557. https://doi.org/10.1523/JNEUROSCI.2521-09.2009

Kolk, S. M., & Rakic, P. (2022). Development of prefrontal cortex. In *Neuropsychopharmacology* (Vol. 47, Issue 1, pp. 41–57). Springer Nature. https://doi.org/10.1038/s41386-021-01137-9

Kroon, T., van Hugte, E., van Linge, L., Mansvelder, H. D., & Meredith, R. M. (2019). Early postnatal development of pyramidal neurons across layers of the mouse medial prefrontal cortex. *Scientific Reports*, *9*(1). https://doi.org/10.1038/s41598-019-41661-9

Kubota, Y., Hattori, R., & Yui, Y. (1994). Three distinct subpopulations of GABAergic neurons in rat frontal agranular cortex. In *Brain Research* (Vol. 649).

Kubota, Y., & Kawaguchi, Y. (1994). Three classes of GABAergic interneurons in neocortex and neostriatum. *The Japanese Journal of Physiology*, *44 Suppl 2*.

La Manno, G., Gyllborg, D., Codeluppi, S., Nishimura, K., Salto, C., Zeisel, A., Borm, L. E., Stott, S. R. W., Toledo, E. M., Villaescusa, J. C., Lönnerberg, P., Ryge, J., Barker, R. A., Arenas, E., & Linnarsson, S. (2016). Molecular Diversity of Midbrain Development in Mouse, Human, and Stem Cells. *Cell*, *167*(2). https://doi.org/10.1016/j.cell.2016.09.027

Labouesse, M. A., Cola, R. B., & Patriarchi, T. (2020). GPCR-based dopamine sensors—A detailed guide to inform sensor choice for in vivo imaging. In *International Journal of Molecular Sciences* (Vol. 21, Issue 21, pp. 1–41). MDPI AG. https://doi.org/10.3390/ijms21218048

Lammel, S., Hetzel, A., Häckel, O., Jones, I., Liss, B., & Roeper, J. (2008). Unique Properties of Mesoprefrontal Neurons within a Dual Mesocorticolimbic Dopamine System. *Neuron*, *57*(5), 760–773. https://doi.org/10.1016/j.neuron.2008.01.022

Lammel, S., Lim, B. K., Ran, C., Huang, K. W., Betley, M. J., Tye, K. M., Deisseroth, K., & Malenka, R. C. (2012). Input-specific control of reward and aversion in the ventral tegmental area. *Nature*, *491*(7423), 212–217. https://doi.org/10.1038/nature11527

Larsen, B., & Luna, B. (2018). Adolescence as a neurobiological critical period for the development of higher-order cognition. *Neuroscience and Biobehavioral Reviews*, *94*(March), 179–195. https://doi.org/10.1016/j.neubiorev.2018.09.005

Lazarus, M. S., Krishnan, K., & Huang, Z. J. (2015). GAD67 deficiency in parvalbumin interneurons produces deficits in inhibitory transmission and network disinhibition in mouse prefrontal cortex. *Cerebral Cortex*, *25*(5). https://doi.org/10.1093/cercor/bht322

Le Magueresse, C., & Monyer, H. (2013). GABAergic Interneurons Shape the Functional Maturation of the Cortex. *Neuron*, *77*(3), 388–405. https://doi.org/10.1016/j.neuron.2013.01.011

Lee, F. H., Zai, C. C., Cordes, S. P., Roder, J. C., & Wong, A. H. (2013). *Abnormal interneuron development in disrupted-in-schizophrenia-1 L100P mutant mice*. http://www.molecularbrain.com/content/6/1/20

Lee, S. P., So, C. H., Rashid, A. J., Varghese, G., Cheng, R., Lança, A. J., O'Dowd, B. F., & George, S. R. (2004). Dopamine D1 and D2 receptor co-activation generates a novel phospholipase C-mediated calcium signal. *Journal of Biological Chemistry*, *279*(34), 35671–35678. https://doi.org/10.1074/jbc.M401923200

Leslie, C. A., Robertson, M. W., Cutler, A. J., & Bennett, J. P. (1991). Postnatal development of D1 dopamine receptors in the medial prefrontal cortex, striatum and nucleus accumbens of normal and neonatal 6-hydroxydopamine treated rats: a quantitative autoradiographic analysis. In *Developmental Brain Research* (Vol. 62).

Levey, A. I., Hersch, S. M., Rye, D. B., Sunaharat, R. K., Niznikt, H. B., Kitt, C. A., Price, D. L., Maggio1, R., Brann Ii, M. R., & Ciliax, B. J. (1993). Localization of D1 and D2 dopamine receptors in brain with subtype-specific antibodies. In *Proc. Natl. Acad. Sci. USA* (Vol. 90).

Levitt, P., & Moore, R. Y. (1979). Development of the noradrenergic innervation of neocortex. *Brain Research*, *162*(2), 243–259. https://doi.org/10.1016/0006-8993(79)90287-7

Lewis, D. A. (1997). Development of the prefrontal cortex during adolescence: Insights into vulnerable neural circuits in schizophrenia. In *Neuropsychopharmacology* (Vol. 16, Issue 6). https://doi.org/10.1016/S0893-133X(96)00277-1

Lidow, M. S., Koh, P. O., & Arnsten, A. F. T. (2003). D1 dopamine receptors in the mouse prefrontal cortex: Immunocytochemical and cognitive neuropharmacological analyses. *Synapse*, *47*(2), 101–108. https://doi.org/10.1002/syn.10143

Lieberman, O. J., McGuirt, A. F., Mosharov, E. V., Pigulevskiy, I., Hobson, B. D., Choi, S., Frier, M. D., Santini, E., Borgkvist, A., & Sulzer, D. (2018). Dopamine Triggers the Maturation of Striatal Spiny Projection Neuron Excitability during a Critical Period. *Neuron*, *99*(3), 540-554.e4. https://doi.org/10.1016/j.neuron.2018.06.044

Lim, L., Mi, D., Llorca, A., & Marín, O. (2018). Development and Functional Diversification of Cortical Interneurons. *Neuron*, *100*(2), 294–313. https://doi.org/10.1016/j.neuron.2018.10.009

Liu, T., Bai, W., Xia, M., & Tian, X. (2018). Directional hippocampal-prefrontal interactions during working memory. *Behavioural Brain Research*, *338*. https://doi.org/10.1016/j.bbr.2017.10.003

Lord, C., Elsabbagh, M., Baird, G., & Veenstra-Vanderweele, J. (2018). Autism spectrum disorder. In *The Lancet* (Vol. 392, Issue 10146, pp. 508–520). Lancet Publishing Group. https://doi.org/10.1016/S0140-6736(18)31129-2

Maddaloni, G., Bertero, A., Pratelli, M., Barsotti, N., Boonstra, A., Giorgi, A., Migliarini, S., & Pasqualetti, M. (2017). Development of serotonergic fibers in the post-natal mouse brain. *Frontiers in Cellular Neuroscience*, *11*(July), 1–11. https://doi.org/10.3389/fncel.2017.00202

Mandic-Maravic, V., Grujicic, R., Milutinovic, L., Munjiza-Jovanovic, A., & Pejovic-Milovancevic, M. (2022). Dopamine in Autism Spectrum Disorders—Focus on D2/D3 Partial Agonists and Their Possible Use in Treatment. In *Frontiers in Psychiatry* (Vol. 12). Frontiers Media S.A. https://doi.org/10.3389/fpsyt.2021.787097

Manitt, C., Eng, C., Pokinko, M., Ryan, R. T., Torres-Berrío, A., Lopez, J. P., Yogendran, S. V., Daubaras, M. J. J., Grant, A., Schmidt, E. R. E., Tronche, F., Krimpenfort, P., Cooper, H. M., Pasterkamp, R. J., Kolb, B., Turecki, G., Wong, T. P., Nestler, E. J., Giros, B., & Flores, C. (2013). Dcc orchestrates the development of the prefrontal cortex during adolescence and is altered in psychiatric patients. *Translational Psychiatry*, *3*. https://doi.org/10.1038/tp.2013.105

Margolis, E. B., Lock, H., Chefer, V. I., Shippenberg, T. S., Hjelmstad, G. O., & Fields, H. L. (2005). *opioids selectively control dopaminergic neurons projecting to the prefrontal cortex* (Vol. 103, Issue 8). www.pnas.orgcgidoi10.1073pnas.0511159103

Mastwal, S., Li, X., Stowell, R., Manion, M., Zhang, W., Kim, N.-S., Yoon, K.-J., Song, H., Ming, G.-L., & Hong Wang, K. (2023). *Adolescent neurostimulation of dopamine circuit reverses genetic deficits in frontal cortex function*. *12*, 87414. https://doi.org/10.7554/eLife

Miller, E. K., Freedman, D. J., & Wallis, J. D. (2002). The prefrontal cortex: Categories, concepts and cognition. *Philosophical Transactions of the Royal Society B: Biological Sciences*, *357*(1424), 1123–1136. https://doi.org/10.1098/rstb.2002.1099

Missale, C., Nash, S. R., Robinson, S. W., Jaber, M., & Caron, M. G. (1998). Dopamine Receptors: From Structure to Function. In *PHYSIOLOGICAL REVIEWS* (Vol. 78, Issue 1).

Miyoshi, G., & Fishell, G. (2011). GABAergic interneuron lineages selectively sort into specific cortical layers during early postnatal development. *Cerebral Cortex*, *21*(4), 845–852. https://doi.org/10.1093/cercor/bhq155

Mizoguchi, K., Shoji, H., Tanaka, Y., Maruyama, W., & Tabira, T. (2009). Age-related spatial working memory impairment is caused by prefrontal cortical dopaminergic dysfunction in rats. *Neuroscience*, *162*(4). https://doi.org/10.1016/j.neuroscience.2009.05.023

Mo, R., Freer, A. M., Zinyk, D. L., Crackower, M. A., Michaud, J., Heng, H. H. Q., Chik, K. W., Shi, X. M., Tsui, L. C., Cheng, S. H., Joyner, A. L., & Hui, C. C. (1997). Specific and redundant functions of Gli2 and Gli3 zinc finger genes in skeletal patterning and development. *Development*, *124*(1). https://doi.org/10.1242/dev.124.1.113

Morón, J. A., Brockington, A., Wise, R. A., Rocha, B. A., & Hope, B. T. (2002). Dopamine uptake through the norepinephrine transporter in brain regions with low levels of the dopamine transporter: Evidence from knock-out mouse lines. *Journal of Neuroscience*, *22*(2). https://doi.org/10.1523/jneurosci.22-02-00389.2002

Mukherjee, A., Carvalho, F., Eliez, S., & Caroni, P. (2019). Long-Lasting Rescue of Network and Cognitive Dysfunction in a Genetic Schizophrenia Model. *Cell*, *178*(6), 1387-1402.e14. https://doi.org/10.1016/j.cell.2019.07.023

Murphy, B. L., Arnsten, A. F. T., Goldman-Rakic, P. S., & Roth, R. H. (1996). Increased dopamine turnover in the prefrontal cortex impairs spatial working memory performance

in rats and monkeys. *Proceedings of the National Academy of Sciences of the United States of America*, *93*(3). https://doi.org/10.1073/pnas.93.3.1325

Murray, A. J., Woloszynowska-Fraser, M. U., Ansel-Bollepalli, L., Cole, K. L. H., Foggetti, A., Crouch, B., Riedel, G., & Wulff, P. (2015). Parvalbumin-positive interneurons of the prefrontal cortex support working memory and cognitive flexibility. *Scientific Reports*, *5*. https://doi.org/10.1038/srep16778

Nakamoto, C., Goto, Y., Tomizawa, Y., Fukata, Y., Fukata, M., Harpsøe, K., Gloriam, D. E., Aoki, K., & Takeuchi, T. (2021). A novel red fluorescence dopamine biosensor selectively detects dopamine in the presence of norepinephrine in vitro. *Molecular Brain*, *14*(1). https://doi.org/10.1186/s13041-021-00882-8

Nakamura, S. I., Ito, Y., Shirasaki, R., & Murakami, F. (2000). Local directional cues control growth polarity of dopaminergic axons along the rostrocaudal axis. *Journal of Neuroscience*, *20*(11), 4112–4119. https://doi.org/10.1523/jneurosci.20-11-04112.2000

Naneix, F., Marchand, A. R., Di Scala, G., Pape, J. R., & Coutureau, E. (2012). Parallel maturation of goal-directed behavior and dopaminergic systems during adolescence. *Journal of Neuroscience*, *32*(46), 16223–16232. https://doi.org/10.1523/JNEUROSCI.3080-12.2012

Neve, K. A., Seamans, J. K., & Trantham-Davidson, H. (2004). Dopamine Receptor Signaling. *Journal of Receptor and Signal Transduction Research*, *24*(3), 165–205. https://doi.org/10.1081/lrst-200029981

Noaín, D., Avale, M. E., Wedemeyer, C., Calvo, D., Peper, M., & Rubinstein, M. (2006). Identification of brain neurons expressing the dopamine D4 receptor gene using BAC transgenic mice. *European Journal of Neuroscience*, *24*(9), 2429–2438. https://doi.org/10.1111/j.1460-9568.2006.05148.x

Noisin, E. L., & Thomas, W. E. (1988). Ontogeny of dopaminergic function in the rat midbrain tegmentum, corpus striatum and frontal cortex. In *Developmental Brain Research* (Vol. 41).

Oh, W. C., Rodríguez, G., Asede, D., Jung, K., Hwang, I. W., Ogelman, R., Bolton, M. M., & Kwon, H. B. (2021). Dysregulation of the mesoprefrontal dopamine circuit mediates an early-life stress-induced synaptic imbalance in the prefrontal cortex. *Cell Reports*, *35*(5). https://doi.org/10.1016/j.celrep.2021.109074

Ohira, K. (2019). Dopamine stimulates differentiation and migration of cortical interneurons. *Biochemical and Biophysical Research Communications*, *512*(3). https://doi.org/10.1016/j.bbrc.2019.03.105

Panman, L., Papathanou, M., Laguna, A., Oosterveen, T., Volakakis, N., Acampora, D., Kurtsdotter, I., Yoshitake, T., Kehr, J., Joodmardi, E., Muhr, J., Simeone, A., Ericson, J., & Perlmann, T. (2014). Sox6 and Otx2 control the specification of substantia nigra and ventral tegmental area dopamine neurons. *Cell Reports*, *8*(4). https://doi.org/10.1016/j.celrep.2014.07.016

Pavăl, D. (2017). A Dopamine Hypothesis of Autism Spectrum Disorder. In *Developmental Neuroscience* (Vol. 39, Issue 5). https://doi.org/10.1159/000478725

Pavăl, D., & Miclutia, I. V. (2021). The Dopamine Hypothesis of Autism Spectrum Disorder Revisited: Current Status and Future Prospects. In *Developmental Neuroscience* (Vol. 43, Issue 2, pp. 73–83). S. Karger AG. https://doi.org/10.1159/000515751

Pérez-López, J. L., Contreras-López, R., Ramírez-Jarquín, J. O., & Tecuapetla, F. (2018). Direct Glutamatergic Signaling From Midbrain Dopaminergic Neurons Onto Pyramidal Prefrontal Cortex Neurons. *Frontiers in Neural Circuits*, *12*. https://doi.org/10.3389/fncir.2018.00070

Perlman, G., Tanti, A., & Mechawar, N. (2021). Parvalbumin interneuron alterations in stress-related mood disorders: A systematic review. In *Neurobiology of Stress* (Vol. 15). Elsevier Inc. https://doi.org/10.1016/j.ynstr.2021.100380

Phillips, A. G., Ahn, S., & Floresco, S. B. (2004). Magnitude of Dopamine Release in Medial Prefrontal Cortex Predicts Accuracy of Memory on a Delayed Response Task. *Journal of Neuroscience*, *24*(2). https://doi.org/10.1523/JNEUROSCI.4653-03.2004

Pioli, E. Y., Gaskill, B. N., Gilmour, G., Tricklebank, M. D., Dix, S. L., Bannerman, D., & Garner, J. P. (2014). An automated maze task for assessing hippocampus-sensitive memory in mice. *Behavioural Brain Research*, *261*, 249–257. https://doi.org/10.1016/j.bbr.2013.12.009

Pittolo, S., Yokoyama, S., Willoughby, D. D., Taylor, C. R., Reitman, M. E., Tse, V., Wu, Z., Etchenique, R., Li, Y., & Poskanzer, K. E. (2022). Dopamine activates astrocytes in prefrontal cortex via α1-adrenergic receptors. *Cell Reports*, *40*(13). https://doi.org/10.1016/j.celrep.2022.111426

Poulin, J. F., Caronia, G., Hofer, C., Cui, Q., Helm, B., Ramakrishnan, C., Chan, C. S., Dombeck, D. A., Deisseroth, K., & Awatramani, R. (2018). Mapping projections of molecularly defined dopamine neuron subtypes using intersectional genetic approaches. *Nature Neuroscience*, *21*(9), 1260–1271. https://doi.org/10.1038/s41593-018-0203-4

Poulin, J. F., Gaertner, Z., Moreno-Ramos, O. A., & Awatramani, R. (2020). Classification of Midbrain Dopamine Neurons Using Single-Cell Gene Expression Profiling Approaches. In *Trends in Neurosciences* (Vol. 43, Issue 3, pp. 155–169). Elsevier Ltd. https://doi.org/10.1016/j.tins.2020.01.004

Poulin, J. F., Zou, J., Drouin-Ouellet, J., Kim, K. Y. A., Cicchetti, F., & Awatramani, R. B. (2014). Defining midbrain dopaminergic neuron diversity by single-cell gene expression profiling. *Cell Reports*, *9*(3), 930–943. https://doi.org/10.1016/j.celrep.2014.10.008

Powell, J. M., Plummer, N. W., Scappini, E. L., Tucker, C. J., & Jensen, P. (2019). DEFiNE: A method for enhancement and quantification of fluorescently labeled axons. *Frontiers in Neuroanatomy*, *12*. https://doi.org/10.3389/fnana.2018.00117

Rajput, P. S., Kharmate, G., Somvanshi, R. K., & Kumar, U. (2009). Colocalization of dopamine receptor subtypes with dopamine and cAMP-regulated phosphoprotein (DARPP-32) in rat brain. *Neuroscience Research*, *65*(1), 53–63. https://doi.org/10.1016/j.neures.2009.05.005

Reynolds, L. M., Pokinko, M., Torres-Berrío, A., Cuesta, S., Lambert, L. C., Del Cid Pellitero, E., Wodzinski, M., Manitt, C., Krimpenfort, P., Kolb, B., & Flores, C. (2018). DCC Receptors Drive Prefrontal Cortex Maturation by Determining Dopamine Axon Targeting in Adolescence. *Biological Psychiatry*, *83*(2), 181–192. https://doi.org/10.1016/j.biopsych.2017.06.009

Rinetti-Vargas, G., Phamluong, K., Ron, D., & Bender, K. J. (2017). Periadolescent Maturation of GABAergic Hyperpolarization at the Axon Initial Segment. *Cell Reports*, *20*(1), 21–29. https://doi.org/10.1016/j.celrep.2017.06.030

Rudy. (2013). *Three groups of interneurons account for nearly 100 %*. *71*(1), 45–61. https://doi.org/10.1002/dneu.20853.Three

Santana, N., & Artigas, F. (2017). Laminar and cellular distribution of monoamine receptors in rat medial prefrontal cortex. In *Frontiers in Neuroanatomy* (Vol. 11). Frontiers Media S.A. https://doi.org/10.3389/fnana.2017.00087

Santana, N., Mengod, G., & Artigas, F. (2009). Quantitative analysis of the expression of dopamine D1 and D2 receptors in pyramidal and GABAergic neurons of the rat prefrontal cortex. *Cerebral Cortex*, *19*(4), 849–860. https://doi.org/10.1093/cercor/bhn134

Sawaguchi, T., & Goldman-Rakic, P. S. (1991). D1 Dopamine Receptors in Prefrontal Cortex: Involvement in Working Memory. *Science*, *251*(4996). https://doi.org/10.1126/science.1825731

Schambra, U. B., Duncan, G. E., R Breese, tf G., Fornaretto, M. G., G Caron, ll M., & Fremeau Jr, R. T. (1994). *ONTOGENY OF D, AND D, DOPAMINE RECEPTOR SUBTYPES IN RAT BRAIN USING IN SITU HYBRIDIZATION AND RECEPTOR BINDING* (Vol. 62, Issue 1).

Schneider, C. A., Rasband, W. S., & Eliceiri, K. W. (2012). NIH Image to ImageJ: 25 years of image analysis. In *Nature Methods* (Vol. 9, Issue 7). https://doi.org/10.1038/nmeth.2089

Schubert, D., Martens, G. J. M., & Kolk, S. M. (2015). Molecular underpinnings of prefrontal cortex development in rodents provide insights into the etiology of neurodevelopmental disorders. In *Molecular Psychiatry* (Vol. 20, Issue 7, pp. 795–809). Nature Publishing Group. https://doi.org/10.1038/mp.2014.147

Seamans, J. K., Floresco, S. B., & Phillips, A. G. (1998). D1 receptor modulation of hippocampal-prefrontal cortical circuits integrating spatial memory with executive functions in the rat. *Journal of Neuroscience*, *18*(4). https://doi.org/10.1523/jneurosci.18-04-01613.1998

Sesack, S. R., Aoki, C., & Picke13, V. M. (1994). *Ultrastructural Localization of D, Receptor-like Immunoreactivity in Midbrain Dopamine Neurons and Their Striatal Targets*.

Shaw, P., Gornick, M., Lerch, J., Addington, A., Seal, J., Greenstein, D., Sharp, W., Evans, A., Giedd, J. N., Castellanos, F. X., & Rapoport, J. L. (2007). Polymorphisms of the dopamine D4 receptor, clinical outcome, and cortical structure in attention-deficit/hyperactivity disorder. *Archives of General Psychiatry*, *64*(8). https://doi.org/10.1001/archpsyc.64.8.921

Smidt, M. P., & Burbach, J. P. H. (2007). How to make a mesodiencephalic dopaminergic neuron. *Nature Reviews Neuroscience*, *8*(1), 21–32. https://doi.org/10.1038/nrn2039

Sohal, V. S., Zhang, F., Yizhar, O., & Deisseroth, K. (2009). Parvalbumin neurons and gamma rhythms enhance cortical circuit performance. *Nature*, *459*(7247), 698–702. https://doi.org/10.1038/nature07991

Sonnenschein, S. F., Gomes, F. V., & Grace, A. A. (2020). Dysregulation of Midbrain Dopamine System and the Pathophysiology of Schizophrenia. In *Frontiers in Psychiatry* (Vol. 11). https://doi.org/10.3389/fpsyt.2020.00613

Sotoyama, H., Inaba, H., Iwakura, Y., Namba, H., Takei, N., Sasaoka, T., & Nawa, H. (2022). The dual role of dopamine in the modulation of information processing in the prefrontal cortex underlying social behavior. *FASEB Journal*, *36*(2). https://doi.org/10.1096/fj.202101637R

Stamatakis, A. M., & Stuber, G. D. (2012). Activation of lateral habenula inputs to the ventral midbrain promotes behavioral avoidance. *Nature Neuroscience*, *15*(8), 1105–1107. https://doi.org/10.1038/nn.3145

Stirling, D. R., Swain-Bowden, M. J., Lucas, A. M., Carpenter, A. E., Cimini, B. A., & Goodman, A. (2021). CellProfiler 4: improvements in speed, utility and usability. *BMC Bioinformatics*, *22*(1). https://doi.org/10.1186/s12859-021-04344-9

Tapias-Espinosa, C., Sánchez-González, A., Cañete, T., Sampedro-Viana, D., Castillo-Ruiz, M. del M., Oliveras, I., Tobeña, A., Aznar, S., & Fernández-Teruel, A. (2023). Decreased activation of parvalbumin interneurons in the medial prefrontal cortex in intact inbred Roman rats with schizophrenia-like reduced sensorimotor gating. *Behavioural Brain Research*, *437*. https://doi.org/10.1016/j.bbr.2022.114113

Tarazi, F. I., & Baldessarini, R. J. (2000). Comparative postnatal development of dopamine D1, D2 and D4 receptors in rat forebrain. *International Journal of Developmental Neuroscience*, *18*(1), 29–37. https://doi.org/10.1016/S0736-5748(99)00108-2

Taylor, J. B., Cunningham, M. C., & Benes, F. M. (1998). Neonatal raphe lesions increase dopamine fibers in prefrontal cortex of adult rats. *NeuroReport*, *9*(8). https://doi.org/10.1097/00001756-199806010-00026

Tritsch, N. X., & Sabatini, B. L. (2012). Dopaminergic Modulation of Synaptic Transmission in Cortex and Striatum. *Neuron*, *76*(1), 33–50. https://doi.org/10.1016/j.neuron.2012.09.023

Tseng, K. Y., & O'Donnell, P. (2005). Post-pubertal emergence of prefrontal cortical up states induced by D 1-NMDA co-activation. *Cerebral Cortex*, *15*(1), 49–57. https://doi.org/10.1093/cercor/bhh107

Tseng, K. Y., & O'Donnell, P. (2007). Dopamine modulation of prefrontal cortical interneurons changes during adolescence. *Cerebral Cortex*, *17*(5), 1235–1240. https://doi.org/10.1093/cercor/bhl034

Tsetsenis, T., Broussard, J. I., & Dani, J. A. (2023). Dopaminergic regulation of hippocampal plasticity, learning, and memory. In *Frontiers in Behavioral Neuroscience* (Vol. 16). https://doi.org/10.3389/fnbeh.2022.1092420

Uhlhaas, P. J., & Singer, W. (2011). The development of neural synchrony and large-scale cortical networks during adolescence: Relevance for the pathophysiology of schizophrenia and neurodevelopmental hypothesis. *Schizophrenia Bulletin*, *37*(3), 514–523. https://doi.org/10.1093/schbul/sbr034

Van Aerde, K. I., & Feldmeyer, D. (2015). Morphological and physiological characterization of pyramidal neuron subtypes in rat medial prefrontal cortex. *Cerebral Cortex*, *25*(3), 788–805. https://doi.org/10.1093/cercor/bht278

Van den Heuvel, D. M. A., & Pasterkamp, R. J. (2008). Getting connected in the dopamine system. *Progress in Neurobiology*, *85*(1), 75–93. https://doi.org/10.1016/j.pneurobio.2008.01.003

van Os, J., & Kapur, S. (2009). Schizophrenia. In *The Lancet* (Vol. 374, Issue 9690). https://doi.org/10.1016/S0140-6736(09)60995-8

Veenvliet, J. V., & Smidt, M. P. (2014). Molecular mechanisms of dopaminergic subset specification: Fundamental aspects and clinical perspectives. In *Cellular and Molecular Life Sciences* (Vol. 71, Issue 24, pp. 4703–4727). Birkhauser Verlag AG. https://doi.org/10.1007/s00018-014-1681-5

Verwey, M., Grant, A., Meti, N., Adye-White, L., Torres-Berrío, A., Rioux, V., Lévesque, M., Charron, F., & Flores, C. (2016). Mesocortical dopamine phenotypes in mice lacking the sonic hedgehog receptor Cdon. *ENeuro*, *3*(3), 775–787. https://doi.org/10.1523/ENEURO.0009-16.2016

Vogel, P., Hahn, J., Duvarci, S., & Sigurdsson, T. (2022). Prefrontal pyramidal neurons are critical for all phases of working memory. *Cell Reports*, *39*(2). https://doi.org/10.1016/j.celrep.2022.110659

Volk, D. W., Austin, M. C., Pierri, J. N., Sampson, A. R., & Lewis, D. A. (2000). Decreased glutamic acid decarboxylase67 messenger RNA expression in a subset of prefrontal cortical γ-aminobutyric acid neurons in subjects with schizophrenia. *Archives of General Psychiatry*, *57*(3). https://doi.org/10.1001/archpsyc.57.3.237

Volkow, N. D., & Morales, M. (2015). The Brain on Drugs: From Reward to Addiction. In *Cell* (Vol. 162, Issue 4, pp. 712–725). Cell Press. https://doi.org/10.1016/j.cell.2015.07.046

Voorn, P., Kalsbeek, A., Jorritsma-Byham, B., & Groenewegen, H. J. (1988). The pre- and postnatal development of the dopaminergic cell groups in the ventral mesencephalon and the dopaminergic innervation of the striatum of the rat. *Neuroscience*, *25*(3), 857–887. https://doi.org/10.1016/0306-4522(88)90041-3

Vosberg, D. E., Leyton, M., & Flores, C. (2020). The Netrin-1/DCC guidance system: dopamine pathway maturation and psychiatric disorders emerging in adolescence. *Molecular Psychiatry*, *25*(2), 297–307. https://doi.org/10.1038/s41380-019-0561-7

Wahlsten, D. (2010). Mouse Behavioral Testing: How to Use Mice in Behavioral Neuroscience. In *Mouse Behavioral Testing: How to Use Mice in Behavioral Neuroscience*. https://doi.org/10.1016/C2009-0-30530-9

Wang, F., Flanagan, J., Su, N., Wang, L. C., Bui, S., Nielson, A., Wu, X., Vo, H. T., Ma, X. J., & Luo, Y. (2012). RNAscope: A novel in situ RNA analysis platform for formalin-fixed, paraffin-embedded tissues. *Journal of Molecular Diagnostics*, *14*(1). https://doi.org/10.1016/j.jmoldx.2011.08.002

Wenk, G. L. (1998). Assessment of Spatial Memory Using the T Maze. *Current Protocols in Neuroscience*, *4*(1). https://doi.org/10.1002/0471142301.ns0805bs04

Willing, J., Cortes, L. R., Brodsky, J. M., Kim, T., & Juraska, J. M. (2017). Innervation of the medial prefrontal cortex by tyrosine hydroxylase immunoreactive fibers during adolescence in male and female rats. *Developmental Psychobiology*, *59*(5), 583–589. https://doi.org/10.1002/dev.21525

Wöhr, M., Orduz, D., Gregory, P., Moreno, H., Khan, U., Vörckel, K. J., Wolfer, D. P., Welzl, H., Gall, D., Schiffmann, S. N., & Schwaller, B. (2015). Lack of parvalbumin in mice leads to behavioral deficits relevant to all human autism core symptoms and related neural morphofunctional abnormalities. *Translational Psychiatry*, *5*(3). https://doi.org/10.1038/TP.2015.19

Wonders, C. P., & Anderson, S. A. (2006). The origin and specification of cortical interneurons. *Nature Reviews Neuroscience*, *7*(9), 687–696. https://doi.org/10.1038/nrn1954

Wu, J., Xiao, H., Sun, H., Zou, L., & Zhu, L. Q. (2012). Role of dopamine receptors in ADHD: A systematic meta-analysis. *Molecular Neurobiology*, *45*(3). https://doi.org/10.1007/s12035-012-8278-5

Wu, M., Zhang, X., Feng, S., Freda, S. N., Kumari, P., Dumrongprechachan, V., & Kozorovitskiy, Y. (2024). Dopamine pathways mediating affective state transitions after sleep loss. *Neuron. 2024 Jan 3;112(1):141-154.E8.*, *112*(1), 141–154.

Xia, M., Liu, T., Bai, W., Zheng, X., & Tian, X. (2019). Information transmission in HPC-PFC network for spatial working memory in rat. *Behavioural Brain Research*, *356*, 170–178. https://doi.org/10.1016/j.bbr.2018.08.024

Yang, J. M., Zhang, J., Yu, Y. Q., Duan, S., & Li, X. M. (2014). Postnatal development of 2 microcircuits involving fast-spiking interneurons in the mouse prefrontal cortex. *Cerebral Cortex*, *24*(1), 98–109. https://doi.org/10.1093/cercor/bhs291

Yang, S. S., Mack, N. R., Shu, Y., & Gao, W. J. (2021). Prefrontal GABAergic Interneurons Gate Long-Range Afferents to Regulate Prefrontal Cortex-Associated Complex Behaviors. In *Frontiers in Neural Circuits* (Vol. 15). https://doi.org/10.3389/fncir.2021.716408

Zhang, Y., Behrens, M. M., & Lisman, J. E. (2008). Prolonged exposure to NMDAR antagonist suppresses inhibitory synaptic transmission in prefrontal cortex. *Journal of Neurophysiology*, *100*(2). https://doi.org/10.1152/jn.00079.2008

Zhang, Z. W., Burke, M. W., Calakos, N., Beaulieu, J. M., & Vaucher, E. (2010). Confocal analysis of cholinergic and dopaminergic inputs onto pyramidal cells in the prefrontal cortex of rodents. *Frontiers in Neuroanatomy*, *JUNE*. https://doi.org/10.3389/fnana.2010.00021

8. Acknowledgements

The completion of this thesis would not have been possible without the help and guidance of people who have supported me on this journey.

Firstly, I would like to express my deepest gratitude and appreciation to Prof. Dr. Sandra Blaess for giving me the opportunity to pursue my doctoral study in her lab. Her scientific expertise, intellectual input and attention to detail have been vital to the research project and have enabled me to become a better researcher, for which I am extremely grateful. I am indebted to her for her guidance, support, advice and patience over the years, which have been instrumental in the completion of this thesis.

I would like to thank Prof. Dr. Witke for supporting my PhD candidature as a second referee and Prof. Dr. Gerhard von der Emde and Prof. Dr. Valentin Stein for agreeing to be on my thesis committee.

I am grateful to members of the Institute of Reconstructive Neurobiology for creating a pleasant work environment and lending a helping hand whenever required. I would like to thank Dr. Laura Ewell and Maryam Pasdarnavab for the technical assistance with behavioral experiment and also to the members of Prof. Dr. Beck's lab for their support. I deeply appreciate the support from Dr. Hannes Beckert and the microscopy core facility of the medical faculty at the University of Bonn with confocal imaging.

I would like to thank my former and current colleagues for the wonderful working atmosphere in our group: Ankita Vaswani, Marianna Tolve, Alessandro Petese, Adrián López Fernández, Norisa Meli, Philipp Grunwald, Franca Fries, Rui Lois Tan, Catarina Pacheco, Lena Fahrbach, Paula Siebrecht, Daniel Pliev. I am grateful for their endless help and support and for all the laughter we have shared during my time in the lab. I would particularly like to thank Ankita and Marianna for their help during the initial days of my PhD and express my heartfelt gratitude to Norisa for being the best colleague one could ask for. I gratefully acknowledge the contribution of Anta Sinani, Emmy Sedky, Bianca Broske and Wencke Trein to this thesis. I would also like to extend my sincere thanks to Alesja, Antonia, Annika and all the student assistants who have helped to keep the lab running smoothly.

I am blessed with family and friends who have always been there for me. The highest appreciation is reserved for my parents, Abba and Ma, whose profound belief in my abilities and relentless support have enabled me to come this far. Special thanks go to Amma, Baba,

and Bubu, whose constant encouragement and support have motivated me towards the finish line. I am thankful to have Samma, Zaf, and Jummy in my life, my sources of strength and solace. Lastly and most importantly, I would like to thank my daughters for filling my life with love and joy and my husband for being incredibly supportive and patient throughout this journey, for enduring the rough days, and believing in me. I would like to dedicate this work to them.